

COLORIMETRIC AND FLUORESCENT DETECTION OF NUCLEIC ACID BY STYRYL DYES



A Dissertation Submitted in Partial Fulfillment of the Requirements
for the Degree of Doctor of Philosophy in Chemistry

Department of Chemistry

FACULTY OF SCIENCE

Chulalongkorn University

Academic Year 2021

Copyright of Chulalongkorn University

การตรวจวัดกรดนิวคลีอิกด้วยวิธีเชิงสีและฟลูออเรสเซนซ์โดยใช้สีย้อมสไตริล



วิทยานิพนธ์นี้เป็นส่วนหนึ่งของการศึกษาตามหลักสูตรปริญญาวิทยาศาสตรดุษฎีบัณฑิต

สาขาวิชาเคมี ภาควิชาเคมี

คณะวิทยาศาสตร์ จุฬาลงกรณ์มหาวิทยาลัย

ปีการศึกษา 2564

ลิขสิทธิ์ของจุฬาลงกรณ์มหาวิทยาลัย

กชกร ศุภบวรสถิตย์ : การตรวจวัดกรดนิวคลีอิกด้วยวิธีเชิงสีและฟลูออเรสเซนซ์โดยใช้สีย้อมสไตริล. (COLORIMETRIC AND FLUORESCENT DETECTION OF NUCLEIC ACID BY STYRYL DYES) อ.ที่
 ปริญญาหลัก : ศ. ดร.ธีรยุทธ วิไลวัลย์

สีย้อมกรดนิวคลีอิกเป็นเครื่องมือสำคัญสำหรับการวิเคราะห์ดีเอ็นเอหรืออาร์เอ็นเอในหลอดทดลอง และในการใช้งานแสดงภาพระดับเซลล์ อย่างไรก็ตามแม้ว่าในช่วง 2 – 3 ทศวรรษที่ผ่านมาจะมีสีย้อมกรดนิวคลีอิกจำหน่ายในท้องตลาดหลายชนิด แต่ตัวเลือกในการใช้งานยังคงค่อนข้างจำกัด ซึ่งสีย้อมส่วนมากมักมีราคาแพงมากและยังมีสมบัติที่ไม่พึงประสงค์ เช่น ความเป็นพิษต่อผู้ใช้งาน เป็นต้น ดังนั้นการค้นคว้าและพัฒนาสีย้อมที่ไม่เป็นพิษและพร้อมใช้งานผนวกกับมีลักษณะทางแสงที่ต้องการ และควบคุมได้จึงยังคงมีความสำคัญ ไม่นานมานี้สีย้อมสไตริลได้รับความนิยมในฐานะสีย้อมสีทางชีวภาพที่มีคุณสมบัติเชิงแสงตามต้องการ ได้แก่ มีขั้นตอนการสังเคราะห์ที่ไม่ยุ่งยาก, มีความเสถียรเชิงแสงที่ดีเยี่ยม, สามารถปรับคุณสมบัติเชิงแสงได้ และมีการตอบสนองฟลูออเรสเซนส์สูงเมื่อจับกับกรดนิวคลีอิกเป้าหมายโดยมีสัญญาณพื้นหลังต่ำ นอกจากนี้สีย้อมสไตริลมีการดูดกลืนแสงในช่วงความยาวคลื่นแสงที่มองเห็นได้ และมีการเปลี่ยนช่วงการดูดกลืนในตัวทำละลายที่มีสภาพขั้วต่างกัน สีย้อมสไตริลนี้จึงเหมาะสมที่จะประยุกต์ใช้สำหรับการตรวจวิเคราะห์กรดนิวคลีอิกเชิงสีที่ให้ผลรวดเร็วและราคาไม่แพง ในการศึกษาได้ออกแบบสีย้อมสไตริลชนิดใหม่ที่มีประจุบวกในโมเลกุลสองตำแหน่ง โดยมีตัวดัดแปลงที่มีหมู่ควอเตอร์นารีแอมโมเนียมที่มีประจุบวก เพื่อเพิ่มความสามารถในการจับ และการตอบสนองทางแสงกับดีเอ็นเอผ่านอันตรกิริยาทางไฟฟ้ากับหมู่ฟอสเฟตที่มีประจุลบในโครงสร้างหลักของกรดนิวคลีอิก การทดสอบความสามารถของสีย้อมชนิดใหม่ที่สังเคราะห์ได้ทั้งในแง่ของขีดจำกัดของการตรวจวัด และความเลือกจำเพาะของการตอบสนองของสีย้อม ทำได้โดยการวิเคราะห์คุณสมบัติเชิงแสงของสีย้อมสไตริลที่สังเคราะห์ขึ้นใหม่ ประกอบด้วย การตรวจวัดการเปลี่ยนแปลงการเรืองแสงและ/หรือสีเมื่อมีดีเอ็นเอเป้าหมายเทียบกับดีเอ็นเอที่มีลำดับเบสหลากหลายผลลัพธ์ที่ได้ทั้งจากการทดลอง และทางทฤษฎีสนับสนุนว่าสีย้อมสไตริลที่มีประจุบวกในโมเลกุลสองตำแหน่งที่ถูกพัฒนาขึ้นใหม่มีคุณสมบัติที่ดีกว่าสีย้อมสไตริลที่มีประจุบวกตำแหน่งเดียวที่มีโครงสร้างคล้ายคลึงกันทั้งในแง่ของการจับและการตอบสนองทางแสงต่อดีเอ็นเอ นอกจากนี้การศึกษานี้ยังพบว่าประเภของหมู่แทนที่ที่มีสมบัติให้อิเล็กตรอนในโมเลกุลสีย้อมไม่เพียงแต่ส่งผลถึงคุณสมบัติทางแสงเท่านั้น แต่ยังส่งผลถึงการเลือกจับกับดีเอ็นเอที่มีลำดับเบสแตกต่างกัน ซึ่งเอื้อต่อการปรับแต่งคุณสมบัติเชิงแสงของสีย้อมให้ตรงตามความต้องการใช้งานเฉพาะ อีกทั้งในงานนี้ยังได้มีการประยุกต์ใช้สีย้อมที่พัฒนาขึ้นมาสำหรับการแสดงภาพกรดนิวคลีอิกในเซลล์ และประยุกต์ใช้ในแพลตฟอร์มการตรวจจับโปรตีน (II) ที่ใช้ดีเอ็นเอแอปตาเมอร์ได้อย่างประสบความสำเร็จอีกด้วย

สาขาวิชา เคมี
 ปีการศึกษา 2564

ลายมือชื่อนิสิต
 ลายมือชื่อ อ.ที่ปรึกษาหลัก

5872801323 : MAJOR CHEMISTRY

KEYWORD: Styryl dye, Nucleic acid, Colorimetric detection, Fluorescent detection

Kotchakorn Supabowornsathit : COLORIMETRIC AND FLUORESCENT DETECTION OF NUCLEIC ACID BY STYRYL DYES. Advisor: Prof. TIRAYUT VILAVAN, Ph.D.

Nucleic acid staining dyes are essential tools for the analysis and visualizing of DNA/RNA *in vitro* and in cellular applications. Although there are several commercially available dyes developed during the past few decades, the selection is still relatively limited, and they are often very costly and associated with undesirable characteristics such as toxicity. Consequently, the discovery of nontoxic, readily available dyes, with desirable and controllable optical characteristics remains important. Styryl dyes have recently gained popularity as potential biological staining agents with many desirable properties including a straightforward synthesis procedure, excellent photostability, tunable optical properties, and high responsiveness towards nucleic acid targets with low background fluorescence signals. In addition, because of their strong absorption in the visible region together with solvatochromic behaviors, styryl dyes are also potentially useful as colorimetric stains for rapid and inexpensive detection of nucleic acids. In this study, novel dicationic styryl dyes with positively charged quaternary ammonium modifiers are designed to improve the binding affinity and optical responsiveness with DNA through the favorable electrostatic interaction with the negatively charged phosphate backbones. To explore new dyes that can sensitively and specifically change fluorescence and/or color in the presence of nucleic acid targets, optical characteristics of the newly synthesized styryl dyes have been examined in the presence and absence of DNA in various sequence contexts. The obtained results both experimental and theoretical supported that the dicationic styryl dyes outperformed the analogous monocationic styryl dyes in terms of their binding interaction and optical response towards DNA. Moreover, it was found that not only the optical properties but also the selectivity against different DNA sequences can be affected by the nature of the electron-donating substituent on the dyes' molecule thus providing opportunities for fine-tuning of the dyes properties to meet the demand for specific applications. Applications of the developed dyes for cellular imaging of nucleic acids and aptamer-based mercury(II) detection platforms have also been successfully demonstrated.

Field of Study: Chemistry

Student's Signature

Academic Year: 2021

Advisor's Signature

ACKNOWLEDGEMENTS

Firstly, these things are truly beyond my imagination. I had not expected to have long live to these days, but well, I finally did it. During the long journey, I suffered from lots of mental health issues, and thus I would like to thank all kind people around me for their unconditional support and guidance. I would really like to express my sincere gratitude to my research supervisor, Professor Dr.Tirayut Vilaivan, for providing me the opportunity to learn both hard research skills and also lots of soft skills. I am incredibly appreciative for what he has done to awaken my undiscovered abilities, which I had never ever thought they existed. Also, it was a great privilege and honor to work and study under his guidance. My warmest appreciation also goes to his wife, Chotima Vllaivan, for assisting me with whatever I requested. She is gentle, kind, and considerate. I am extremely glad to be a part of TV lab member, where people are friendly, helpful, and supportive of each other.

My work would not be completed without extraordinary collaborators who devoted their time providing data to fulfill this research. I would like to express my special thanks to Dr.Jaru Taechalertpaisarn, and Dr.Chanat Aonbangkhen. I really appreciate their willingness to help without expecting anything in return. In addition, I would like to thank Chulalongkorn University Drug and Health Products Innovation Promotion Center for providing me a kind permission to use their instrument and facilities.

For my family, especially mom and dad, your taught, your guidance, and all your dedication to me always remind me to get back on track. Regardless of circumstances, I fully devote this success to you. As well, I would like to apologize for keeping you waiting for such a long period, lastly, though, I completed the task.

To my private shield, I believe I would not be able to go through tough situations without you. Thanks for rescuing me when I felt like I was drowning, for your unwavering support in everything you do, and for everything else, my partner in crime.

During my journey, I would want to express my gratitude to my psychologist and psychiatrist for helping me heal from my mental illness. Besides, thanks to TELEX

TELEXs, tempdotband, and Oun Chanissara for inspiring me to be much more comfortable, confident, and content.

Finally, I would like to thank the Science Achievement Scholarship of Thailand, Graduate School, and Faculty of Science, Chulalongkorn University for the financial supports during my Ph.D.-to-be journey. My thanks as well go to all the people who have supported me to complete the research work directly or indirectly.

Kotchakorn Supabowornsathit



TABLE OF CONTENTS

	Page
ABSTRACT (THAI)	iii
ABSTRACT (ENGLISH)	iv
ACKNOWLEDGEMENTS	v
TABLE OF CONTENTS	vii
LIST OF TABLES	x
LIST OF FIGURES	xi
1. CHAPTER I INTRODUCTION	1
1.1 Nucleic acids detection.....	1
1.2 Dyes for nucleic acids detection.....	3
1.3 Cyanine and Styryl dyes	9
1.3.1 Cyanine dyes.....	9
1.3.2 Styryl dyes.....	11
1.3.2.1 Styryl dyes for nucleic acid detection	13
1.4 Rationale and objective of this work	25
2. CHAPTER II EXPERIMENTAL SECTION	27
2.1 Materials.....	27
2.2 Synthesis and characterization of novel cationic styryl dyes	28
2.2.1 <i>N</i> -Methylation of the methyl-substituted nitrogen heterocycles.....	28
2.2.2 Sidechain modification of the aromatic aldehyde to introduce additional positive charge to the molecule.....	29
2.2.2.1 Bromoalkylation of the hydroxyl group of substituted salicylaldehydes	29

2.2.2.2 Introduction of positive charge by quaternization with trimethylamine	30
2.2.3 Synthesis of cationic styryl dyes by Aldol-type condensation	32
2.3 Study of optical properties of newly synthesized dyes both in the presence and absence of nucleic acid targets	37
2.3.1 Fluorescence quantum yield (Φ_F) determination of the cationic styryl dyes	38
2.3.2 Color change mechanism of the cationic styryl dyes upon DNA binding	38
2.4 Fluorescent indication displacement assay	39
2.5 Ionic strength dependence studies	40
2.6 Dyes-DNA binding interaction studies	40
2.7 Docking simulation for DNA-dye interaction study	41
2.8 Applications of styryl dyes-based platform for nucleic acid detection	42
2.8.1 HeLa Cell imaging	42
2.8.1.1 MTT cytotoxicity assays	42
2.8.1.2 Cellular imaging experiments	42
2.8.2 Mercury(II) ion detection based on aptamer and cationic styryl dyes	43
3. CHAPTER III RESULTS AND DISCUSSION	44
3.1 Synthesis of cationic styryl dyes	44
3.2 Optical properties of cationic styryl dyes	47
3.3 Studies of binding modes by fluorescent indication displacement	58
3.4 Binding studies using circular dichroism spectroscopy	65
3.5 Comparison of DNA binding affinity between monocationic dyes and dicationic dyes	67
3.5.1 Double-stranded DNA titration	67

3.5.2 Ionic strength dependence quenching of cationic styryl dyes bound to dsDNA.....	70
3.5.3 Binding constant (K_b) and the number of dsDNA base pairs occupied by one bound dye molecule (n)	73
3.5.4 Effect of linker length	75
3.6 DNA sequence selectivity	77
3.7 Docking simulation for DNA-dye interaction study	83
3.8 Limit of detection of cationic styryl dyes for DNA detection in fluorescence and colorimetric modes	86
3.9 Applications of dicationic styryl dyes in cell imaging	88
3.10 Mercury(II) detection platform based on cationic styryl dyes and DNA aptamer	91
4. CHAPTER IV CONCLUSION	96
REFERENCES	99
APPENDIX.....	111
VITA.....	136

LIST OF TABLES

	Page
Table 2.1 Synthetic DNA oligonucleotides used in this work.....	27
Table 3.1 Optical properties of cationic styryl dyes in the absence and presence of dsDNA: absorption maxima $\lambda_{\max}(\text{abs})$, extinction coefficients (ϵ), emission maxima $\lambda_{\max}(\text{em})$, fluorescence quantum yield (Φ_F) and fluorescence enhancement ratio (F/F_0).....	57
Table 3.2 Fluorescence spectra of the cationic styryl dyes' FID assays and their binding characteristics.....	61
Table 3.3 Quenching constants (K_{SV}) of the cationic styryl dyes.....	71
Table 3.4 Binding constant (K_b) and the number of base pairs in dsDNA occupied by one bound dye molecule (n) values of the synthesized styryl dyes.....	74
Table 3.5 Comparison of the limit of detection of cationic styryl dyes for the determination of dsDNA by fluorescence and UV-visible spectrophotometry	86

LIST OF FIGURES

	Page
Figure 1.1 Nucleic acid structures and components.....	1
Figure 1.2 Binding modes of small molecules to dsDNA.....	3
Figure 1.3 Examples of commercially available fluorescent nucleic acid staining dyes	4
Figure 1.4 Example of commercially available colorimetric dyes for nucleic acid detection.....	6
Figure 1.5 Illustration of the colorimetric method for differentiating between single- and double-stranded oligonucleotides.....	7
Figure 1.6 Colorimetric detection of nucleic acids based on AuNPs and positively charged labeled PNA in Faikhruea work.....	8
Figure 1.7 Various types of cyanine dyes.....	9
Figure 1.8 Generic designs of cationic styryl dyes.....	11
Figure 1.9 Twisted Intramolecular Charge Transfer (TICT) dynamics.....	13
Figure 1.10 2-[4-(Dimethylamino)styryl]-1-methylpyridinium iodide (DASPMI) (a), Binding interaction of dyes with different linker lengths towards DNA in Berdnikova work (b).....	15
Figure 1.11 Bis(styryl)pyridinium dyes with OMe or/and NMe ₂ substituents helical aggregations formed by ctDNA.....	16
Figure 1.12 The screening strategy used in Chang's Study.....	17
Figure 1.13 Indole–quinolinium type styryl dyes developed by Bohländer et al.....	18
Figure 1.14 Molecular structures of quinolinium-based styryl dyes with flexible/rigid side group in Wang work and their fluorescence intensity with various DNA oligomers.	19

Figure 1.15 Styryl-quinolinium derivatives synthesized and evaluated in Saady study	20
Figure 1.17 Chemical structure of the styryl dye used (a), Fluorescence intensity of the styryl–DNA system vs. DNA concentration in Xu’s work (b).....	21
Figure 1.18 Monomer and homodimer styryl dyes based on (<i>p</i> -dimethylaminostyryl) benzothiazolium moiety containing charged spermine-like linkage/tail groups in Tokar’s work	22
Figure 1.19 Monomer and homodimer styryl dyes based on (<i>p</i> -dimethylaminostyryl) benzothiazolium moiety in Akbay’s work.....	23
Figure 1.20 Nucleolus and chromosome imaging and digest experiments by RNase and DNase according to Wang.....	24
Figure 1.21 Clickable styryl dyes for fluorescence labeling of pyrrolidiny PNA probes for the detection of base mutations in DNA.	25
Figure 1.22 The concept of this work.....	26
Figure 2.1 Cationic styryl dye structures with shorten names used in this work.....	33
Figure 3.1 Main synthesis steps of cationic styryl dyes	44
Figure 3.2 The structures of cationic styryl dye being studied in this work.....	45
Figure 3.3 Synthetic routes for the cationic styryl dyes in this work.....	46
Figure 3.4 Normalized absorption spectra of cationic styryl dyes PY series (a), BT series (b), 4QL series (c), 2QL2+ (d), TMIN2+ (e) and AD2+ (f) in the absence and presence of DNA.....	47
Figure 3.5 Normalized absorption spectra of 4QL2+ (10 μ M) in various solvents (a), Absorption spectra of 4QL2+ aqueous solution (1 – 50 μ M) (b), Relationship between absorption wavenumber ($1/\lambda_{\max}(\text{abs}), \text{cm}^{-1}$) and $E_T(30)$ scale (c), and Illustration explained energy gaps of 4QL2+ in different polarity environment (d).....	50

Figure 3.6 Normalized fluorescence spectra of the styryl dyes PY series (a), BT series (b), 4QL series (c), 2QL2+ (d), TMIN2+ (e) and AD2+ (f) in the absence (dotted lines) and presence of DNA (solid lines).....	51
Figure 3.7 Fluorescence spectra of 4QL2+ (10 μ M) in the absence and presence of DNA (450 μ M, in bp) in water (a) glycerol (b), Absorption spectra of 4QL2+ (10 μ M) in the presence and absence of DNA (450 μ M, in bp) in glycerol (c), Fluorescence spectra of 4QL2+ (10 μ M) in glycerol (0 – 90 $^{\circ}$ C) (d), Fluorescence spectra of 4QL2+ (10 μ M) in various solvents, $\lambda_{\text{ex}} = 548$ nm (e), Lippert-Mataga plot of the Stokes shift and orientation polarizability of the solvents surrounding the dye molecules of 4QL2+ dissolved in various solvents (f), Illustration explained fluorescence change mechanism of the dye (g).....	56
Figure 3.8 Fluorescent indication displacement concept in this work.....	58
Figure 3.9 Melting temperature (T_m) investigation of d(AT) ₁₀ (a) and d(GC) ₁₀ (b) as the selected DNAs to study binding mode by fluorescent indication displacement	59
Figure 3.10 Determination of optimal ratios between [EtBr]:[DNA] (a) and [DAPI]:.....	60
Figure 3.11 Summary of binding characteristics of cationic styryl dyes determining by fluorescence indication displacement assay	64
Figure 3.12 Circular dichroism (solid line) and absorption (dotted line) spectra of (a) PY2+(C4) , (b) BT2+(NEt₂) , (c) BT2+(OMe) , (d) 4QL2+ in the presence and absence of dsDNA.....	65
Figure 3.13 The proposed enhancement of electrostatic interaction between dicationic styryl dyes and DNA	67
Figure 3.14 UV-vis and fluorescence titration with DNA (3 – 450 μ M, in bp) and plot of relative change of maximum absorption (expressed as A_f/A_i , which referred to the ratios between the absorption maxima of the free dye (A_i) and of the DNA-bound dye (A_f)) and maximum fluorescence emission (expressed as F/F_0) (c) vs. concentration ratio of DNA (bp) and the dyes PY+/PY2+(C4) (a), BT+/BT2+(NEt₂) (b), 4QL+/4QL2+ (c).	69

Figure 3.15 Salt displacement principle displaying ionic strength dependence quenching mechanism of cationic styryl dyes bound to dsDNA.....	70
Figure 3.16 Quenching of the complexes of BT+ and BT2+(NEt₂) (a), PY2+(C4) , BT2+(NEt₂) , and 4QL2+ (b) (1 μ M) with DNA (15 μ M, in bp) in the presence of NaCl (50 mM – 200 mM).....	71
Figure 3.17 Plots of fluorescence intensity dependence on $F \times [\text{Dye}]/[\text{DNA}](\text{bp})$ ratio (square) and its approximation by the modified McGhee and von Hippel equation (equation 5) (dotted line) for PY+ (a), PY2+(C4) (b), BT+ (c), BT2+(NEt₂) (d), 4QL+ (e), 4QL2+ (f).....	73
Figure 3.18 UV-vis and fluorescence titration with DNA (3 – 450 μ M, in bp) (a) and plot of relative change of maximum absorption (expressed as A_f/A_i , which referred to the ratios between the absorption maxima of the free dye (A_i) and of the DNA-bound dye (A_f)) (b) and maximum fluorescence emission (expressed as F/F_0) (c) vs. concentration ratio of DNA (bp) and the dyes with different linker length (PY+ , PY2+(C2) , PY2+(C3) and PY2+(C4)).....	76
Figure 3.19 Preliminary visual screening of the responsiveness of the dyes towards different base sequence.....	78
Figure 3.20 Normalized fluorescence spectra of BT2+(NEt₂) (a) and BT2+(OMe) (c) towards different nucleobases DNA sequences and bar graphs represented responsiveness of BT2+(NEt₂) (b) and BT2+(OMe) (d) towards different nucleobases DNA sequences using F/F_0 ratio.....	79
Figure 3.21 Fluorescent properties of the dyes mixture BT2+(NEt₂) and BT2+(OMe) (a),(d) or 4QL2+ and BT2+(OMe) (b), (c), (e) and (f) in the absence and presence of DNA mixture with different AT/CG compositions.....	82
Figure 3.22 Molecular docking of BT+ , BT2+(NEt₂) , 4QL2+ and PY2+(C4) on a minor-groove DNA (4C64) (a) and at an intercalative site of DNA (108D) (b).....	85
Figure 3.23 Cytotoxicity study of BT+ , BT2+(NEt₂) and BT2+(OMe) by MTT assay (HeLa cells, 1×10^4 cells per plate, 24 h incubation).....	88

Figure 3.24 Fluorescence image analysis of HeLa cells treated with indicated compound at of PhenoVue512 (500nM) and BT2+(NEt₂) (20 μM) (a), DAPI (0.2 μg/mL) and BT2+(OMe) (200 μM) (b).	90
Figure 3.25 Detection platform for mercury(II) ions based on cationic styryl dyes and dT ₃₀ DNA aptamer	91
Figure 3.26 The styryl dye-aptamer based mercury(II) detection platform developed by Tiarpattaradilok.....	93
Figure 3.27 Calibration curves and LODs for the developed mercury(II) detection platform based on dT ₃₀ aptamer and cationic styryl dyes BT2+(NEt₂) (a) and BT2+(OMe) (b). Screening experiments with various metal ions to determine the selectivity of the developed platform for BT2+(NEt₂) (c) and BT2+(OMe) (d).	94
Figure A1 ¹ H (500 MHz, DMSO- <i>d</i> ₆) NMR spectrum of 1,4-dimethylpyridin-1-ium iodide	112
Figure A2 ¹ H (500 MHz, DMSO- <i>d</i> ₆) NMR spectrum of 1,4-dimethylquinolin-1-ium iodide	112
Figure A3 ¹ H (500 MHz, DMSO- <i>d</i> ₆) NMR spectrum of 2,3-dimethylbenzo[<i>d</i>]thiazol-3-ium iodide.....	113
Figure A4 ¹ H (500 MHz, DMSO- <i>d</i> ₆) NMR spectrum of 1,2-dimethylquinolin-1-ium iodide	113
Figure A5 ¹ H (500 MHz, DMSO- <i>d</i> ₆) NMR spectrum of 1,2,3,3-tetramethyl-3 <i>H</i> -indol-1-ium iodide.....	114
Figure A6 ¹ H (500 MHz, DMSO- <i>d</i> ₆) NMR spectrum of 9,10-dimethylacridin-10-ium iodide	114
Figure A7 ¹ H (500 MHz, CDCl ₃) NMR spectrum of 2-(2-bromoethoxy)-4-(diethylamino)benzaldehyde	115
Figure A8 ¹ H (500 MHz, CDCl ₃) NMR spectrum of 2-(3-bromopropoxy)-4-(diethylamino)benzaldehyde	115

Figure A9 ^1H (500 MHz, CDCl_3) NMR spectrum of 2-(4-bromobutoxy)-4-(diethylamino)benzaldehyde	116
Figure A10 ^1H (500 MHz, CDCl_3) NMR spectrum of 2-(4-bromobutoxy)-4-methoxybenzaldehyde	116
Figure A11 ^1H (500 MHz, $\text{DMSO-}d_6$) NMR spectrum of 2-(5-(diethylamino)-2-formylphenoxy)- <i>N,N,N</i> -trimethylethan-1-aminium bromide.....	117
Figure A12 ^1H (500 MHz, $\text{DMSO-}d_6$) NMR spectrum of 3-(5-(diethylamino)-2-formylphenoxy)- <i>N,N,N</i> -trimethylpropan-1-aminium bromide	117
Figure A13 ^1H (500 MHz, $\text{DMSO-}d_6$) NMR spectrum of 4-(5-(diethylamino)-2-formylphenoxy)- <i>N,N,N</i> -trimethylbutan-1-aminium bromide.....	118
Figure A14 ^1H (500 MHz, $\text{DMSO-}d_6$) NMR spectrum of 4-(2-formyl-5-methoxyphenoxy)- <i>N,N,N</i> -trimethylbutan-1-aminium bromide.....	118
Figure A15 ^1H (500 MHz, $\text{DMSO-}d_6$) (a) and ^{13}C (126 MHz, $\text{DMSO-}d_6$) (b) NMR spectra of compound PY+	119
Figure A16 ^1H (500 MHz, $\text{DMSO-}d_6$) (a) and ^{13}C (126 MHz, $\text{DMSO-}d_6$) (b) NMR spectra of compound PY2+(C2)	120
Figure A17 ^1H (500 MHz, $\text{DMSO-}d_6$) (a) and ^{13}C (126 MHz, $\text{DMSO-}d_6$) (b) NMR spectra of compound PY2+(C3)	121
Figure A18 ^1H (500 MHz, $\text{DMSO-}d_6$) (a) and ^{13}C (126 MHz, $\text{DMSO-}d_6$) (b) NMR spectra of compound PY2+(C4)	122
Figure A19 ^1H (500 MHz, $\text{DMSO-}d_6$) (a) and ^{13}C (126 MHz, $\text{DMSO-}d_6$) (b) NMR spectra of compound BT+	123
Figure A20 ^1H (500 MHz, $\text{DMSO-}d_6$) (a) and ^{13}C (126 MHz, $\text{DMSO-}d_6$) (b) NMR spectra of compound BT2+(NEt₂)	124
Figure A21 ^1H (500 MHz, $\text{DMSO-}d_6$) (a) and ^{13}C (126 MHz, $\text{DMSO-}d_6$) (b) NMR spectra of compound BT2+(OMe)	125

Figure A22 ^1H (500 MHz, $\text{DMSO-}d_6$) (a) and ^{13}C (126 MHz, $\text{DMSO-}d_6$) (b) NMR spectra of compound 4QL+	126
Figure A23 ^1H (500 MHz, $\text{DMSO-}d_6$) (a) and ^{13}C (126 MHz, $\text{DMSO-}d_6$) (b) NMR spectra of compound 4QL2+	127
Figure A24 ^1H (500 MHz, $\text{DMSO-}d_6$) (a) and ^{13}C (126 MHz, $\text{DMSO-}d_6$) (b) NMR spectra of compound 2QL2+	128
Figure A25 ^1H (500 MHz, $\text{DMSO-}d_6$) (a) and ^{13}C (126 MHz, $\text{DMSO-}d_6$) (b) NMR spectra of compound TMIN2+	129
Figure A26 ^1H (500 MHz, $\text{DMSO-}d_6$) (a) and ^{13}C (126 MHz, $\text{DMSO-}d_6$) (b) NMR spectra of compound AD2+	130
Figure A27 HRMS (MALDI-TOF) of PY+	131
Figure A28 HRMS (MALDI-TOF) of PY2+(C2)	131
Figure A29 HRMS (MALDI-TOF) of PY2+(C3)	132
Figure A30 HRMS (MALDI-TOF) of PY2+(C4)	132
Figure A31 HRMS (MALDI-TOF) of BT+	133
Figure A32 HRMS (MALDI-TOF) of BT2+(NEt₂)	133
Figure A33 HRMS (MALDI-TOF) of BT2+(OMe)	134
Figure A34 HRMS (MALDI-TOF) of 4QL+	134
Figure A35 HRMS (MALDI-TOF) of 4QL2+	135

CHAPTER I

INTRODUCTION

1.1 Nucleic acids detection

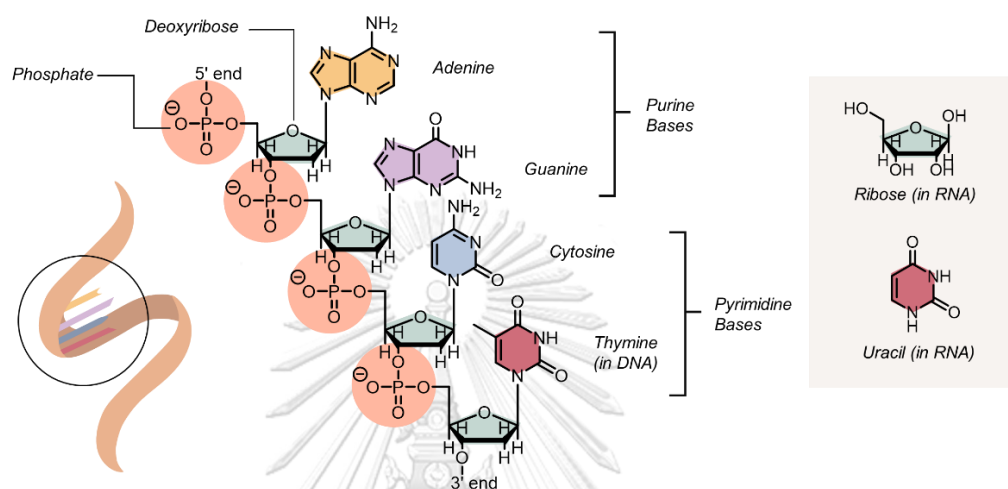


Figure 1.1 Nucleic acid structures and components

Nucleic acids¹ (Figure 1.1) are the molecules that carry the genetic information and play indispensable roles in the production of proteins that are essential for the cell structure and functions. They also possess hereditary characteristics whereby such information can be forwarded to descendants in a highly precise manner. The information is stored in the form of base sequence which is unique for each species and to the level of individual member of the species. Accordingly, the nucleic acid sequence can reveal the identity of the species or the individual organism. Even a slight change in the base sequence of nucleic acids, either through internal factors such as aging or external factors such as exposure to chemicals or radiation, could result in the production of abnormal proteins or stop the protein production altogether. Such event could lead to genetic diseases that can be transmitted to descendants. Thus, the detection of nucleic acids is important in many areas including medical,² forensic,³ agricultural,⁴ and food⁵ applications.

Generally, the nucleic acids assays are performed in the liquid and solid phase formats.⁶ The techniques commonly employed for nucleic acids detection are real-time PCR,⁷ blotting assay,⁸ electrophoresis,^{9,10} and mass spectrometry.¹¹ Since nucleic acid molecules themselves have no intrinsic properties that are suitable for the direct detection (except UV absorption, which is relatively insensitive), a secondary detection technology (e.g., stains, labels) is often required to improve the sensitivity of the assays. The label may bind to the nucleic acid molecule either through a covalent bond to form a probe,¹² or by noncovalent binding to a specific sequence or structure of nucleic acid targets.¹³ The latter is more convenient as no complicated modification and purification steps are required, although the specificity may not be as good as the probe-based assay. For certain type of assays, the label may exhibit permanent signal (always on). In such cases, a mechanism to distinguish between the positive and negative events must be incorporated. This is typically performed in heterogeneous assay format whereby the bound and unbound labels (or labeled probes) are partitioned in separated phases, followed by washing to eliminate the unbound labels or probes. Alternatively, the use of smart labels or probes that can exhibit the signal in response to the correct nucleic acid target, thus providing low background signal in the absence of nucleic acids and gave high response in their presence. This allows the assay to be performed in a homogeneous format that is more convenient and more compatible with the detection of nucleic acid targets in living cells.

1.2 Dyes for nucleic acids detection

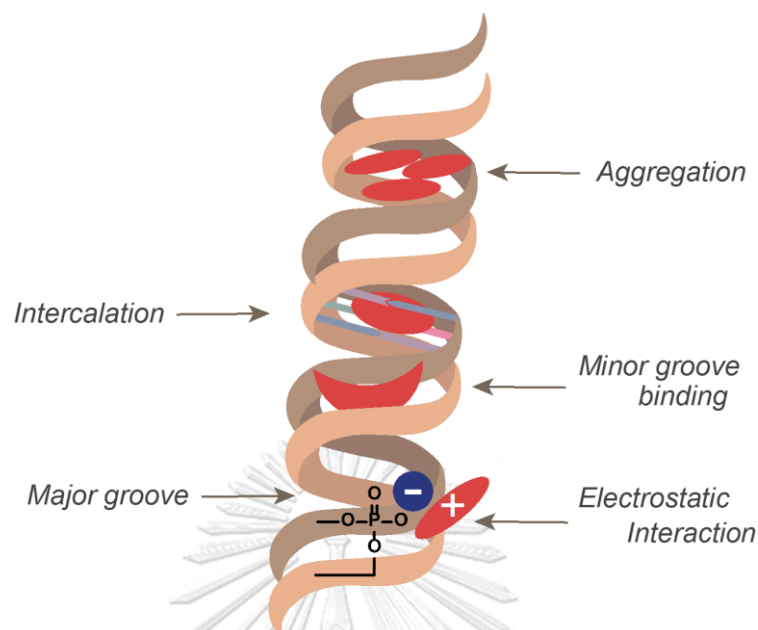


Figure 1.2 Binding modes of small molecules to dsDNA

In recent years, fluorescent organic dye molecules which are typically highly conjugated aromatic compounds have become an essential tool for qualitative and quantitative analysis of nucleic acids both *in vitro* and in the cells. These dyes can bind non-covalently to nucleic acids in one or more of several possible modes typical for the interactions between small molecules and nucleic acids including intercalation, groove binding, aggregation, and electrostatic interaction¹⁴ (Figure 1.2). Ethidium bromide is a classic example of DNA intercalator that became highly fluorescent upon binding to double-stranded DNA (dsDNA) thus it used to be a popular staining agent for visualizing nucleic acids following gel electrophoresis.¹⁵⁻¹⁷ However, ethidium bromide is well-known for its toxicity and mutagenic properties.¹⁸ There have been several commercially available alternative nucleic acid staining dyes – some of which can be used for imaging of cellular nucleic acids, but they are costly and suffers several other limitations. For example, SYBR dyes, which are marketed as replacement for ethidium bromide with less mutagenicity, are also

possible carcinogen due to the high DNA binding affinity of such molecules.¹⁹ Another example of commercially available fluorescent nucleic acid staining dyes is acridine orange. Intercalation is the primary mode of interaction between acridine orange with double-stranded DNA, but electrostatic forces are considered to be the major mode of interaction with single-stranded DNA (ssDNA) and RNA, and multiple acridine orange molecules can stack onto the nucleic acid strands.²⁰ Acridine orange bound to dsDNA showed a maximum emission wavelength of 525 nm (green), while a maximum emission wavelength of 650 nm (red) was observed when the dye bound to ssDNA (and RNA). The difference are easily distinguishable spectroscopically.²⁰ However, acridine orange are also suspected of causing genetic defects. As stated in product safety data sheet, the dye was remarked to cause DNA damage and morphological transformation in mouse and hamster, respectively.²¹

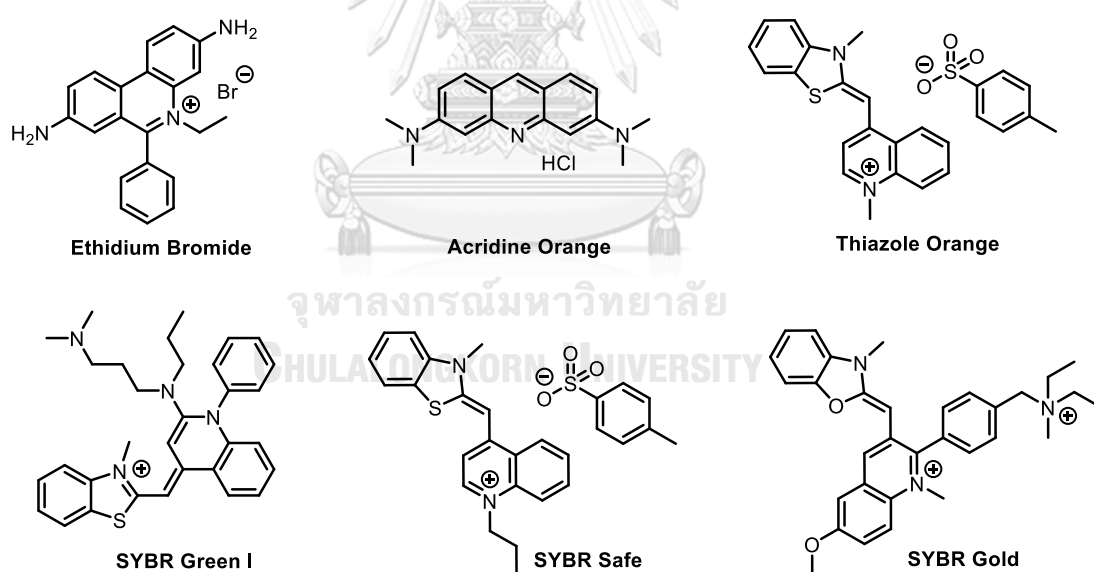


Figure 1.3 Examples of commercially available fluorescent nucleic acid staining dyes

In addition to fluorescence, another optical mode for dye-based nucleic acid detection is colorimetric detection. Only few colorimetric dyes for nucleic acids are known. These include merocyanine,²²⁻²⁴ which is also conjugated organic molecules that can bind to minor groove of nucleic acids at alternative adenine/thymine (AT)

base pairs region. The color change mechanism for the merocyanine is mainly the aggregation of individual dye monomers in the presence of the DNA “template”. When the dye bound to DNA, a face-to-face dimer (*J*-aggregate) is formed and hence leads to bathochromic shift of the dye absorption.²⁵ An additional example of colorimetric conjugated organic dye molecules is crystal violets,^{26, 27} a triphenylmethane dye which is able to bind to major groove of nucleic acids and often used as nuclear staining agents in cellular imaging applications. Crystal violet (CV) exhibits a violet color in aqueous solution. When sulfite ion - a strong nucleophile - is added to the central carbon of CV, the conjugated system collapses resulting in the transformation into a colorless leuco crystal violet (LCV). In the presence of dsDNA, the CV molecule present in chemical equilibrium with the LCV binds to the major groove of dsDNA and forms a CV-dsDNA complex, thus shifting the equilibrium towards the CV side. The CV-DNA binding was stabilized by the electrostatic interaction between the negative charge of the phosphate group of dsDNA and the positive charge on the quinoid ring of CV. Due to steric hindrance and electrostatic interactions, the CV molecule bound to dsDNA is resistant to the nucleophilic attack by the sulfite ion. As a result, the colorless solution of LCV changed to violet of CV in the presence of DNA.²⁶ Therefore, the colorimetric nucleic acid dyes offer a great potential for the development of rapid, instrument-free and low-cost assays suitable for point of care testings. Nevertheless, only limited selection of such dyes is commercially available.

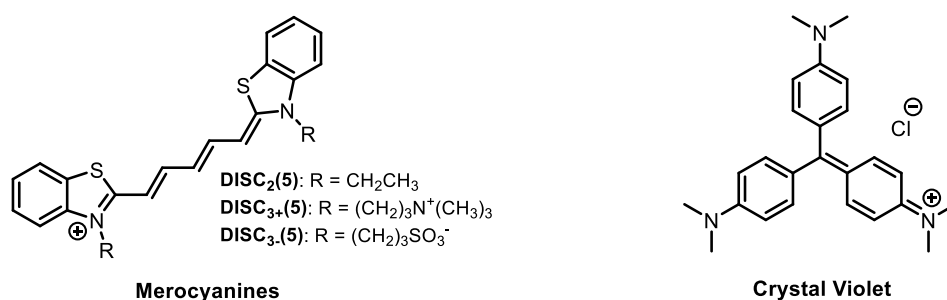


Figure 1.4 Example of commercially available colorimetric dyes for nucleic acid detection

Apart from colorimetric dye molecules, metallic nanoparticles have been also utilized for colorimetric detection of nucleic acids due to their unique localized surface plasmon resonance (LSPR) properties. LSPR is a phenomenon that occurs on metal nanoparticles of similar or smaller size than the wavelength of light. The incident light near the surface stimulates the electron's resonant oscillation, and the maximum optical absorption of the particles occurs at the plasmon resonant frequency.²⁸ The most widely used metallic nanoparticles is gold nanoparticles (AuNPs) which exhibit size-dependent LSPR property. The LSPR wavelength shifts towards the longer wavelength causing an obvious color change from red to purple upon increasing the size of the AuNPs, including aggregation. It has been discovered that the binding of single stranded nucleic acids binds to AuNPs surface through the nucleobases can stabilize the AuNPs towards salt-induced aggregation and thus the solution color remains red. On the other hand, dsDNA cannot interact with AuNPs in the same way because all the nucleobases are involved in the base pairing.²⁹ This principle has been widely used for colorimetric nucleic acid assays.^{30, 31}

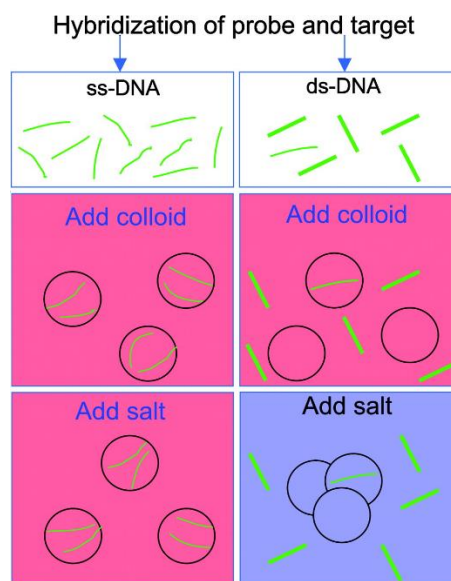


Figure 1.5 Illustration of the colorimetric method for differentiating between single- and double-stranded oligonucleotides. The circles represent colloidal gold nanoparticles.²⁹ (Copyright (2004) National Academy of Sciences)

In 2022, Faikhruea and co-workers reported the use of AuNPs and positively charged PNA probes for dual-mode fluorescent and colorimetric detection of DNA and RNA.³² For colorimetric detection, since PNA probe carried neutral peptide backbone, multiple positive charges were introduced to the PNA probe to enhance the AuNPs aggregation. When the PNA probe and the complementary DNA/RNA target were mixed before adding the AuNPs, the red color of the AuNPs remained stable because the PNA–DNA hybrid with net negative charges could not effectively induce aggregation of the AuNPs. On the other hand, in the presence of mismatched nucleic acid target or no nucleic acid target at all (i.e., PNA probe alone), the positively charged PNA probe induced immediate aggregation of AuNPs leading to obvious color change from red to purple. In addition, AuNPs can also act as an effective quencher. Thus, when the PNA probe was labeled with a fluorescent label such as fluorescein, a fluorescence-based assay could also be achieved simultaneously. Thus, the free PNA probe bound to the AuNPs resulting in

fluorescence quenching of the probe as well as aggregation of the AuNPs. In contrast, the presence of DNA target inhibited both the fluorescence quenching and AuNPs aggregation resulting in red-colored solution with green fluorescence as shown in Figure 1.6. Thus, the use of PNA probe in combination with AuNPs allowed the dual-mode discrimination of target and non-target nucleic acids with good sensitivity and specificity.

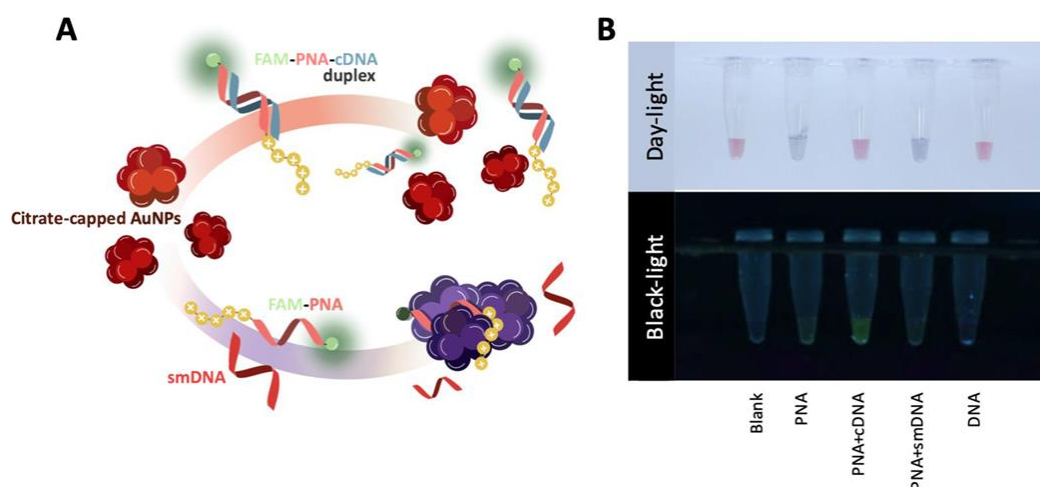


Figure 1.6 Colorimetric detection of nucleic acids based on AuNPs and positively charged labeled PNA in Faikhruea work.³² (Reprinted with permission from *ACS Appl. Bio Mater.* **2022**, 5 (2), 789-800. Copyright (2022) American Chemical Society.)

Nevertheless, the use of metallic nanoparticles is quite difficult to control because the nanoparticles are extremely sensitive to environment change such as salt and other components in the samples such as proteins, etc. Consequently, the development of alternative dyes which are non-toxic, readily accessible, with tunable optical properties and target binding affinity/selectivity is still desirable and challenging, and thus conjugated organic molecules are outstanding candidates with promising properties.³³

1.3 Cyanine and Styryl dyes

1.3.1 Cyanine dyes

Cyanine dyes are highly conjugated organic molecules containing two nitrogen atoms in the molecule, one of which carries a positive charge, while the other is neutral. The two nitrogen atoms are connected via a polymethine bridge, which consists of an odd number of conjugated carbon atom(s). These two nitrogen atoms of cyanine dyes could exist as open chain or be a part of heterocycles, such as pyrrole, imidazole, thiazole, pyridine, quinoline, indole, and benzothiazole, etc. When only one of the nitrogen atoms is part of the heterocyclic ring, the dyes are called hemicyanines.^{34,35} Examples of the most common cyanine dyes include Cy3 and Cy5, as shown in Figure 1.7.

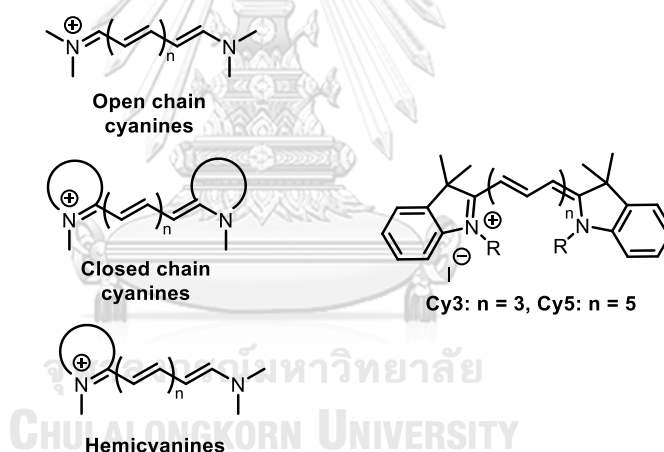


Figure 1.7 Various types of cyanine dyes

Due to extensive conjugated system of the cyanine dyes, their absorption and fluorescence are in the visible to near infrared range of the electromagnetic spectrum. The significant absorption of light at various wavelengths results in a variety of brightly colored solutions, leading to a wide range of applications in single-molecule and super-resolution imaging, as well as other biophysical studies.³⁶ For instance, they have been applied for laser printing,³⁷ pH sensors,³⁸ fluorescence

imaging *in vivo*,³⁹ data storage,⁴⁰ and medicine.⁴¹ In addition, cyanine dyes have found widespread uses as nucleic acid labels.^{42, 43} The binding of individual cyanine dye molecules or their self-assembling to form *J*-aggregate in the presence of double-helical DNA templates caused change in optical properties such as fluorescence⁴⁴ or color change²³ which can be used for nucleic acids detection.

The most popular cyanine dyes currently used for high-performance nucleic acid labeling purposes are Cy3 and Cy5. Due to different length in conjugated system of both dyes, the Cy3 exhibits green emission, while the Cy5 gave red emission. Both dyes are typically not environment sensitive and should exhibit permanent signal (always on). However, it was found that the nucleobase sequence of the labeled oligonucleotides can have a strong influence on the fluorescence intensity of Cy3 and Cy5 dyes which may complicate quantitation in nucleic acid sequencing^{45, 46} and microarray applications.⁴⁷

Another common cyanine dye for nucleic acids detection which is also commercially available is thiazole orange (and the structurally related SYBR safe).⁴⁸ Thiazole orange was first developed as a photographic dye.⁴⁹ Its use as nucleic acid stains subsequently followed after the finding that the dye gave large fluorescence enhancement upon binding to nucleic acids as a monomer to dsDNAs and poly(dA), both as a monomer and as a dimer to poly(dG) and mainly as a dimer to poly(dC) and poly(dT).⁵⁰ Moreover, the dye can permeate live cell membranes thus it was applicable for cellular nucleic acid detection.⁵¹ Apart from dsDNA, thiazole orange showed strong binding affinity to G-quadruplex (G4) and gave strong fluorescence enhancement. The strong response of thiazole orange to G4 suggests its potential for various medical applications since G4s are important noncanonical secondary structures of nucleic acids that are associated with some diseases, such as tumors, diabetes, and neurodegenerative diseases.⁵² However, thiazole orange stains DNA

non-selectively, thus sequence-specific detection requires additional probe molecule. Due to the low responsiveness of thiazole orange to single stranded PNA, the PNA probe covalently modified with thiazole orange has found widespread uses as hybridization responsive probes which gave high fluorescence enhancement in the presence of complementary DNA target.⁵³⁻⁵⁵

1.3.2 Styryl dyes

Styryl dye is a class of conjugated organic dyes which shares structural similarity to the cyanine dyes. The styryl dye structures possess a styryl group (Ar-CH=CH-) derived from styrene. It consists of two aromatic moieties with complementary electronic properties. The majority of these dyes consists of an electron-rich aromatic ring system linking to an electron-deficient heteroaromatic ring system via one or more conjugated double bonds.⁵⁶

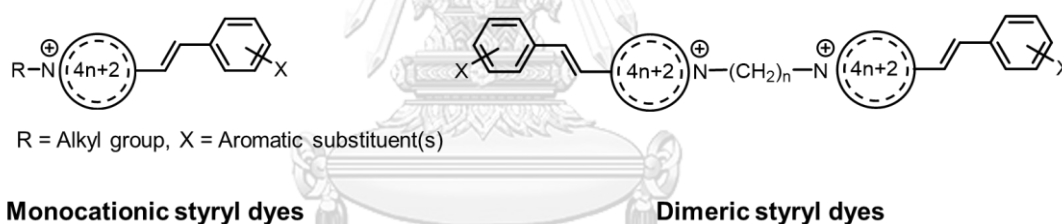


Figure 1.8 Generic designs of cationic styryl dyes

The synthesis of styryl dyes was firstly reported in 1920 by Kong et al.⁵⁶ Since then, styryl dyes have been widely employed as sensitizers and additives in photographic industries.^{57, 58} These dyes have been utilized in several other applications, such as molecular photovoltaic cells,⁵⁹ optical molecular systems⁶⁰ and artificial photosynthesis,⁶¹ Recently, styryl dyes have been employed as fluorescent probes for numerous analytical methods especially for chemosensing of peroxidase activities,⁶² selected ions⁶³ or biomolecules.⁶⁴ This class of dye is often highly sensitive to environment⁶⁵ like solvent polarity, viscosity or pH, leading to visible

response in terms of color and/or fluorescence change even upon small change in environment. Also, styryl dyes show high photostability and high fluorescence quantum yield (Φ_f).

The asymmetrical donor- π -acceptor structure of styryl dyes, which is often referred to as push-pull molecules, gives rise to their interesting optical characteristics. The optical properties of these dyes can be greatly altered by the environment such as solvent polarity due to their dipolar nature. The comparison of these dyes' permanent dipole moments can explain their solvatochromic behavior in solution. If the excited state has a greater dipole moment than the ground state, the more polar solvent preferentially stabilizes it, and the energy gap between the two states becomes more narrow, causing the absorption and emission spectra to shift to the red region.⁶⁶

In addition, the styryl dyes are characterized as molecular rotors due to their ability to form twisted states by rotating one of the molecule's segments in relation to the remainder of the molecule in the excited state. Twisted intramolecular charge transfer (TICT) complexes are the name given to this class of fluorophores. A molecular rotor can return to the ground state after photon absorption, either from the locally energized (LE) state or from the twisted state. The energy gaps between the LE and twisted states and the ground state are vastly different, and de-excitation from the twisted state results in either a red-shifted emission wavelength or no emission at all. However, if the molecular motion is restricted, such as by binding to a host molecule, the non-radiative relaxation pathway is inhibited, resulting in higher fluorescent quantum yields.⁶⁷

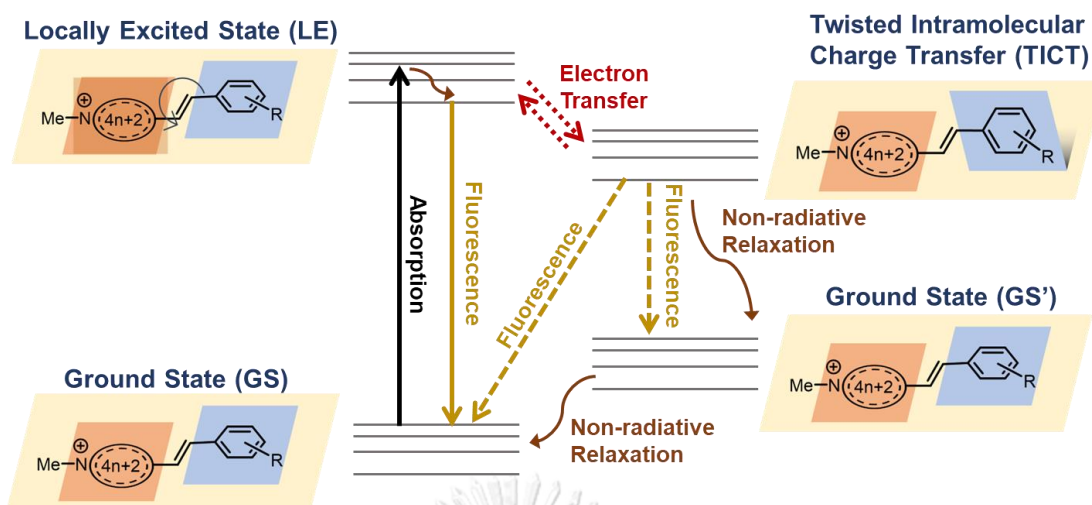


Figure 1.9 Twisted Intramolecular Charge Transfer (TICT) dynamics

1.3.2.1 Styryl dyes for nucleic acid detection

Styryl dyes have been extensively used as fluorescent probes for nucleic acids sensing applications.^{44, 65, 68-77} Fluorescence enhancement mechanism of styryl dyes in the presence of nucleic acids can be explained by the restriction in conformational freedom of the styryl dye molecules once they are intercalated or inserted in the grooves of DNA with a proper space. This phenomenon prevented the non-radiative pathway for relaxation of the dye in the excited state and therefore resulting in the observed fluorescence increase.⁷⁸ In addition, the change of absorption maxima up to a few tens of nanometers has been previously noted in some styryl dyes upon binding to nucleic acids.⁷⁹ Since colorimetric detection of nucleic acids based on styryl dyes have been currently reported, the styryl dyes also showed promising properties to be colorimetric dyes for nucleic acids detection.

Pyridinium-based styryl dyes such as 2-[4-(dimethylamino)styryl]-1-methylpyridinium iodide (DASPMI) is a well-established styryl dye that has been used for selective labeling of mitochondria.⁸⁰ This dye was reported to bind to dsDNA in a groove binding mode based on Sahoo⁸¹ and Ramadass⁸² studies. Fluorescence enhancement of DASPMI in the presence of calf thymus DNA (ct-DNA) was only

about 2 folds in the presence of 1.8 equiv. of DNA total concentration (strand).⁸¹ The binding mode changed to intercalative when the dye was encapsulated in a vesicular medium. The vesicles interact with the base pairs to achieve DNA compaction, and in this environment of favorable electrostatic conditions and π - π interaction between the charge transfer dye sitting on the vesicles and the base pairs, the dye DASPMI partially exits the vesicles and stacks between the DNA base pairs via intercalative binding. For retro-addition of the vesicles to dye molecules that have already been groove-bound, the dye-DNA binding mechanism (minor groove) remained unchanged.⁸³

The mode of binding between related pyridinium-based styryl dyes and DNA was further studied in 2018 by Berdnikova and co-workers.⁸⁴ They reported that the pyridinium-based dyes with a short C₃ linker bound to DNA in the intercalation mode. However, when the linker length was extended to C₆, the mode of DNA binding changed to minor groove binding. When the linker was extended further to C₁₀, the interaction between dyes and DNA changed to major groove binding. The explanation is that the longer substituent increased hydrophobicity, that is not suitable for the dye molecule to intercalate to DNA base pairs, since the hydrophobic part would be exposed to the water molecules in polar environment. On the other hand, the groove binding mode would provide the hydrophobic environment that can accommodate the hydrophobic substituent better.

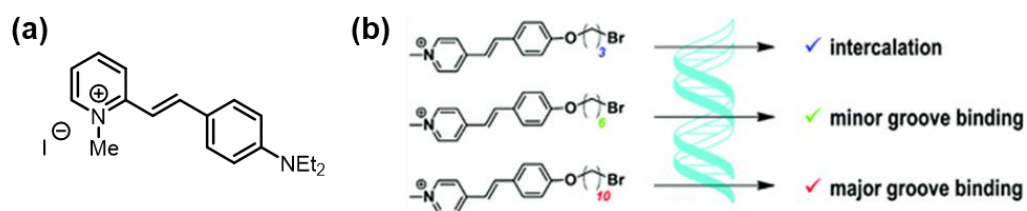


Figure 1.10 2-[4-(Dimethylamino)styryl]-1-methylpyridinium iodide (DASPMI) (a), Binding interaction of dyes with different linker lengths towards DNA in Berdnikova work.⁸⁴ (b) (Used with permission of Royal Society of Chemistry, from Governing the DNA-binding mode of styryl dyes by the length of their alkyl substituents - from intercalation to major groove binding, Daria V. Berdnikova, Nikolai I. Sosnin, Olga A. Fedorova, Heiko Ihmels, *Org. Biomol. Chem.* **2018**, *16*, 545-554.; permission conveyed through Copyright Clearance Center, Inc.)

In a recent study of the pyridinium-based styryl dye-DNA interaction, three distinct dimeric styryl pyridinium dyes with OMe or/and NMe₂ substituents on the phenyl moiety were synthesized and their interaction with calf thymus DNA (ct-DNA) was explored by Ustimova in 2021.⁸⁵ The dyes containing the NMe₂ group showed a greater fluorescence enhancement when bound to DNA. At high dye concentrations, the molecules interact with ct-DNA by forming aggregates in the minor groove. The bis(styryl) dye with an OMe substituent forms right-handed chiral helical dye aggregate, whereas the dye with an NMe₂ group forms left-handed chiral aggregates in the minor groove of DNA as shown by CD spectroscopy.

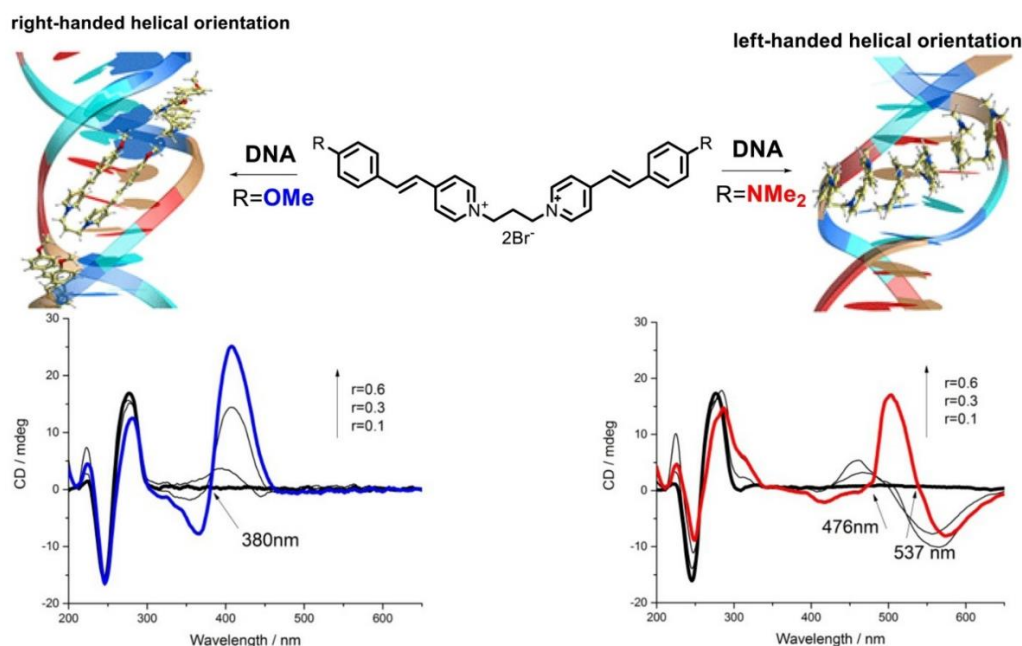


Figure 1.11 Bis(styryl)pyridinium dyes with OMe or/and NMe₂ substituents helical aggregations formed by ctDNA.⁸⁵ (Reprinted from *Journal of Photochemistry and Photobiology A: Chemistry*, Volume 418, Maria A. Ustimova, Yury V. Fedorov, Vladimir B. Tsvetkov, Sergey D. Tokarev, Nikolai A. Shepel, Olga A. Fedorova, Helical aggregates of bis(styryl) dyes formed by DNA templating, *J. Photochem. Photobiol. A: Chem.* **2021**, 418, 113378., Copyright (2021), with permission from Elsevier.)

In 2003 Chang et al.⁸⁶ developed a combinatorial synthesis of quinolinium-based styryl dyes and cell-based screening approach to identify novel structural motifs for DNA sensor. From the screening of a 855-member styryl dyes library, several molecules with desirable optical properties were selected for further studies. Eventually, one of them was identified as a cell permeable nuclear staining dye useful for live cell imaging which showed 13 times fluorescence increase in the presence of DNA. In a subsequent work in 2006, the same group also reported RNA-selective dyes with live cell imaging properties for studying nuclear structure and function.⁶⁹ Screening of 88 styryl dyes was first carried out to select dyes with good nucleolar targeting ability, high fluorescence intensity, low photobleaching, and the

smallest effect on cell survival. The study had identified three novel styryl dyes that could be employed to stain live cells (HeLa, A549, 3T3 and 3T3-L1 cells) providing 5.5-55 times of fluorescence increase in the presence of RNA.

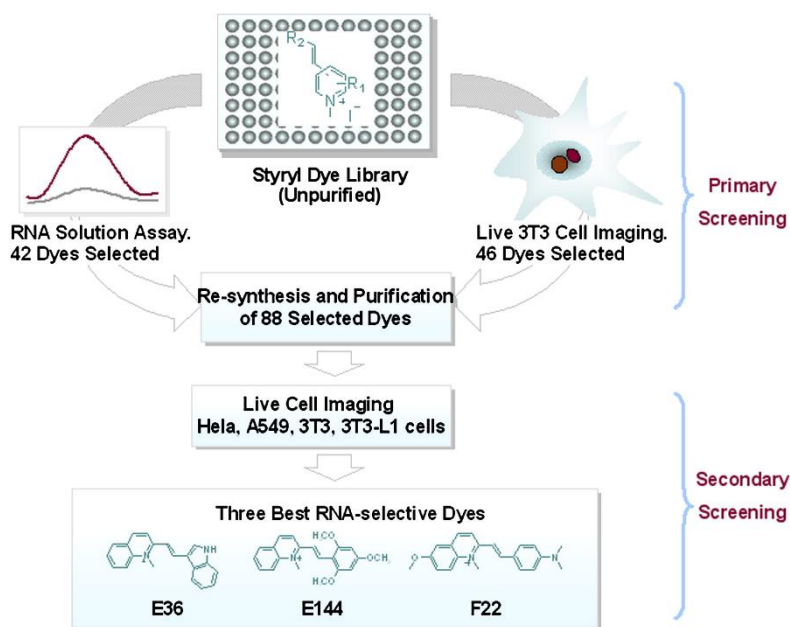


Figure 1.12 The screening strategy used in Chang's Study ⁶⁹ (Reprinted from Chemistry & Biology, 13, Qian Li, Yunkyung Kim, Joshua Namm, Amita Kulkarni, Gus R. Rosania, Young-Hoon Ahn, Young-Tae Chang, RNA-Selective, Live Cell Imaging Probes for Studying Nuclear Structure and Function, 615-623, Copyright (2006), with permission from Elsevier.)

During the last few decades, many designs of styryl dyes have been continued emerging with the objective to find styryl dyes with desirable optical characteristics that are suitable for nucleic acids detection such as tunable color, high responsiveness, and photostability. For example, in 2013, Bohländer et al.⁷⁰ demonstrated that the photostability of indole–quinolinium type (CyIQ) styryl dyes could be greatly improved while maintaining or even improving their excellent optical properties, such as brilliant fluorescence in the presence of DNA. The attachment of the vinylene bridge to the 4-position of the quinolinium part increases

both optical properties and photostabilities of the resulting dyes. Furthermore, methylation of the indole nitrogen and/or the addition of a methoxy group to the quinolinium portion results in fluorophores that are remarkably photostable.

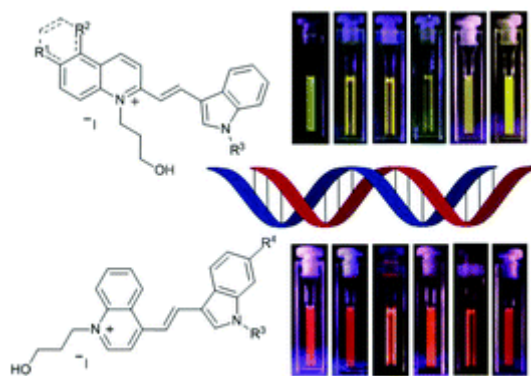


Figure 1.13 Indole–quinolinium type styryl dyes developed by Bohländer et al.⁷⁰ (Used with permission of Royal Society of Chemistry, from Synthesis and evaluation of cyanine-styryl dyes with enhanced photostability for fluorescent DNA staining, Bohländer, Peggy R.; Wagenknecht, Hans-Achim, *Org. Biomol. Chem.* **2013**, *11*, 7458-7462.; permission conveyed through Copyright Clearance Center, Inc.)

Another example is the quinolinium-based styryl dyes for selective sensing of G-quadruplex DNAs published by Wang in 2018.⁷¹ The appropriate styrene-like side group connected to the *N*-methylquinolinium framework was found to play an important role in determining the target selectivity. The results showed that incorporation of a flexible side group (*N*-methylpiperazinylphenyl) resulted in a styryl dye which gave highly selective fluorescence response to G-quadruplex over duplex DNAs down to the nanomolar range. The dye was shown to selectively stabilize the parallel G-quadruplex structure according to CD studies. Additionally, docking investigations revealed that the dye molecule interacts with G-quadruplex structures mostly through the groove binding mode. These discoveries could be useful in the development of a highly specific G-quadruplex probe and provide important

structural information that could lead to different specificity of dye binding to various types of nucleic acids.

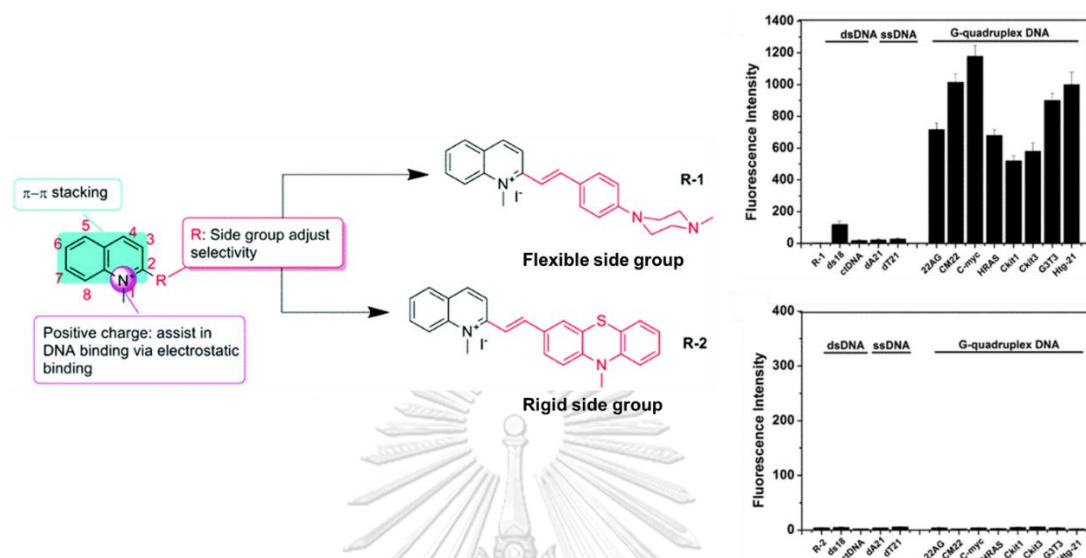


Figure 1.14 Molecular structures of quinolinium-based styryl dyes with flexible/rigid side group in Wang work and their fluorescence intensity with various DNA oligomers.⁷¹ (Used with permission of Royal Society of Chemistry, from Synthesis of quinolinium-based probes and studies of their effects for selective G-quadruplex DNA targeting, Wang, Ming-Qi; Liu, Xiao-Ning; Guo, Zhong-Jian; Feng, Chunlai; Rui, Mengjie, *New J. Chem.* **2018**, 42, 4933-4939.; permission conveyed through Copyright Clearance Center, Inc.)

Saad et al.⁶⁵ also developed the quinolinium-based styryl dye which specifically stained nucleoli and cytoplasm with no sign of toxicity in 2020. It was also reported that the developed dye showed higher affinity of for rRNA, comparing with nuclear dsDNA. The explanation was investigated that the dye bound to secondary structures of rRNA that are possibly double stranded. However, for nuclear dsDNA, the histones forming the nucleosomes on cellular DNA cause hindered for dye binding, and thus result in lower fluorescent response.

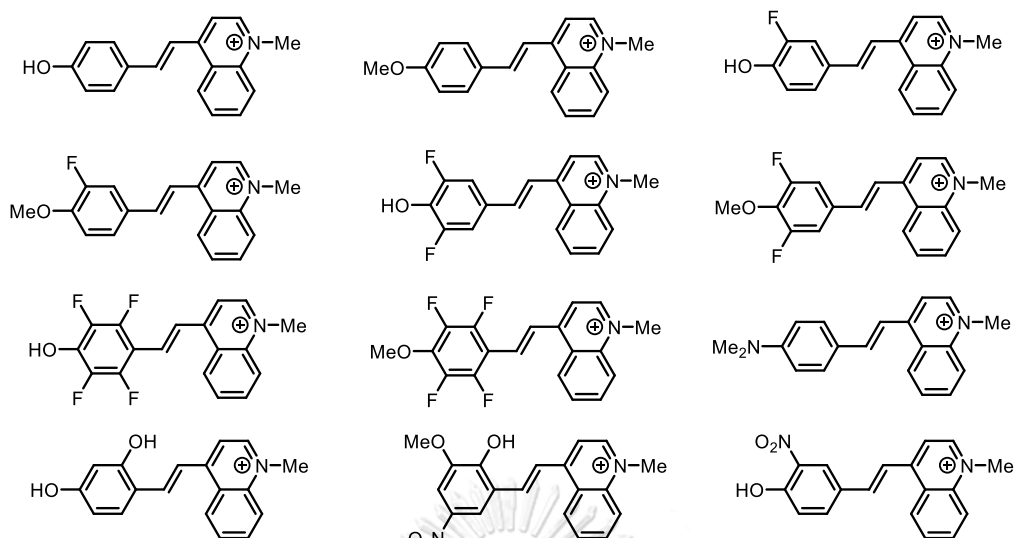


Figure 1.15 Styryl-quinolinium derivatives synthesized and evaluated in Saady study.⁶⁵

In addition to pyridinium- and quinolinium-based styryl dyes exemplified above, benzothiazole is another extensively used heterocyclic part. In 2004, Xu and co-workers developed a benzothiazolium-based styryl dye as a probe for the fluorescent-based determination of non-specific nucleic acids including calf thymus DNA (CT DNA) and fish sperm DNA (FS DNA).⁴⁴ It was proposed that fluorescence enhancement of the dye towards DNA was caused by the binding of a single styryl molecule in the minor groove of DNA or the self-assembling of the styryl dye *J*-aggregate in the presence of a double-helical DNA template. The limits of detection were 5 and 7 ng mL⁻¹ for CT DNA and FS DNA, respectively. However, the detection was non-specific and any types of DNA would give similar responses.

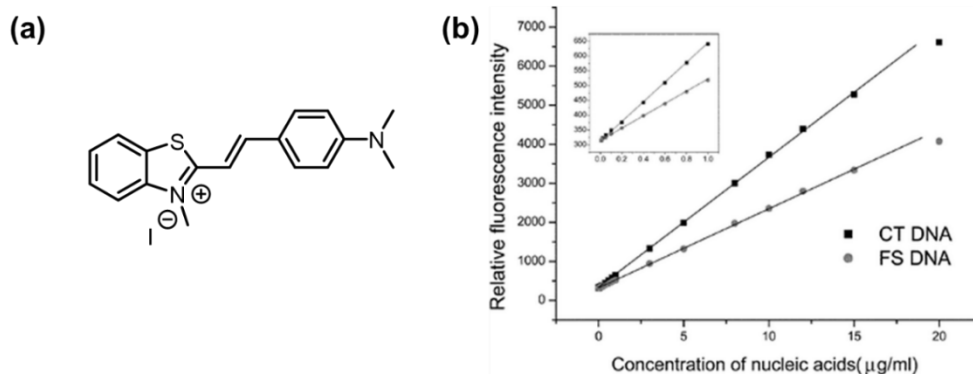


Figure 1.16 Chemical structure of the styryl dye used (a), Fluorescence intensity of the styryl–DNA system vs. DNA concentration in Xu’s work.⁴⁴ (b) (Used with permission of Royal Society of Chemistry, from Fluorescence enhancement method for the determination of nucleic acids using cationic cyanine as a fluorescence probe, Zhu, Chang-Qing; Zhuo, Shu-Juan; Zheng, Hong; Chen, Jin-Long; Li, Dong-Hui; Li, Shun-Hua; Xu, Jin-Gou, *Analyst* **2004**, *129*, 254-258.; permission conveyed through Copyright Clearance Center, Inc.)

From 2005 to 2008, Yarmoluk’s group developed a series of monomeric and homodimeric styryl dyes based on the (*p*-dimethylaminostyryl)pyridinium,^{77, 87} benzothiazolium,^{77, 79, 88} benzoxazolium⁷⁷ and indolium⁷⁷ cores. For benzothiazolium-based styryl dyes, charged spermine-like linkage/tail groups were incorporated into the monomeric and homodimeric styryl dyes in Tokar work.⁷⁹ The use of spermine-like linkage/tail groups for the dye design increases fluorescence intensity in the presence of DNA when compared to the dyes with non-modified charged groups. The styryl dyes were proposed as effective fluorescent probes for DNA detection and imaging under both single-photon excitation (SPE) and two-photon excitation (TPE). The mechanistic studies of the DNA binding of the benzothiazolium-based monomer and homodimer styryl dyes were also reported by the same group in the year 2008.⁸⁸ According to the study, the binding constant (K_b) and the number of dsDNA base pairs occupied by one bound dye molecule (n) of

each dye were determined by modified McGhee and von Hippel equation. The presence of spermine-like linkage/tail group was found to increase the dye-DNA binding constants. Both groove-binding and intercalation mechanisms are supported by the binding constants, the study of dyes sensitivity for AT- and GC-sequences of DNA, and the values of dsDNA base pairs occupied by one bound dye molecule. For monomer (Sbt and Bos-5) and homodimer DBos-13 having linkage group bound to nitrogen atoms of benzothiazole ring, the results suggested the intercalative binding mode, whereas homodimer DBsu-10 with the linkage group bound in 6-positions of benzothiazole heterocycle was considered to bind to DNA via the groove-binding mechanism.

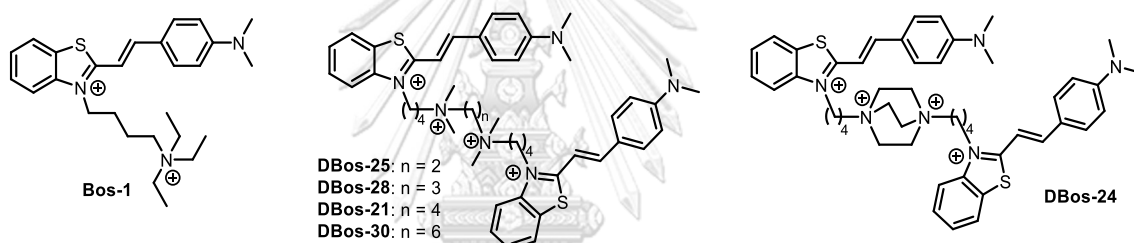


Figure 1.17 Monomer and homodimer styryl dyes based on (*p*-dimethylaminostyryl) benzothiazolium moiety containing charged spermine-like linkage/tail groups in Tokar's work⁷⁹

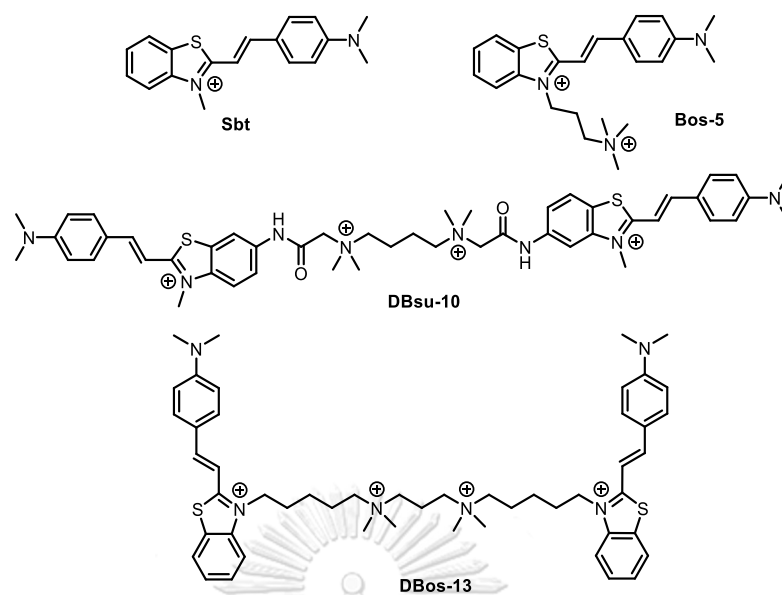


Figure 1.18 Monomer and homodimer styryl dyes based on (*p*-dimethylaminostyryl) benzothiazolium moiety in Akbay's work⁸⁸

Application of similar benzothiazolium-based styryl dye for localization of cellular nucleic acids have also been recently demonstrated. In 2018, Wang et al.⁷¹ reported two benzothiazolium-based styryl dyes to visualize nucleoli and chromosomes during the cell cycles with real time manner. Based on molecular simulation studies, the dye molecule was proposed to bind to dsDNA at hydrophobic minor grooves which was further stabilized by hydrogen bonding between nucleobases. On the other hand, the simulation indicated that the dye might bind to RNA at hydrophobic major grooves by π -cation interaction and hydrogen bonding.

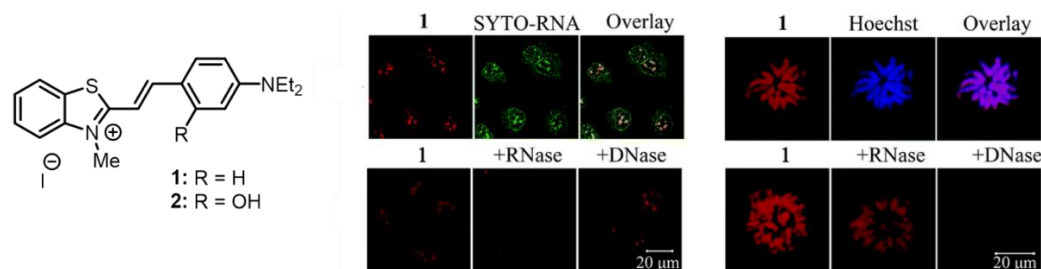


Figure 1.19 Nucleolus and chromosome imaging and digest experiments by RNase and DNase according to Wang.⁷¹ (Used with permission of Royal Society of Chemistry (Great Britain), from Red fluorescent probes for real-time imaging of the cell cycle by dynamic monitoring of the nucleolus and chromosome, Cao, Qian; Chao, Xi-Juan; He, Liang; Liu, Bing; Mao, Zong-Wan; Tan, Cai-Ping; Wang, Kang-Nan; Zhang, Chen; Zheng, Xiao-Hui; Zhou, Dan-Jie, *Chem. Commun.* **2018**, *54*, 2635-2638.; permission conveyed through Copyright Clearance Center, Inc.)

In all aforementioned examples, the styryl dyes could at best only distinguish between various DNA/RNA structures at global levels, i.e. DNA from RNA, dsDNA from G4 DNA, etc. To enable sequence-specific detection of nucleic acid, a combination with another selective probe is required. In 2019, Ditmangklo and co-workers successfully developed novel “clickable” alkyne-modified styryl dyes that can be conjugated onto the conformationally rigid pyrrolidiny PNA by click chemistry.⁷⁴ The fluorescence of the alkyne-modified styryl dye was low in the free state but increased dramatically (up to 125-fold) in the presence of DNA in a non-selective fashion. Unexpectedly, the styryl-dye-labeled acpcPNA probes gave only low fluorescence response to complementary DNA target. Nevertheless, they produced significantly increased fluorescence when hybridized to a mutated DNA containing base mismatch, abasic site, and most notably, base insertion. Based on spectroscopic investigations and modeling, it was proposed that the defect in the PNA-DNA duplex

structure provides a binding site that can accommodate the styryl dye positioned nearby, resulting in the observed fluorescence enhancement.

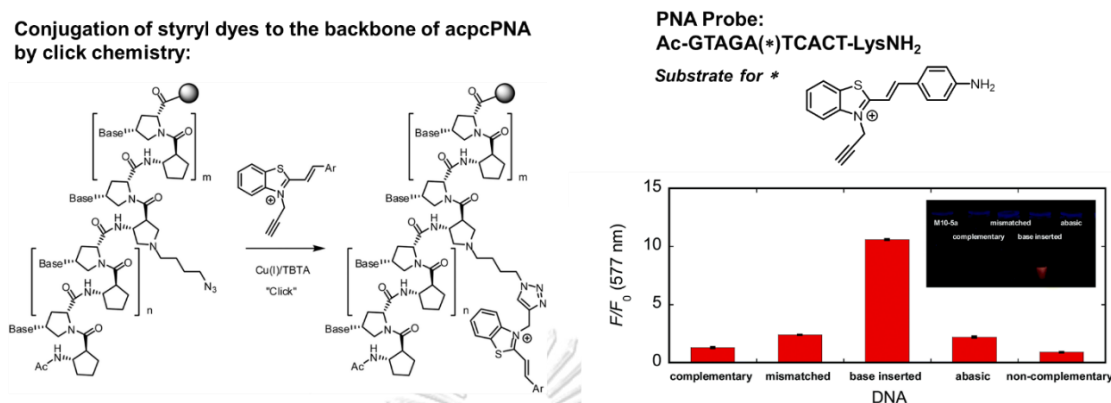


Figure 1.20 Clickable styryl dyes for fluorescence labeling of pyrrolidiny PNA probes for the detection of base mutations in DNA.⁷⁴ (Used with permission of Royal Society of Chemistry, from Clickable styryl dyes for fluorescence labeling of pyrrolidiny PNA probes for the detection of base mutations in DNA, Ditmangklo, Boonsong; Taechalertpaisarn, Jaru; Siriwong, Khatcharin; Vilaivan, Tirayut, *Org. Biomol. Chem.* **2019**, *17*, 9712-9725.; permission conveyed through Copyright Clearance Center, Inc.)

1.4 Rationale and objective of this work

In this work, novel dicationic styryl dyes were designed by incorporation of additional positively charged sidechain with the aim to improve the binding strength with target nucleic acids through the electrostatic interaction with the negatively charged phosphate backbone (Figure 1.22). The optical properties of novel styryl dyes will be examined in the presence and absence of nucleic acid targets in order to develop new dyes that can change fluorescence or color in response to different sequence of nucleic acid targets, especially for DNA. Furthermore, dye-nucleic acid binding interaction and optical properties were investigated to acquire a better understanding of the structural-properties relationship by both experimental and theoretical approaches. The enhanced performances of the dicationic dyes as

staining agents for cellular imaging and for the aptamer-based detection of mercury(II) ion were also demonstrated.

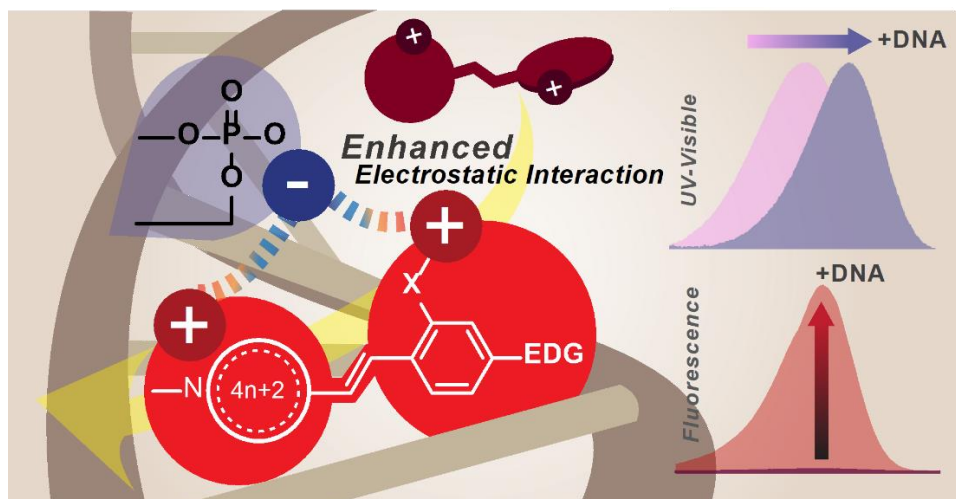
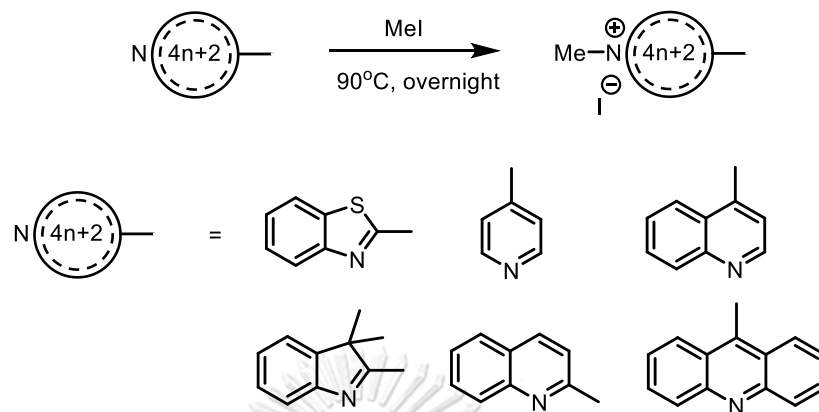


Figure 1.21 The concept of this work



2.2 Synthesis and characterization of novel cationic styryl dyes

2.2.1 N-Methylation of the methyl-substituted nitrogen heterocycles



The mixture of the methyl-substituted nitrogen heterocycle (5 mmol) and iodomethane (10 mmol) were heated overnight at 90°C. The obtained precipitate (57 – 100 %yield) was washed with diethyl ether and then dried under vacuum.

1,4-Dimethylpyridin-1-ium iodide

1.260 g (100 %yield), ¹H NMR (500 MHz, DMSO-*d*₆) δ (ppm): 8.83 (d *J* = 6.6 Hz, 2H), 7.96 (d *J* = 6.4 Hz, 2H), 4.28 (s, 3H), 2.60 (s, 3H).

1,4-Dimethylquinolin-1-ium iodide

1.3686 g (96 %yield), ¹H NMR (500 MHz, DMSO-*d*₆) δ (ppm): 9.35 (d *J* = 6.0 Hz, 1H), 8.54 (d *J* = 7.8 Hz, 1H), 8.49 (d *J* = 8.9 Hz, 1H), 8.27 (t *J* = 8.4 Hz, 1H), 8.06 (dd *J* = 13.0, 6.5 Hz, 2H), 4.58 (s, 3H), 3.01 (s, 3H).

2,3-Dimethylbenzo[*d*]thiazol-3-ium iodide

1.3684 g (94 %yield), ¹H NMR (500 MHz, DMSO-*d*₆) δ (ppm): 8.43 (d *J* = 8.1 Hz, 1H), 8.29 (d *J* = 8.5 Hz, 1H), 7.90 (t *J* = 7.9 Hz, 1H), 7.80 (t *J* = 7.7 Hz, 1H), 4.20 (s, 3H), 3.17 (s, 3H).

1,2-Dimethylquinolin-1-ium iodide

1.4292 g (100 %yield), ^1H NMR (500 MHz, $\text{DMSO-}d_6$) δ (ppm): 9.11 (d J = 8.5 Hz, 1H), 8.60 (d J = 9.0 Hz, 1H), 8.41 (d J = 8.0 Hz, 1H), 8.23 (t J = 7.9 Hz, 1H), 8.13 (d J = 8.5 Hz, 1H), 7.99 (t J = 7.5 Hz, 1H), 4.45 (s, 3H), 3.09 (s, 3H).

1,2,3,3-Tetramethyl-3H-indol-1-ium iodide

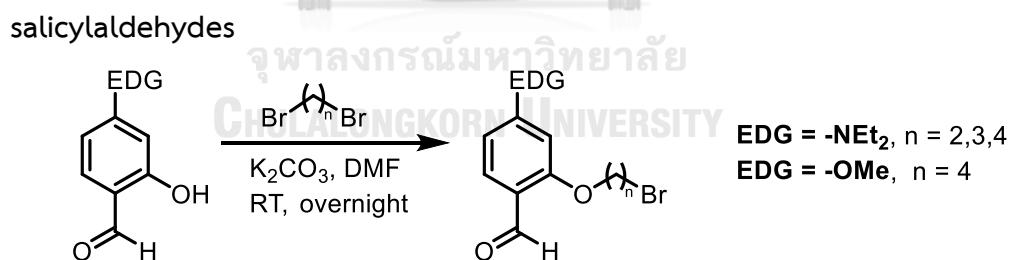
1.4983 g (100 %yield), ^1H NMR (500 MHz, $\text{DMSO-}d_6$) δ (ppm): 7.92 (d J = 8.4 Hz, 1H), 7.83 (d J = 7.7 Hz, 1H), 7.65 – 7.58 (m, 2H), 3.98 (s, 3H), 2.78 (s, 3H), 1.53 (s, 6H).

9,10-Dimethylacridin-10-ium iodide

0.9503 g (57 %yield), ^1H NMR (500 MHz, $\text{DMSO-}d_6$) δ (ppm): 8.92 (d J = 8.5 Hz, 2H), 8.82 – 8.71 (m, 2H), 8.43 (t J = 6.6 Hz, 2H), 8.07 – 7.98 (m, 2H), 4.81 (s, 3H), 3.45 (s, 3H).

2.2.2 Sidechain modification of the aromatic aldehyde to introduce additional positive charge to the molecule

2.2.2.1 Bromoalkylation of the hydroxyl group of substituted salicylaldehydes



The salicylaldehyde substrate bearing a diethylamino or a methoxy as electron donating substituent (2.5 mmol) was dissolved in DMF (2 mL). The solution was stirred at room temperature, followed by addition of anhydrous K_2CO_3 (3 mmol). Then, the dibromoalkane (12.5 mmol) was added to the stirred mixture. The reaction was stirred overnight at room temperature and partitioned in water-dichloromethane followed by washing with water to remove DMF. The organic layer was combined

and the solvent was removed under reduced pressure. The crude product was purified by column chromatography [hexanes:EtOAc (4:1)] to afford the benzaldehyde with bromoalkoxy side chain as brown oil (18 – 84 %yield).

2-(2-Bromoethoxy)-4-(diethylamino)benzaldehyde

0.1651 g (22 %yield), ^1H NMR (500 MHz, CDCl_3) δ (ppm): 10.21 (s, 1H), 7.74 (d J = 8.9 Hz, 1H), 6.36 (d J = 8.3 Hz, 1H), 6.09 (s, 1H), 4.38 (t J = 6.1 Hz, 2H), 3.69 (t J = 6.1 Hz, 2H), 3.42 (q J = 7.1 Hz, 4H), 1.22 (t J = 6.9 Hz, 6H).

2-(3-Bromopropoxy)-4-(diethylamino)benzaldehyde

0.1414 g (18 %yield), ^1H NMR (500 MHz, CDCl_3) δ (ppm): 10.17 (s, 1H), 7.74 (d J = 8.9 Hz, 1H), 6.37 (d J = 6.0 Hz, 1H), 6.21 (s, 1H), 4.21 (t J = 5.7 Hz, 2H), 3.63 (t J = 6.3 Hz, 2H), 3.43 (q J = 7.1 Hz, 4H), 2.38 (p J = 6.0 Hz, 2H), 1.23 (t J = 7.1 Hz, 6H).

2-(4-Bromobutoxy)-4-(diethylamino)benzaldehyde

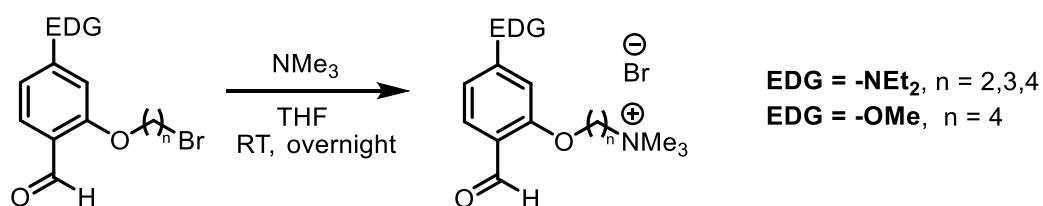
0.6893 g (84 %yield), ^1H NMR (500 MHz, CDCl_3) δ (ppm): 10.15 (s, 1H), 7.71 (d J = 8.9 Hz, 1H), 6.31 (d J = 5.3 Hz, 1H), 6.07 (s, 1H), 4.07 (t J = 5.9 Hz, 2H), 3.49 (t J = 6.4 Hz, 2H), 3.41 (q J = 7.1 Hz, 4H), 2.04 (tt J = 12.7, 7.0 Hz, 4H), 1.21 (t J = 7.1 Hz, 6H).

2-(4-Bromobutoxy)-4-methoxybenzaldehyde

0.5560 g (78 %yield), ^1H NMR (500 MHz, CDCl_3) δ (ppm): 10.32 (s, 1H), 7.81 (d J = 8.7 Hz, 1H), 6.55 (d J = 8.6 Hz, 1H), 6.43 (s, 1H), 4.09 (t J = 5.8 Hz, 2H), 3.87 (s, 3H), 3.50 (t J = 6.3 Hz, 2H), 2.06 (ddd J = 20.1, 14.0, 7.8 Hz, 4H).

2.2.2.2 Introduction of positive charge by quaternization with

trimethylamine



To introduce a positive charge to the obtained benzaldehyde with bromoalkoxy sidechain, the product from **2.2.2.1** was dissolved in THF (2 mL). Then, trimethylamine (2 mL) was added to the solution. The reaction mixture was stirred overnight at room temperature. The solvent was removed by rotary evaporator. The residue was washed with diethyl ether to eliminate nonpolar impurities and dried under vacuum to obtain the product as white precipitate (67 – 100 %yield)

2-(5-(Diethylamino)-2-formylphenoxy)-*N,N,N*-trimethylethan-1-aminium bromide

0.1323 g (67 %yield), ^1H NMR (500 MHz, $\text{DMSO-}d_6$) δ (ppm): 10.00 (s, 1H), 7.53 (d J = 8.9 Hz, 1H), 6.40 (d J = 8.9 Hz, 1H), 6.20 (s, 1H), 4.58 (s, 2H), 3.89 – 3.82 (m, 2H), 3.47 (q, J = 7.0 Hz, 4H), 3.21 (s, 9H), 1.14 (t J = 7.0 Hz, 6H).

3-(5-(Diethylamino)-2-formylphenoxy)-*N,N,N*-trimethylpropan-1-aminium bromide

0.1630 g (97 %yield), ^1H NMR (500 MHz, $\text{DMSO-}d_6$) δ (ppm): 10.07 (s, 1H), 7.52 (d J = 8.9 Hz, 1H), 6.37 (d J = 9.0 Hz, 1H), 6.14 (d J = 2.0 Hz, 1H), 4.18 (t J = 5.7 Hz, 2H), 3.59 – 3.51 (m, 2H), 3.45 (q J = 7.0 Hz, 4H), 3.13 (s, 9H), 2.23 (td J = 11.4, 5.6 Hz, 2H), 1.13 (t J = 7.0 Hz, 6H).

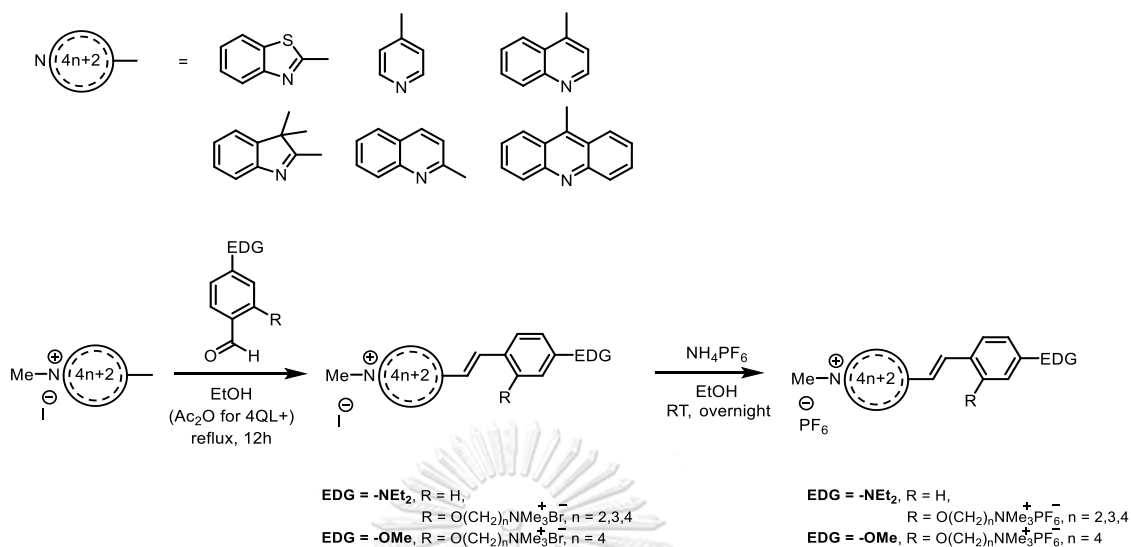
4-(5-(Diethylamino)-2-formylphenoxy)-*N,N,N*-trimethylbutan-1-aminium bromide

0.7403 g (91 %yield), ^1H NMR (500 MHz, $\text{DMSO-}d_6$) δ (ppm): 10.03 (s, 1H), 7.51 (d J = 8.9 Hz, 1H), 6.35 (d J = 8.9 Hz, 1H), 6.14 (s, 1H), 4.14 (t J = 5.8 Hz, 2H), 3.44 (dd J = 14.2, 7.1 Hz, 6H), 3.07 (s, 9H), 1.95 – 1.84 (m, 2H), 1.83 – 1.74 (m, 2H), 1.12 (t J = 7.0 Hz, 6H).

4-(2-Formyl-5-methoxyphenoxy)-*N,N,N*-trimethylbutan-1-aminium bromide

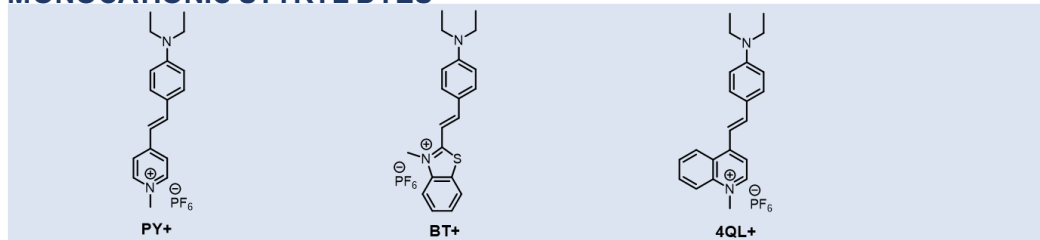
0.6752 g (100 %yield), ^1H NMR (500 MHz, $\text{DMSO-}d_6$) δ (ppm): 10.23 (s, 1H), 7.68 (d J = 8.4 Hz, 1H), 6.69 (s, 2H), 4.17 (s, 2H), 3.86 (s, 3H), 3.45 – 3.36 (m, 2H), 3.06 (s, 9H), 1.96 – 1.85 (m, 2H), 1.81 (dd J = 11.7, 5.6 Hz, 2H).

2.2.3 Synthesis of cationic styryl dyes by Aldol-type condensation



The Aldol-type condensation between the *N*-methylated heterocyclic compound bearing an acidic methyl group (0.5 mmol) and an aromatic aldehyde (0.5 mmol) was carried out in refluxing ethanol (2 mL) without any added catalyst for 8-12 hours. For **4QL+**, the reaction was performed in acetic anhydride (2 mL, 20 mmol) to allow acid catalyzed pathway. The counterion was replaced with PF₆⁻ by the treatment of the bromide or iodide salts with ammonium hexafluorophosphate (1 mmol) in ethanol (2 mL). The products were generally obtained as dark-colored crystalline solid in 11 – 78 %yield. The dyes **PY+**,⁸⁹ **BT+**,⁷¹ and **BT2+(NEt₂)**⁹⁰ have been previously reported in the literature, but the rest are new compounds. It should be noted that the dye **4QL+** is unknown, but the analogue with dimethylamino substituent in place of diethylamino in **4QL+** has been recently reported.⁶⁵

MONOCATIONIC STYRYL DYES



DICATIONIC STYRYL DYES

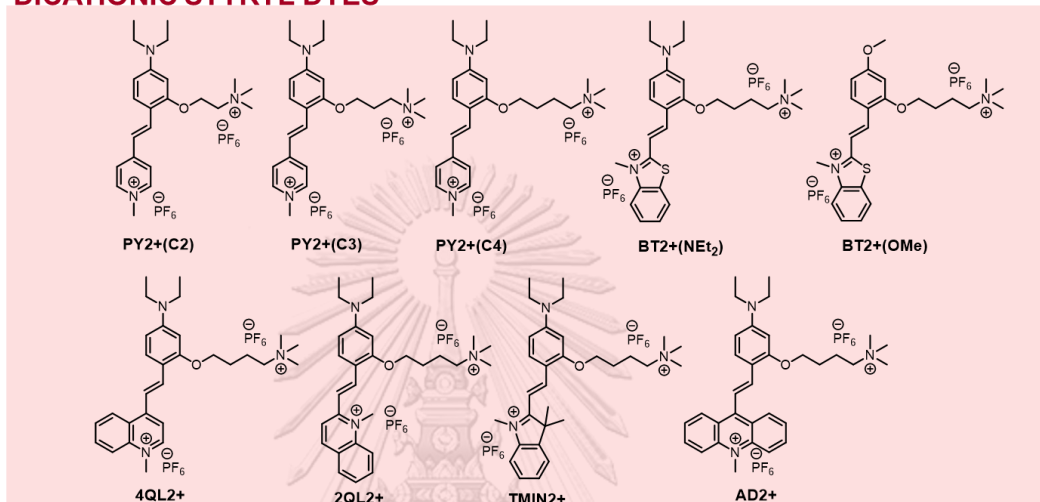


Figure 2.1 Cationic styryl dye structures with shorten names used in this work

(*E*)-4-(4-(Diethylamino)styryl)-1-methylpyridin-1-ium hexafluorophosphate (PY+)

87 mg (55 %yield); ^1H NMR (500 MHz, $\text{DMSO-}d_6$) δ 8.64 (d J = 6.9 Hz, 2H), 8.01 (d J = 6.9 Hz, 2H), 7.87 (d J = 16.1 Hz, 1H), 7.56 (d J = 9.0 Hz, 1H), 7.10 (d J = 16.1 Hz, 1H), 6.74 (d J = 9.0 Hz, 1H), 4.15 (s, 3H), 3.40 – 3.44 (m, 4H), 1.12 (t, J = 7.0 Hz, 6H); ^{13}C NMR (126 MHz, $\text{DMSO-}d_6$) δ 153.5, 149.5, 144.3, 142.0, 130.6, 122.0, 121.7, 116.5, 111.4, 46.3, 43.9, 12.6.; HRMS (MALDI-TOF): m/z calcd for $\text{C}_{18}\text{H}_{23}\text{N}_2^+$: 267.1856 $[M]^+$ found: 267.1851.

(*E*)-4-(4-(Diethylamino)-2-(2-(trimethylammonio)ethoxy)styryl)-1-methylpyridin-1-ium hexafluorophosphate (PY2+(C2))

260 mg (79 %yield); ^1H NMR (500 MHz, $\text{DMSO-}d_6$) δ 8.61 (d J = 4.9 Hz, 2H), 7.96 (m, 3H), 7.62 (d J = 8.5 Hz, 1H), 7.12 (d J = 16.0 Hz, 1H), 6.44 (d J = 8.1 Hz, 1H), 6.25 (s,

1H), 4.58 (t, 2H), 4.16 (s, 3H), 3.93 (t, 2H), 3.45 (m, 4H), 3.22 (s, 9H), 1.15 (t, 6H); ¹³C NMR (126 MHz, DMSO-*d*₆) δ 158.5, 153.7, 151.2, 144.2, 136.1, 130.2, 121.8, 116.5, 110.8, 105.4, 94.6, 64.4, 61.8, 53.2, 46.3, 44.1, 12.7.; HRMS (MALDI-TOF): *m/z* calcd for C₂₃H₃₄N₃O⁺: 368.2701 [*M-H*]⁺ found: 368.2725.

(E)-4-(4-(Diethylamino)-2-(3-(trimethylammonio)propoxy)styryl)-1-methylpyridin-1-ium hexafluorophosphate (PY2+(C3))

260 mg (78 %yield); ¹H NMR (500 MHz, DMSO-*d*₆) δ 8.60 (d *J* = 6.9 Hz, 2H), 7.96 (m, 3H), 7.58 (d *J* = 9.0 Hz, 1H), 7.13 (d *J* = 16.1 Hz, 1H), 6.42 (dd *J* = 9.0, 2.2 Hz, 1H), 6.21 (s, 1H), 4.20 – 4.12 (m, 5H), 3.58 – 3.52 (m, 2H), 3.46 (q, 4H), 3.14 (s, 9H), 2.32 (dd *J* = 10.5, 5.7 Hz, 2H), 1.14 (t, *J* = 7.0 Hz, 6H); ¹³C NMR (126 MHz, DMSO-*d*₆) δ 159.4, 153.8, 151.2, 144.1, 136.9, 130.8, 121.8, 116.6, 111.1, 105.2, 94.6, 65.2, 63.1, 52.4, 46.2, 44.1, 22.6, 12.6.; HRMS (MALDI-TOF): *m/z* calcd for C₂₄H₃₆N₃O⁺: 382.2858 [*M-H*]⁺ found: 382.2897.

(E)-4-(4-(Diethylamino)-2-(4-(trimethylammonio)butoxy)styryl)-1-methylpyridin-1-ium hexafluorophosphate (PY2+(C4))

344 mg (100 %yield); ¹H NMR (500 MHz, DMSO-*d*₆) δ 8.60 (d *J* = 5.9 Hz, 2H), 7.97 (m, 3H), 7.57 (d *J* = 8.0 Hz, 1H), 7.16 (d *J* = 16.0 Hz, 1H), 6.40 (d *J* = 8.9 Hz, 1H), 6.21 (s, 1H), 4.16 (m, 5H), 3.54 – 3.43 (m, 6H), 3.09 (s, 9H), 1.89 (d *J* = 6.9 Hz, 4H), 1.13 (t, *J* = 6.6 Hz, 3H); ¹³C NMR (126 MHz, DMSO-*d*₆) δ 159.7, 153.8, 151.2, 144.1, 137.1, 131.2, 121.7, 116.5, 111.2, 105.0, 94.5, 67.1, 65.1, 52.2, 46.2, 44.1, 25.6, 19.5, 12.6.; HRMS (MALDI-TOF): *m/z* calcd for C₂₅H₃₈N₃O⁺: 396.3015 [*M-H*]⁺ found: 396.3040.

(E)-2-(4-(Diethylamino)styryl)-3-methylbenzo[d]thiazol-3-ium hexafluorophosphate (BT+)

194 mg (83 %yield); ¹H NMR (500 MHz, DMSO-*d*₆) δ 8.27 (d *J* = 8.9 Hz, 1H), 8.05 (d *J* = 8.4 Hz, 1H), 8.01 (d *J* = 15.2 Hz, 1H), 7.86 (d *J* = 8.9 Hz, 2H), 7.76 (t, 1H), 7.67 (t, 1H), 7.55 (d *J* = 15.2 Hz, 1H), 6.80 (d *J* = 9.1 Hz, 2H), 4.19 (s, 3H), 3.53 – 3.46 (m, 4H), 1.15

(t, $J = 7.1$ Hz, 3H); ^{13}C NMR (126 MHz, DMSO- d_6) δ 171.2, 151.5, 150.1, 142.0, 133.3, 128.9, 127.4, 126.7, 123.8, 121.1, 115.9, 111.6, 105.6, 44.3, 35.5, 12.6.; HRMS (MALDI-TOF): m/z calcd for $\text{C}_{20}\text{H}_{23}\text{N}_2\text{S}^+$: 323.1576 $[M]^+$ found: 323.1575.

(E)-2-(4-(Diethylamino)-2-(4-(trimethylammonio)butoxy)styryl)-3-methylbenzo[d]thiazol-3-ium hexafluorophosphate (BT2+(NEt₂))

234 mg (63 %yield); ^1H NMR (500 MHz, DMSO- d_6) δ 8.18 (d $J = 7.9$ Hz, 1H), 8.12 (d $J = 15.1$ Hz, 1H), 8.03 (d $J = 8.3$ Hz, 1H), 7.90 (d $J = 9.1$ Hz, 1H), 7.75 (t $J = 7.7$ Hz, 1H), 7.64 (t $J = 7.6$ Hz, 1H), 7.50 (d $J = 15.2$ Hz, 1H), 6.54 (d $J = 8.9$ Hz, 1H), 6.21 (s, 1H), 4.21 (t, 2H), 4.12 (s, 3H), 3.64 – 3.47 (m, 6H), 3.09 (s, 9H), 1.92 (q, 4H), 1.18 (t, $J = 6.9$ Hz, 6H); ^{13}C NMR (126 MHz, DMSO- d_6) δ 171.1, 161.3, 153.8, 146.3, 144.2, 142.0, 128.8, 127.2, 126.2, 123.6, 115.6, 111.0, 106.3, 104.4, 93.9, 67.3, 65.1, 52.3, 44.5, 35.1, 25.6, 19.2, 12.7.; HRMS (MALDI-TOF): m/z calcd for $\text{C}_{27}\text{H}_{38}\text{N}_3\text{OS}^+$: 452.2735 $[M-H]^+$ found: 452.2774.

(E)-2-(4-Methoxy-2-(4-(trimethylammonio)butoxy)styryl)-3-methylbenzo[d]thiazol-3-ium hexafluorophosphate (BT2+(OMe))

204 mg (58 %yield); ^1H NMR (500 MHz, DMSO- d_6) δ 8.33 (d $J = 8.0$ Hz, 1H), 8.21 (m, 2H), 8.10 (d $J = 8.8$ Hz, 1H), 7.86 (m, 2H), 7.77 (t $J = 7.7$ Hz, 1H), 6.78 (dd $J = 8.8, 2.2$ Hz, 1H), 6.73 (d $J = 2.2$ Hz, 1H), 4.27 (s, 3H), 4.23 (t $J = 5.4$ Hz, 2H), 3.90 (s, 3H), 3.42 – 3.39 (m, 2H), 3.09 (s, 9H), 1.92 (q, 4H); ^{13}C NMR (126 MHz, DMSO- d_6) δ 172.4, 165.2, 160.1, 143.3, 142.1, 132.2, 129.4, 128.2, 127.3, 124.0, 116.7, 115.6, 110.7, 107.6, 99.2, 67.8, 65.0, 56.0, 52.3, 36.0, 25.5, 19.1.; HRMS (MALDI-TOF): m/z calcd for $\text{C}_{24}\text{H}_{31}\text{N}_2\text{O}_2\text{S}^+$: 411.2106 $[M-H]^+$ found: 411.2129.

(E)-4-(4-(Diethylamino)styryl)-1-methylquinolin-1-ium hexafluorophosphate (4QL+)

125 mg (54 %yield); ^1H NMR (500 MHz, DMSO- d_6) δ 9.05 (d $J = 6.5$ Hz, 1H), 8.99 (d $J = 8.5$ Hz, 1H), 8.30 (m, 2H), 8.23 – 8.09 (m, 2H), 7.94 (m, 2H), 7.83 (d $J = 8.5$ Hz, 2H), 6.78

(d J = 8.6 Hz, 2H), 4.41 (s, 3H), 3.44 (m, 4H), 1.15 (t J = 6.8 Hz, 6H); ^{13}C NMR (126 MHz, DMSO- d_6) δ 153.2, 150.1, 146.7, 144.8, 138.8, 134.6, 131.9, 128.6, 126.3, 125.7, 122.5, 119.1, 113.7, 112.5, 111.5, 44.1, 44.0, 12.6.; HRMS (MALDI-TOF): m/z calcd for $\text{C}_{22}\text{H}_{25}\text{N}_2^+$: 317.2012 $[M]^+$ found: 317.2015.

(E)-4-(4-(Diethylamino)-2-(4-(trimethylammonio)butoxy)styryl)-1-methylquinolin-1-ium hexafluorophosphate (4QL2+)

96 mg (26 %yield); ^1H NMR (500 MHz, DMSO- d_6) δ 8.93 (d J = 6.5 Hz, 1H), 8.84 (d, J = 8.5 Hz, 1H), 8.28 (m, 2H), 8.17 (m, 2H), 8.01 – 7.91 (m, 3H), 6.47 (d, J = 9.0 Hz, 1H), 6.24 (s, 1H), 4.40 (s, 3H), 4.21 (t, 2H), 3.54 – 3.47 (m, 6H), 3.07 (s, 9H), 1.93 (q, 4H), 1.17 (t J = 6.7 Hz, 3H); ^{13}C NMR (126 MHz, DMSO- d_6) δ 160.2, 153.4, 152.0, 146.3, 139.3, 138.9, 134.5, 131.7, 128.5, 125.9, 125.6, 119.1, 113.1, 112.1, 112.0, 105.4, 94.3, 67.2, 65.2, 52.3, 44.2, 43.9, 25.8, 19.4, 12.7.; HRMS (MALDI-TOF): m/z calcd for $\text{C}_{29}\text{H}_{40}\text{N}_3\text{O}^+$: 446.3171 $[M-H]^+$ found: 446.3202.

(E)-2-(4-(Diethylamino)-2-(4-(trimethylammonio)butoxy)styryl)-1-methylquinolin-1-ium hexafluorophosphate (2QL2+)

195 mg (54 %yield); ^1H NMR (500 MHz, DMSO- d_6) δ 8.67 (d J = 9.1 Hz, 1H), 8.37 (dd J = 16.8, 9.1 Hz, 2H), 8.27 (d J = 15.3 Hz, 1H), 8.20 (d J = 7.9 Hz, 1H), 8.05 (t J = 8.0 Hz, 1H), 7.81 (t J = 8.6 Hz, 2H), 7.54 (d J = 15.4 Hz, 1H), 6.49 (d J = 9.0 Hz, 1H), 6.24 (s, 1H), 4.34 (s, 3H), 4.22 (t J = 5.3 Hz, 2H), 3.51 (q J = 6.9 Hz, 6H), 3.09 (s, 9H), 1.93 (s, 4H), 1.17 (t J = 7.0 Hz, 6H). ^{13}C NMR (126 MHz, DMSO- d_6) δ 161.40, 157.02, 153.19, 144.45, 141.72, 139.78, 134.51, 133.90, 130.28, 128.19, 126.95, 120.30, 119.03, 112.21, 111.31, 106.03, 94.60, 67.77, 65.61, 52.74, 44.80, 39.01, 26.16, 19.89, 13.13.

(E)-2-(4-(Diethylamino)-2-(4-(trimethylammonio)butoxy)styryl)-1,3,3-trimethyl-3H-indol-1-ium hexafluorophosphate (TMIN2+)

343 mg (91 %yield); ^1H NMR (500 MHz, DMSO- d_6) δ 8.41 (d J = 15.4 Hz, 1H), 8.06 (d J = 8.9 Hz, 1H), 7.70 (d J = 7.3 Hz, 1H), 7.63 (d J = 8.0 Hz, 1H), 7.53 (t J = 8.2 Hz, 1H),

7.44 (t $J = 7.7$ Hz, 1H), 7.19 (d $J = 15.5$ Hz, 1H), 6.60 (d $J = 7.4$ Hz, 1H), 6.23 (s, 1H), 4.23 (s, 2H), 3.86 (s, 3H), 3.58 (q $J = 7.0$ Hz, 6H), 3.09 (s, 9H), 1.91 (s, 4H), 1.70 (s, 6H), 1.19 (t $J = 7.1$ Hz, 6H). ^{13}C NMR (126 MHz, DMSO- d_6) δ 179.04, 162.70, 155.47, 142.78, 142.32, 129.27, 127.36, 123.00, 113.49, 112.62, 107.54, 94.15, 67.92, 65.53, 52.73, 50.64, 45.25, 32.97, 27.65, 26.22, 19.80, 13.16.

(E)-9-(4-(Diethylamino)-2-(4-(trimethylammonio)butoxy)styryl)-10-methylacridin-10-ium hexafluorophosphate (AD2+)

170 mg (43 %yield); ^1H NMR (500 MHz, DMSO- d_6) δ 8.71 (d, $J = 8.4$ Hz), 8.39 (d, $J = 9.0$ Hz), 8.34 (d, $J = 15.0$ Hz), 8.22 – 8.17 (m), 8.14 (d, $J = 9.2$ Hz), 7.87 (d, $J = 15.0$ Hz), 7.81 – 7.74 (m), 6.59 (d, $J = 8.9$ Hz), 6.25 (s), 4.47 (s), 4.17 (s), 3.57 (d, $J = 7.0$ Hz), 2.96 (s), 1.77 (s), 1.20 (t, $J = 6.9$ Hz). ^{13}C NMR (126 MHz, DMSO- d_6) δ 164.29, 161.43, 157.42, 153.84, 148.22, 148.19, 141.06, 136.79, 132.13, 129.05, 125.94, 123.48, 118.35, 106.92, 90.31, 67.75, 65.47, 52.62, 49.93, 45.11, 38.04, 26.21, 19.61, 13.23.

2.3 Study of optical properties of newly synthesized dyes both in the presence and absence of nucleic acid targets

Optical properties of the cationic styryl dyes in the presence and absence of nucleic acids were studied by measuring the absorption and fluorescence change upon dyes-nucleic acids binding. The absorption spectra were measured on a CARY 100 Bio UV-vis spectrophotometer (Varian) and the fluorescence spectra were collected on a Cary Eclipse Fluorescence Spectrophotometer (Varian/Agilent Technologies) using a quartz cuvette with a path length of 1.0 cm at ambient temperature. Double-stranded DNA (dsDNA) used in this work is stated in Table 2.1, prepared by mixing the respective single stranded synthetic oligodeoxynucleotides in 10 mM sodium phosphate buffer (pH 7.0). Samples for absorption and fluorescence studies of cationic styryl dyes in the presence and absence of dsDNA were prepared

in 10 mM sodium phosphate buffer pH 7.0. The concentration of the DNA was determined by UV spectrophotometry using the molar extinction coefficient at 260 nm (ϵ_{260}) as calculated from the base sequence (<http://www.chemistry.sc.chula.ac.th/dna/DNARNA.asp>).

2.3.1 Fluorescence quantum yield (Φ_F) determination of the cationic styryl dyes

The fluorescence quantum yield (Φ_F) of the free dyes, bound dyes with dsDNA were calculated using fluorescein ($\Phi_F = 0.95$, $\lambda_{ex} = 470 - 490$ nm), rhodamine 6G ($\Phi_F = 0.95$, $\lambda_{ex} = 470 - 510$ nm), cresyl violet ($\Phi_F = 0.54$, $\lambda_{ex} = 540 - 590$ nm) as the standards. The integrated fluorescence intensities and the absorbance values (at λ_{ex}) of the standard and the samples were plotted and the slopes were investigated to give $grad_{standard}$ and $grad_{sample}$, respectively.⁹¹

The quantum yield can be calculated according to equation (1):

$$\Phi_{sample} = \Phi_{standard} (grad_{sample} / grad_{standard}) (\eta_{sample}^2 / \eta_{standard}^2) \quad (1)$$

Where $grad$ is the slope from the plot of integrated fluorescence intensity as a function of absorbance and η is the refractive index of the solvent used for the fluorescence measurement.

2.3.2 Color change mechanism of the cationic styryl dyes upon DNA binding

To investigate the mechanism of the optical change of the cationic styryl dyes in the presence of DNA, 4QL2+ was dissolved in water, acetonitrile, acetone, ethyl acetate, DMSO, methanol, glycerol, ethanol, and dichloromethane to the same concentration at 10 μ M with the final volume of 1 mL in all cases. Solvatochromic behavior of the dye in various solvents was studied using Lippert-Mataga equation (2).⁹²

$$\Delta\bar{\nu} = \bar{\nu}_A - \bar{\nu}_f = \frac{2}{hc} \left(\frac{\epsilon - 1}{2\epsilon + 1} - \frac{n^2 - 1}{2n^2 + 1} \right) \frac{(\mu_E - \mu_G)^2}{a^3} + k \quad (2)$$

Where h = Planck constant, c = light speed in vacuum, a = radius of the cavity where the dyes is allocated, $\bar{\nu}_A$ = absorption wavenumber, $\bar{\nu}_f$ = emission wavenumber, k = difference between the absorption and emission wavenumbers in the vacuum.

$$\Delta f = \frac{\epsilon - 1}{2\epsilon + 1} - \frac{n^2 - 1}{2n^2 + 1} \quad (3)$$

Where Δf = orientation polarizability which is the combination of dielectric constant (ϵ) and refractive index (n) parameters of solvents.

2.4 Fluorescent indication displacement assay

In this study, two DNA sequences were utilized. Firstly, d(AT)₁₀ was used for groove binding study. For intercalation study, d(GC)₁₀ was employed. The dyes utilized in this study were **PY+/PY2+(C4)**, **BT+/BT2+(NEt₂)/BT2+(OMe)**, and **4QL+/4QL2+**. Ethidium bromide (EtBr) and 4',6-diamidino-2-phenylindole (DAPI) were used as reference intercalator and groove binding dyes. The optimal ratios between indicator dyes and DNAs were determined at a fixed DNA concentration at 20 μ M (bp) prior to the displacement assay, and the optimal ratios for EtBr:DNA (bp) and DAPI:DNA (bp) to give the maximum signals were 2:5 and 1:10, respectively. For the displacement titration assay, the indicator dyes were first incubated with DNA at the optimal ratio for 30 minutes at room temperature. Then, various concentrations of the cationic styryl dyes were added to the prepared mixtures, with the DNA concentration fixed (bp) at 20 μ M. After 15 minutes incubation, the fluorescence spectra were recorded on Cary Eclipse Fluorescence Spectrophotometer (Varian/Agilent Technologies).

2.5 Ionic strength dependence studies

The samples containing dsDNA (15 μ M bp) and representative dyes, including **BT+**, **BT2+(NEt₂)**, **PY2+(C4)** and **4QL2+** (1 μ M) in 10 mM sodium phosphate buffer (pH 7.0) were prepared in a 96-well microplate. Next, various concentrations of NaCl (50 – 200 mM) were added with the final volume adjusted to 200 μ L in all cases, followed by fluorescent measurement on a PerkinElmer, EnSight Multimode Microplate Reader. Optimal excitation wavelength of each styryl dyes, referred to the previous session was used. The measured fluorescence intensities at the wavelengths of interest (600 nm for **PY2+(C4)**, **BT+** and **BT2+(NEt₂)**, 670 nm for **4QL2+**) were used to calculate the Stern-Volmer quenching constant according to equation (4).⁸¹

$$F_0/F = 1 + K_{SV}[Q] \quad (4)$$

where F_0 and F are the fluorescence intensities in the absence and presence of NaCl (50 – 200 mM), as the quencher [Q] and K_{SV} is the Stern-Volmer quenching constant.

2.6 Dyes-DNA binding interaction studies

In this study, the binding constant (K_b) and binding site (n) values of each dye were determined to compare the relative binding affinity between dye molecules and DNA strands. To achieve the spectroscopic data, the dsDNA (30 bp) as sequence shown in Table 2.1 was used. The selected dyes consisted of **PY+**, **PY2+(C4)**, **BT+**, **BT2+(NEt₂)**, **4QL+**, and **4QL2+**. The dye-DNA mixtures at various dye-DNA (in bp) ratios were prepared in 10 mM sodium phosphate buffer (pH 7.0) at a fixed concentration of dyes (2 μ M) in 96-well microplate with a final volume of 200 μ L. Next, fluorescent intensities at desired wavelengths were recorded on PerkinElmer, EnSight Multimode Microplate Reader. The intensities were recorded until they reached constant values which represented excess amounts of DNA in the system. Only the data at optimal ratios for dye-DNA(in bp) which showed linear response

were further collected to calculate the binding parameters K_b and n . According to Akbay and co-workers,⁸⁸ the McGhee and von Hippel equation was modified based on an assumption that only one type of interaction between dye and DNA leading to non-cooperative binding. Therefore, K_b and n values can be calculated from fluorescent titration curves using equation (5):

$$Y = F_{\max} - \frac{X \left(1 - \left[(n-1) \frac{X}{F_{\max}}\right]\right)}{C_{\text{dye}} K_b \left(1 - n \frac{X}{F_{\max}}\right)^n} \quad (5)$$

where Y =fluorescence intensity at maximum emission wavelength (F) and $X = F \times C_{\text{dye}} / C_{\text{DNA}}$ (bp). Therefore, K_b , n and F_{\max} values can be calculated as approximation parameters of fitting by the Eq. 5 the experimentally obtained data plotted as the dependence of Y on X .

2.7 Docking simulation for DNA-dye interaction study

(This part of the work was performed by Dr. Jaru Taechalertpaisarn from Department of Chemistry and Biochemistry, University of California, Santa Cruz, California, United States)

To calculate free energy of DNA-dye binding (ΔG), **BT+**, **BT2+(NEt₂)**, **PY2+(C4)**, and **4QL2+** were chosen as model ligands. Initially, SMILES string of each ligand was generated by PerkinElmer ChemDraw[®], followed by 3D model building, minimization, torsion adjustment and atomic partial charges calculation by Discovery Studio 2018. DNA structures were obtained from RCSB with removal of water, ligands, and salts molecules by ChimeraX, and addition of polar H atoms and Gasteiger charges by AutodockTools. Drew-Dickerson (PDB code: 4C64) DNA crystal structure was used as a model for a minor groove interaction, while the most-averaged NMR structure of a dsDNA-intercalator complex (PDB code: 108D) was employed as an intercalation

model. Docking simulations of DNA-dye interaction were performed by AutoDock 4.2.6.⁹³ Grid boxes were generated with 60 × 75 × 120 Å and 60 × 110 × 60 Å dimensions to cover the entire 4C64 and 108D DNA models, respectively. Lamarckian Genetic Algorithm (LGA) was selected as a docking algorithm in which each docking consisted of 20 independent runs, with a maximum number of 5×10^6 energy evaluations, and a maximum number of 27,000 generations. The best docking structures were visualized by ChimeraX software.

2.8 Applications of styryl dyes-based platform for nucleic acid detection

2.8.1 HeLa Cell imaging

(This part of the work was performed by Mr. Kriangsak Faikhruea under supervision of Dr. Chanat Aonbangkhaen)

2.8.1.1 MTT cytotoxicity assays

HeLa cells (a gift from the Lampson Lab, Department of Biology, the University of Pennsylvania, PA, USA) were seeded in 96-well plates at 1×10^4 cells per well. The cells were incubated at 37 °C in a humidification incubator with 5% CO₂. After incubation, the cells were treated with different concentrations of 0.1, 1, 10, 25 μM dyes (**BT+**, **BT2+(NEt₂)** and **BT2+(OMe)**). They were incubated under the same conditions for 24 hours. MTT solution (5 mg/mL of 3-(4,5-dimethylthiazol-2-yl)-2,5-diphenyltetrazolium bromide in PBS) was added to the wells and again incubated at 37 °C for 3 hours. The media was then removed and mixed with DMSO. The absorbance at 570 nm was measured with a PerkinElmer, EnSight Multimode Microplate Reader and the cytotoxicity was calculated.

2.8.1.2 Cellular imaging experiments

HeLa cells were cultured in Dulbecco's Modified Eagle's Medium (DMEM, HyClone™ Thermo Scientific, USA) containing 4.5 g/L D-glucose, 4 mM L-glutamine and supplemented with 10% of heat-inactivated fetal bovine serum (FBS; Gibco™

Invitrogen) and 1% penicillin at 37 °C at 5% CO₂. The HeLa cells were seeded on a 24-well chamber cell culture plate at 5 × 10⁴ cells per well. The cells were grown in an incubator at 37 °C and 5% CO₂. The live cells were stained with 20 μM **BT2+(NEt₂)**, 500 nM PhenoVue512 or 200 μM **BT2+(OMe)** at 37 °C. After 18 h of treatment, the cells were stained with DAPI (0.2 μg/mL) and incubated for 15 minutes. The fluorescence images of the live cells were recorded using fluorescence microscope (ZEISS Axio Observer).

2.8.2 Mercury(II) ion detection based on aptamer and cationic styryl dyes

All procedures and conditions in a previous work by Tiarpattaradilok was used without modifications.⁹⁴ The aptamer used to detect mercury(II) ion was dT₃₀ (The aptamer sequence is shown in Table 2.1). The cationic styryl dyes employed in this study include **BT2+(NEt₂)** and **BT2+(OMe)**. The samples for fluorescence studies consist of the cationic styryl dyes (2 μM) and the aptamer (1 μM, in strand) in the presence of various concentrations of mercury(II) ion were prepared in 10 mM Tris-HCl buffer (pH 7.4). The samples were incubated for 30 minutes prior to the fluorescence measurement by Cary Eclipse Fluorescence Spectrophotometer (Varian/Agilent Technologies) and PerkinElmer, EnSight Multimode Microplate Reader. For selectivity screening, separate stock solutions of 9 metal(II) ions, consisting of mercury(II), nickel(II), copper(II), zinc(II), lead(II), cobalt(II), cadmium(II), iron(II), and manganese(II) ion, were prepared at 10 mM concentration. The samples consist of the metal(II) ion (500 μM) and dT₃₀ (25 μM, in strand)) were then prepared in 10 mM Tris-HCl buffer (pH 7.4). After 30 minutes incubation time, the dyes (**BT2+(NEt₂)** or **BT2+(OMe)**) were added with final concentration of 50 μM. The results were observed under UV light (365 nm).

CHAPTER III

RESULTS AND DISCUSSION

3.1 Synthesis of cationic styryl dyes

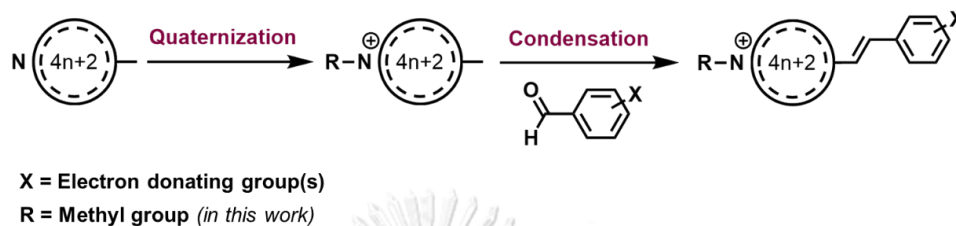


Figure 3.1 Main synthesis steps of cationic styryl dyes

Cationic styryl dyes are generally synthesized from two components: an *N*-alkylated heterocyclic ring system with an acidic methyl group, and a substituted benzaldehyde derivative. In this work, the *N*-methylated heteroaromatic compounds were prepared in the first step by simply heating the heteroaromatic substrates (4-picoline – PY, 2-methylbenzothiazole – BT, 4-methylquinoline – 4QL, 2-methylquinoline – 2QL, 2,3,3-trimethylindolenine - TMIN, and 9-methylacridine - AD) with iodomethane under neat conditions to quaternize the nitrogen atom on the heterocycles. The obtained quaternized compounds were next condensed with the substituted benzaldehydes via an aldol-type reaction in refluxing ethanol to yield the desired cationic styryl dyes, as summarized in Figure 3.1.

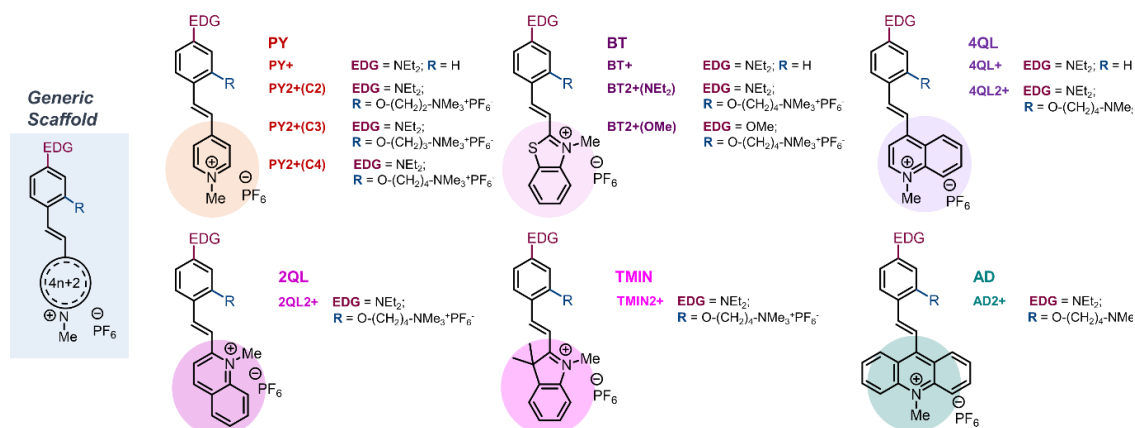
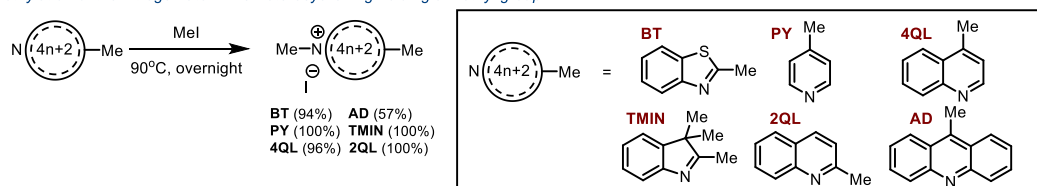


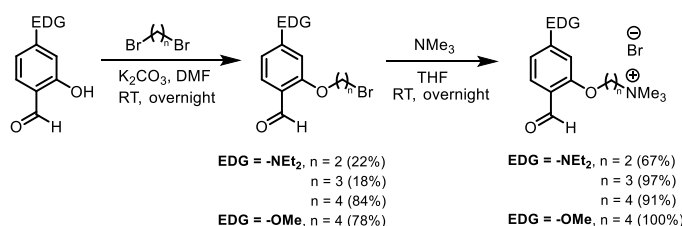
Figure 3.2 The structures of cationic styryl dye being studied in this work

To introduce the additional positive charge to the styryl dye molecules, the aromatic aldehyde was modified with a trimethyl ammonium group attached to the hydroxy substituent on the aromatic ring via an alkylene linker. The effect of linker length was investigated in the PY series with pyridine as the heteroaromatic core structure by varying the alkylene linker lengths from ethoxy (C2), propoxy (C3), to butoxy (C4) in **PY2+(C2)**, **PY2+(C3)**, and **PY2+(C4)**, respectively. The dyes **BT2+(NEt₂)**, **4QL2+**, **2QL2+**, **TMIN2+**, and **AD2+** carried the same tetramethylene (C4) linker as **PY2+(C4)** in order to compare the effects of different heteroaromatic cores. The dye **BT2+(OMe)** was also synthesized to compare the effects of different electron-donating aromatic substituents (-NEt₂ and -OMe, which are strong and weak electron donors, respectively). To assess the influence of the additional positive charge on the dyes' optical characteristics, selected monocationic dyes including **PY+**,⁸¹ **4QL+**,⁶⁵ and **BT+**⁷¹ without the quaternary ammonium group were also prepared for comparison following the literature methods.

N-methylation of the nitrogen atom in a heterocyclic ring holding a methyl group:



Sidechain modification of aromatic aldehyde to introduce additional positive charge to molecule:



Aldol-type condensation of the methyl group on the heterocyclic ring with an aromatic aldehyde:

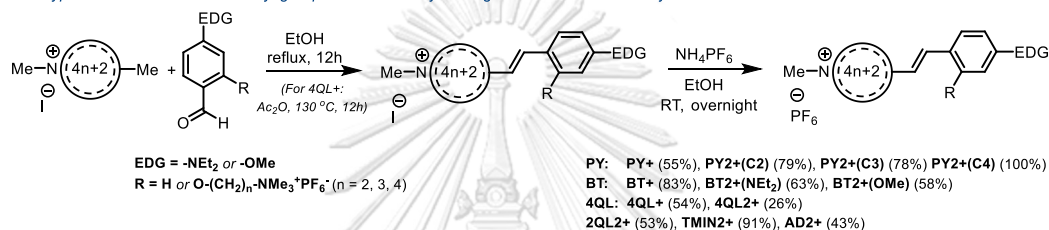


Figure 3.3 Synthetic routes for the cationic styryl dyes in this work

The starting quaternary ammonium-modified benzaldehydes were prepared by alkylation of the hydroxy groups of 4-(diethylamino)salicylaldehyde and 4-methoxysalicylaldehyde with excess of the appropriate α,ω -dibromoalkane (C2, C3, or C4) to afford the corresponding bromoalkylated salicylaldehyde derivatives in 18 – 84% yield. This was followed by another nucleophilic substitution with trimethylamine in THF to obtain the desired quaternized benzaldehyde substrates in good yields (67 – 100%). For the condensation step, simple refluxing in ethanol without any catalysts was applicable for almost dyes. In the case of **4QL2+**, a poor yield was obtained due to the high pK_a of the quinolinium methyl group.⁹⁵ In addition, the synthesis of the dye **4QL+** required heating the starting materials in acetic anhydride at 130 °C, and the reaction probably proceeded through the acid-catalyzed pathway.^{71, 96} The counterions in all cationic dyes were exchanged from bromide and/or iodide to hexafluorophosphate (PF_6^-) by treatment of the crude

product with an excess of NH_4PF_6 in ethanol to facilitate the isolation of the products. In all cases, the precipitated salts were isolated by simple filtration. The overall yields for cationic styryl dyes are ranging from low to quantitative yields (11 – 78%) as illustrated in Figure 3.3.

3.2 Optical properties of cationic styryl dyes

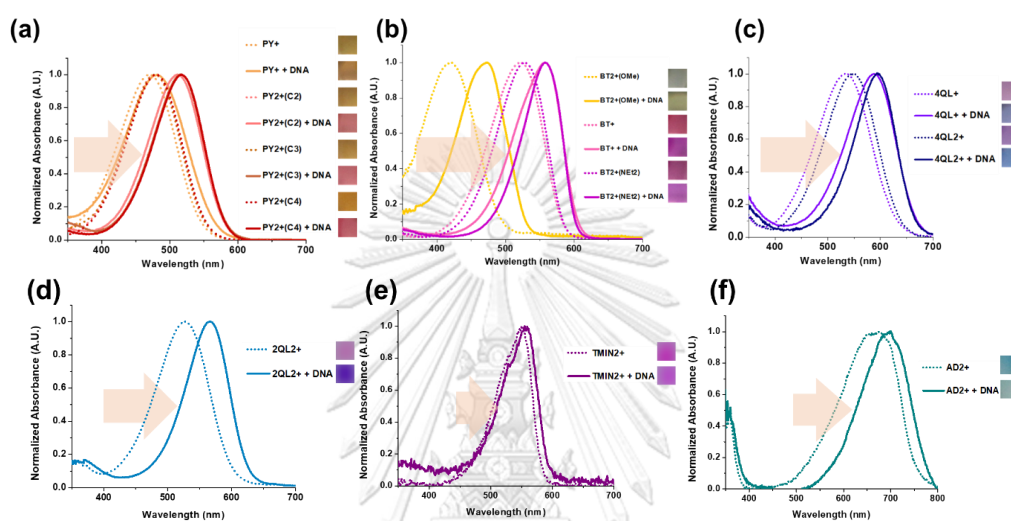


Figure 3.4 Normalized absorption spectra of cationic styryl dyes PY series (a), BT series (b), 4QL series (c), 2QL2+ (d), TMIN2+ (e) and AD2+ (f) in the absence and presence of DNA. Conditions: [Dye] = 10 μM , [DNA (in bp)] = 450 μM , except for [TMIN2+] = 1 μM , [DNA (in bp)] = 45 μM . Inset: colors of the dyes in daylight in the absence and presence of DNA. Conditions: [Dye] = 50 μM , [DNA (in bp)] = 2,250 μM . All experiments were performed in 10 mM sodium phosphate buffer pH 7.0.

Due to the presence of substantial conjugation in the structure, all cationic styryl dyes absorbed strongly in the visible region (470 to 550 nm). When all other factors are equal, the heteroaromatic component exerts a considerable impact on absorption. The absorption maxima moved towards the longer wavelengths as the conjugated system became larger (PY < BT < QL). The maximum absorption wavelengths of the $-\text{NEt}_2$ substituted dyes without the DNA target were 471 – 480 (PY

series), 523 – 528 (BT series), 533 – 547 (4QL series), 527 (**2QL2+**), 551 (**TMIN2+**), and 678 (**AD2+**) nm as shown in Figures 3.4a – f (dotted line). As evidenced by the significantly blue-shifted absorption maxima of the **BT2+(OMe)** carrying the weakly electron-donating -OMe substituent (OMe) when compared to the **BT2+(NEt₂)** bearing the strong electron-donating -NEt₂ substituent (420 vs 528 nm), the nature of the substituent on the aromatic ring has an impact on the absorption wavelength. The $n \rightarrow \pi^*$ transition in the styryl dye is facilitated by the stronger electron-donating substituent, resulting in the observed longer wavelength absorption. The presence of an additional positive charge due to the quaternary ammonium group linked to the ring via the alkoxy linker has little effect on the dye's absorption characteristics, and the absorption spectra were only slightly red-shifted (less than 10 nm) in most cases.

To investigate the optical properties of the dyes in the presence of DNA, the model double-stranded DNA oligonucleotide (dsDNA) with 30 base pairs (bp) was selected (see the sequence in Table 2.1). The sequence of the dsDNA was chosen so that it contained 63% GC and 37% AT which are uniformly distributed along the DNA strand. This very same dsDNA model was also utilized for the binding affinity studies which required an unbiased response of the synthesized dyes towards DNA target. In the presence of the dsDNA target, the absorption spectra of all cationic styryl dyes shifted towards the longer wavelength by 10 – 50 nm (Figure 3.4 – solid line). The relationship between the solvent polarity and red-shifting in the absorption maxima of similar dyes has long been observed in previous literature.⁹⁷ The **4QL2+** dye was chosen as a model for further studies of color-changing behavior because it showed the most pronounced absorption change in the presence of dsDNA (up to 48 nm red-shifting).

To investigate the solvatochromic properties, the absorption and fluorescence spectra of **4QL2+** were measured in various solvents including water, ethyl acetate, acetone, dimethyl sulfoxide, ethanol, methanol, dichloromethane, acetonitrile, and glycerol (Figure 3.5a). It was evidenced that the maximum absorption wavelength (λ_{max}) changed with the polarities of the solvents, becoming more red-shifted in less polar solvents and vice versa. It's worth noting that the shape and λ_{max} of the absorption spectra of **4QL2+** in aqueous solution at different concentrations remained constant over a broad concentration range of 1 to 50 μM (Figure 3.5b). The results showed that under the typical conditions studied, the color shift was not related to changes in the dye aggregation states.

The trend in the relationship between absorption energy (wavenumber of the maximum absorption) and $E_{\text{T}}(30)$, which represented an empirical solvent polarity scale^{98, 99} of each solvent (Figure 3.5c) revealed a positive correlation. This pattern is explained by the fact that the ground state of styryl dyes is more polar than the excited state.¹⁰⁰ The dye molecule in the ground state was better stabilized in more polar solvents due to substantial delocalization caused by an intramolecular charge transfer, resulting in a greater energy difference between the ground state and the excited state. As a result, the electronic transition occurred at a shorter wavelength, resulting in the observed hypsochromic shift as the solvent polarity increased. The observed results are to be expected for typical donor-acceptor dyes.¹⁰¹ The change in the local environment of the dye from polar to nonpolar was related to the red-shifting of the absorption maxima of **4QL2+** as illustrated in Figure 3.5d. However, it should be emphasized that the structure of the excited state is only speculative based on a possible resonance form. More accurate structure should be further investigated by an appropriate theoretical calculation, e.g. by the configuration interaction singles (CIS) approach.¹⁰² Other dyes in this work showed similar trends in

the absorption spectra change. However, the differences were less noticeable ($\Delta\lambda_{\text{abs}} = 11 - 37$ nm for PY series, $30 - 35$ nm for BT series, 33 nm for **2QL2+**, 22 nm for **AD2+** and 8 nm for **TMIN2+**).

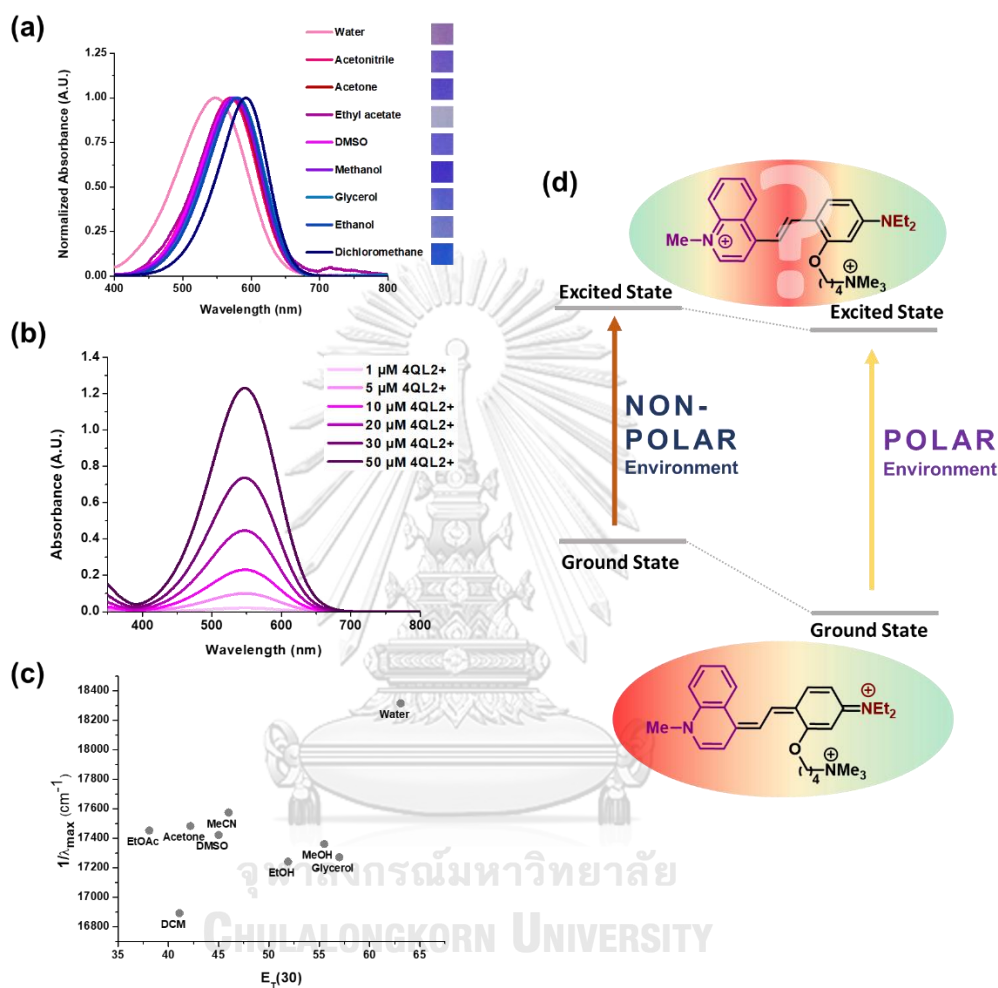


Figure 3.5 Normalized absorption spectra of **4QL2+** (10 μM) in various solvents (a), Absorption spectra of **4QL2+** aqueous solution (1 – 50 μM) (b), Relationship between absorption wavenumber ($1/\lambda_{\text{max}}(\text{abs})$, cm^{-1}) and $E_{\text{T}}(30)$ scale (c), and Illustration explained energy gaps of **4QL2+** in different polarity environment (d). The color contour illustrated electron density distribution from red (δ^+) to green (δ^-).

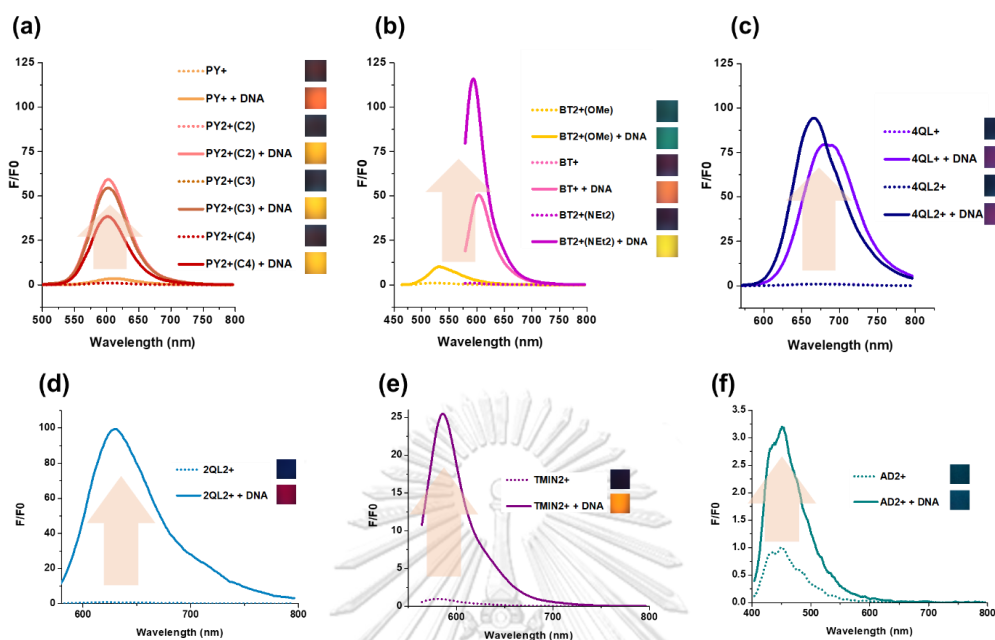


Figure 3.6 Normalized fluorescence spectra of the styryl dyes PY series (a), BT series (b), 4QL series (c), 2QL2+ (d), TMIN2+ (e) and AD2+ (f) in the absence (dotted lines) and presence of DNA (solid lines). Conditions: [Dye] = 10 μM , [DNA (in bp)] = 450 μM , except for [BT+] = [BT2+(NEt₂)] = [TMIN2+] = 1 μM , [DNA] = 1.5 μM , BT2+(OMe) λ_{ex} = 450 nm, PY+, PY2+(C2), PY2+(C3), PY2+(C4) λ_{ex} = 480 nm, BT+, BT2+(NEt₂) λ_{ex} = 565 nm, 4QL+, 4QL2+ λ_{ex} = 548 nm, 2QL2+ λ_{ex} = 560 nm, TMIN2+ λ_{ex} = 550 nm, AD2+ = 390 nm. Inset: emission color of the dyes under UV illumination (365 nm) in the absence and presence of DNA. Conditions: [Dye] = 50 μM , [DNA (in bp)] = 2,250 μM . All experiments were performed in 10 mM sodium phosphate buffer pH 7.0.

For fluorescence properties, the emission maxima of the unbound dyes also showed a similar trend to the absorption properties. The heteroaromatic components and electron (-NEt₂ or -OMe) substituents also exert substantial effects on the emission wavelength. The maximum emission wavelengths of the -NEt₂ substituted dyes without the DNA target were 599 – 612 (PY series), 591 – 595 (BT

series), 665 – 680 (4QL series), 626 (**2QL2+**), 581 (**TMIN2+**), while **BT2+(OMe)** with -OMe substituent showed an emission maximum as 521 nm. Importantly, all free styryl dyes showed very weak fluorescence emission as reflected by the low fluorescence quantum yields ($\Phi_F = 0.001 - 0.004$). In the presence of an excess of the dsDNA target, the ratios of fluorescence emission (F/F_0) and quantum yield ($\Phi_{F(DNA)}/\Phi_{F(dye)}$) were increased by 3.2 to 126 times, and 3.4 to 87.5 times, respectively (Table 3.1, Figures 3.6a – f).

It should be noted that the fluorescence response of the dye **AD2+** did not follow this general trend. The results showed that the emission maximum of **AD2+** was only 450 nm, while the emission wavelength should be expected to be longer due to the larger conjugated system of acridine compared to pyridine or quinoline. Also, the fluorescence increase was very weak compared to other systems. It is possible that the emission range for **AD2+** may occur in the near-IR range that is beyond the capability of the current instrument to measure.

The restricted motion of the dye molecules in the excited state,¹⁰³ which inhibits the nonradiative relaxation pathways of the dyes' photoexcited states, has been previously proposed as an explanation for the significant increase in the fluorescence quantum yields of benzothiazole-based⁷⁴ and pyridine-based⁸² styryl dyes related to BT and PY series, respectively. In this study, the fluorescence spectra of the **4QL2+** dye were also examined in aqueous and glycerol solution both in the absence and presence of DNA (Figures 3.7a – b) to investigate whether the proposed mechanism is also in operation with the quinoline dye family. Indeed, the fluorescence intensities increased in the presence of glycerol which increased the viscosity of the solution. This behavior is consistent with the molecular rotor nature of the dye that shows restricted motion in solvents with high viscosity resulting in the observed increased fluorescence.⁶⁷ The fluorescence intensity and emission maxima

of the dye in glycerol and the DNA-bound dye in water were almost the same. In the presence of DNA, the dye in glycerol showed no further change in the fluorescence spectra. The findings show that the fluorescence increase in the presence of DNA is caused by a restriction of the **4QL2+** dye's conformational freedom when it binds to DNA, similar to other styryl dyes reported in the literature.⁷⁸ On the other hand, the absorption spectra of **4QL2+** in glycerol both in the absence and presence of DNA showed the same maximum absorption wavelength (Figure 3.7d). Accordingly, the color change of the dye is due to the effect of local polarity change (*vide infra*, section 1.3.2) rather than the motion restriction.

To confirm that molecular motion has an impact on the fluorescence intensity, the fluorescence of the **4QL2+** dye in an aqueous glycerol solution was examined at different temperatures. The sample was equilibrated at 0 °C, then heated to 30, 60, and 90 °C before cooling down to 0 °C and the fluorescence spectra were recorded at each temperature. The fluorescence emission intensity decreases as the temperature rises in a reversible fashion. Evidently, high temperature increases the molecular motion, thus enabling the non-radiative relaxation pathway to operate. The results are completely consistent with the proposed mechanism of fluorescence enhancement based on decreased molecular motion.

The fluorescence spectra of **4QL2+** were also measured in various organic solvents. Similar to the absorbance, the Stokes shifts of **4QL2+** showed a strong dependency on solvent polarity (Figure 3.7e). The Lippert-Mataga plot⁹² (Figure 3.7f) shows a positive correlation between the Stokes shift and the orientation polarizability (Δf) of the solvents surrounding the dye molecules. This implies that solvents influence molecular dipole moment change between the ground and excited states of dye.¹⁰⁴ Furthermore, the findings revealed that polarity, in addition

to solvent viscosity (or molecular motion), influences the fluorescence characteristics of **4QL2+** (Figure 3.7g), both in terms of fluorescence emission maxima and intensities. This can also be used to explain the optical properties of other styryl dyes in this study in the same way.

The dyes **BT2+(OMe)** and **BT2+(NEt₂)**, which shared the same benzothiazolium core structure but carried different electron donating substituents on the aromatic-ring (-OMe and -NEt₂, respectively), revealed quite different optical characteristics (Table 3.1). The dye **BT2+(OMe)** with a weaker electron-donating substituent (-OMe group) showed the absorption at a shorter wavelength when compared to **BT2+(NEt₂)**. In the presence of DNA, the maximum absorption was shifted from near UV (420 nm) to visible (473 nm) regions. In terms of fluorescence response, a relatively poor fluorescence enhancement ($F/F_0 = 10.9$) was observed for the dye **BT2+(OMe)** in the presence of DNA. For comparison, the **BT2+(NEt₂)** showed a much larger fluorescence increase ($F/F_0 = 125.7$) in the presence of DNA.

In summary, both the heteroaromatic moieties (PY, BT, 4QL, 2QL, TMIN) as well as the substituents on the electron-rich aromatic moiety (-NEt₂ and -OMe) exert substantial impacts on the dye's absorption and fluorescence characteristics. The results suggest that the styryl dye's optical characteristics can be easily tuned by modifying the heteroaromatic core and the aromatic ring substituent. Meanwhile, the introduction of the quaternary ammonium group via a non-conjugated alkoxy linker had only minor effects on the dyes' optical properties in terms of absorption and fluorescence emission maxima, but the responsiveness towards DNA significantly increased. As presented in Table 3.1, when compared to the monocationic dyes with the same heteroaromatic series (**PY+**, **BT+**, and **4QL+**), the dicationic dyes (**PY2+(C2, C3, C4)**, **BT2+(NEt₂)** and **4QL2+**) demonstrated a larger absorption change ($\Delta\lambda_{\text{abs}}$) and fluorescence enhancement (F/F_0) in the presence of DNA. In addition, the

brightness parameter ($\epsilon \times \Phi_F$) and fluorescence quantum yield of the dyes in the presence and absence of DNA ($\Phi_{F(DNA)}/\Phi_{F(dye)}$) also follows the same trend as the fluorescence enhancement ratios (F/F_0), which confirmed the significant impact of the additional positive charge modifier to dye molecules towards DNA responsiveness of the dicationic styryl dyes.



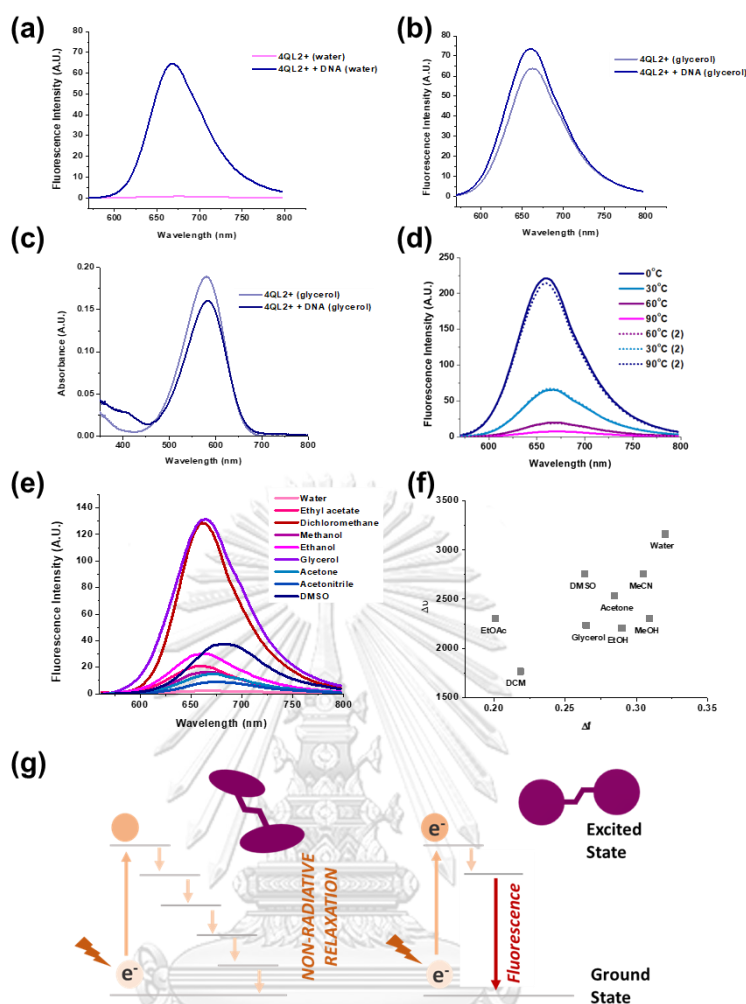


Figure 3.7 Fluorescence spectra of 4QL2+ (10 μM) in the absence and presence of DNA (450 μM , in bp) in water (a) glycerol (b), Absorption spectra of 4QL2+ (10 μM) in the presence and absence of DNA (450 μM , in bp) in glycerol (c), Fluorescence spectra of 4QL2+ (10 μM) in glycerol (0 – 90 $^{\circ}\text{C}$) (d), Fluorescence spectra of 4QL2+ (10 μM) in various solvents, $\lambda_{\text{ex}} = 548 \text{ nm}$ (e), Lippert-Mataga plot of the Stokes shift and orientation polarizability of the solvents surrounding the dye molecules of 4QL2+ dissolved in various solvents (f), Illustration explained fluorescence change mechanism of the dye (g).

Table 3.1 Optical properties of cationic styryl dyes in the absence and presence of dsDNA: absorption maxima $\lambda_{\text{max}}(\text{abs})$, extinction coefficients (ϵ), emission maxima $\lambda_{\text{max}}(\text{em})$, fluorescence quantum yield (Φ_F) and fluorescence enhancement ratio (F/F_0)^a

Dye	ϵ^b ($\times 10^4$ $\text{M}^{-1} \text{cm}^{-1}$)		λ_{max} (nm)		F/F_0^d		Φ_F		Brightness ^e ($\times 10^3$)	
	abs (Dye)	abs (Dye+DNA)	em (Dye)	em (Dye+DNA)	value	wavelength (nm)	Dye	+DNA	Dye	+DNA
PY+	471	482	612	612	3.5	600	0.002	0.008	0.10	0.40
PY2+(C2)	478	511	605	603	60.5	600	0.002	0.114	0.10	5.9
PY2+(C3)	479	516	599	603	54.8	600	0.002	0.133	0.086	5.7
PY2+(C4)	480	517	603	600	38.5	600	0.002	0.127	0.11	6.8
BT+	523	558	595	605	56.6	600	0.004	0.053	0.13	1.7
BT2+(NEt ₂)	528	558	591	595	125.7	600	0.004	0.371	0.11	1.04
BT2+(OMe)	420	473	521	531	10.9	530	0.004	0.014	0.064	0.22
4QL+	533	587	680	682	80.1	670	0.001	0.038	0.22	0.84
4QL2+	547	595	665	670	98.4	670	0.001	0.057	0.25	1.4
2QL2+	527	560	626	632	91.9	620	ND	ND	ND	ND
TMIN2+	551	559	581	586	23.9	580	ND	ND	ND	ND
AD2+	678	700	450	451	3.2	450	ND	ND	ND	ND

^a Conditions: [Dye] = 2 μM , [DNA] = 1 μM ; [DNA(in bp)]: [Dye] = 15 : 1; all measurements were performed in 10 mM sodium phosphate buffer pH 7.0. dsDNA = 5'-CGGGGGGTACAGTAGTACTACCATGCCCTGG-3' + 3'-

CGCCGCATGTCACCTAGATGTCACGGGACC-5'.

^b in MeOH. ^c Estimated from absorption spectra of each dye at single concentration. ^d Fluorescence intensity with dsDNA (F) and without dsDNA (F_0). ^e Brightness = $\epsilon \times \Phi_F$. ND = not determined

3.3 Studies of binding modes by fluorescent indication displacement

According to the concept of fluorescence displacement assay, the indicator dye was first bound to the DNA strand and titrated with the dye of interest. The new dye can displace the indicator dyes if it interacts more strongly and in the same binding mode as the indicator dye.¹⁰⁵ The change in absorption or fluorescence emission can be monitored to indicate the extent of the displacement. In this study, ethidium bromide (EtBr) was used as the indicator dye for the intercalative binding mode,¹⁰⁶ while 4',6-diamidino-2-phenylindole (DAPI) was used as the indicator dye for the groove binding mode.¹³ Figure 3.8 shows a brief illustration to explain the concept of the fluorescent indicator displacement assay.

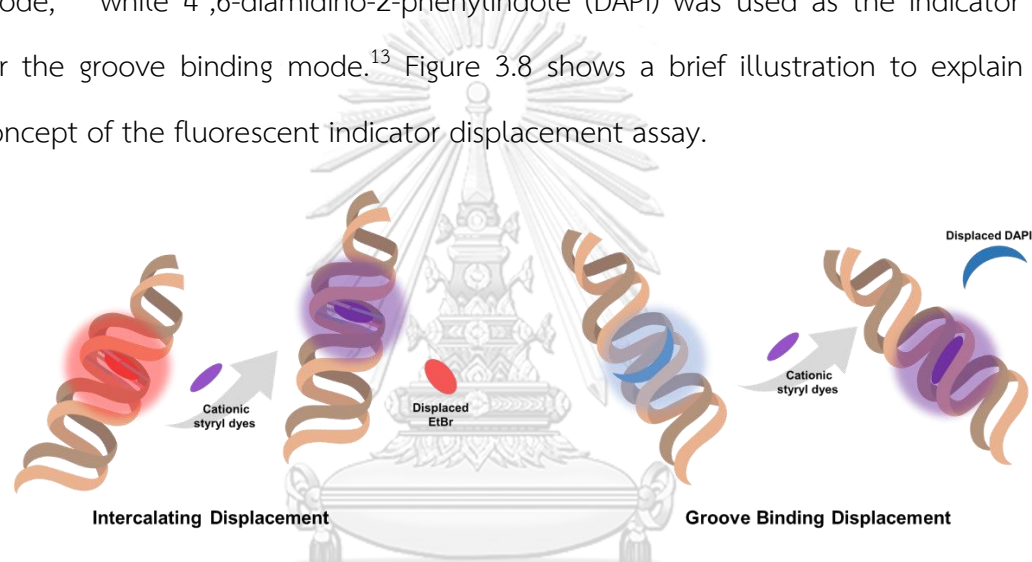


Figure 3.8 Fluorescent indication displacement concept in this work

To investigate the binding mode between the dicationic styryl dyes and DNA. Two DNA sequences including d(AT)₁₀ and d(GC)₁₀ were chosen as representative DNA sequences for groove binding and intercalating studies, respectively. Melting temperatures (T_m) were first determined to make sure that the chosen DNAs were in the double-stranded form required for the assay. The melting temperature was measured by the collection of DNA absorption at 260 nm, which is the average absorption of DNA nucleobase. The temperature was slowly increased from 20 °C to 95 °C at a rate of 1.0 °C/min. The plot between the temperature and normalized absorbance at 260 nm typically gives an S-curve, from which the temperature at

which the double-stranded DNA completely separated from each other can be determined via the 1st derivative of the plot. The results in Figure 3.9 showed that the melting temperatures of both DNAs were higher than room temperature, the T_m for d(AT)₁₀ was 37 °C, while the T_m for d(GC)₁₀ was 66 and >95 °C. The complex melting curve in the case of d(GC)₁₀ could be explained by the presence of several co-existing secondary structures. These results indicated that the chosen DNA sequences should be appropriate as the model dsDNA for the indicator displacement titration experiments.

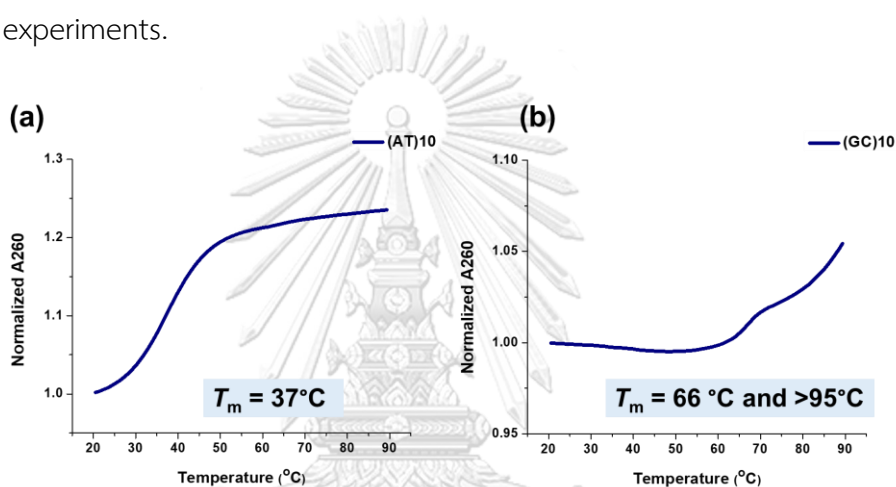


Figure 3.9 Melting temperature (T_m) investigation of d(AT)₁₀ (a) and d(GC)₁₀ (b) as the selected DNAs to study binding mode by fluorescent indication displacement

Next, the binding experiment of the indicator dyes at a fixed concentration of DNA was performed to examine the optimal ratio between the indicator dyes and DNAs. From the results in Figure 3.10, the optimal ratio of DNA (in bp) to ethidium bromide that gave the maximum response was 5:2 for both d(AT)₁₀ and d(GC)₁₀. The corresponding ratio of DNA to DAPI was 10:1 for d(AT)₁₀ and no fluorescent response was observed in the case of d(GC)₁₀. From the titration experiment, the DAPI molecules showed selectivity towards d(AT)₁₀ over d(GC)₁₀, while ethidium bromide gave similar fluorescent responses to both DNA models.

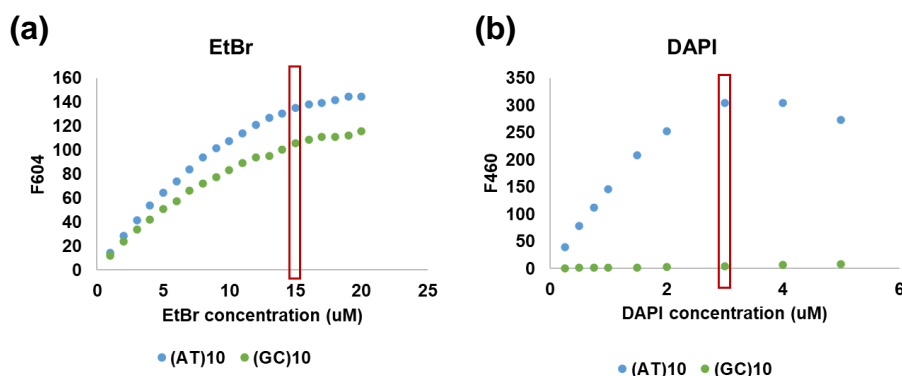


Figure 3.10 Determination of optimal ratios between [EtBr]:[DNA] (a) and [DAPI]:[DNA] (b)

Next, the displacement experiments were performed by titration of the cationic styryl dye to the DNA-indicator dye complexes at a fixed concentration. From the results, the cationic styryl dyes can be categorized into two groups. The first group is the styryl dyes that can bind to dsDNA only in the groove binding mode. The pyridinium-based styryl dyes (**PY+** and **PY2+(C4)**) belong to this group. As shown in Table 3.2 and Figure 3.11, the dyes could only displace DAPI which is a reference groove binder from the DNA strands but could not displace EtBr. Another group of the dyes may bind to dsDNA in both groove binding and intercalating modes. The dyes in the second group could displace both DAPI and EtBr from the dsDNA, which revealed both binding characteristics. The dyes in this group include the benzothiazolium-based styryl dyes (**BT+**, **BT2+(NEt₂)**, and **BT2+(OMe)**) and quinolinium-based styryl dyes (**4QL+** and **4QL2+**). A summary of the binding characteristics of the cationic styryl dyes is shown in Table 3.2 and Figure 3.11. The obtained results are consistent with reported literature which stated that pyridinium-based styryl dyes are groove binders,⁸¹ while benzothiazolium-based styryl dyes⁸⁸ could exhibit both groove binding and intercalating behaviors. In the case of quinolinium-based styryl dyes, even no literature specified exact binding mode of

the dye and DNA, the planarity of the quinolinium core structure should support the intercalative binding mode and hence provided possibility of the dyes to be both groove binder and intercalator.

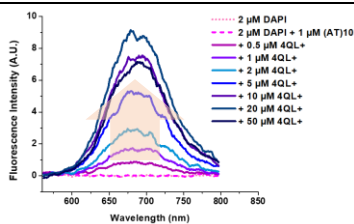
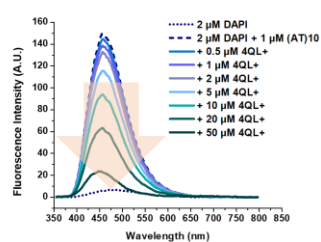
Table 3.2 Fluorescence spectra of the cationic styryl dyes' FID assays and their binding characteristics

Dye	Indicator dye excitation ^a	Styryl dye excitation ^a	Groove binding	Intercalation
PY+ <i>DAPI displacement</i>			✓	
<i>EtBr displacement</i>				✗
PY2+(C4) <i>DAPI displacement</i>			✓	
<i>EtBr displacement</i>				✗

4QL+

DAPI

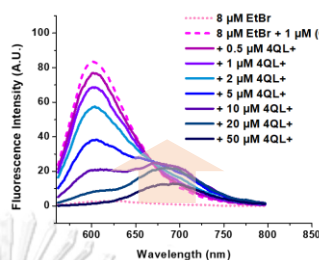
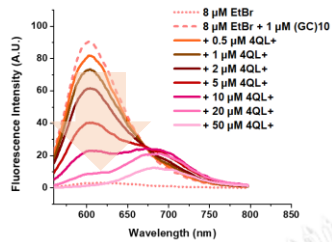
displacement



✓

EtBr

displacement

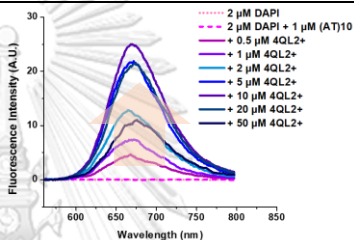
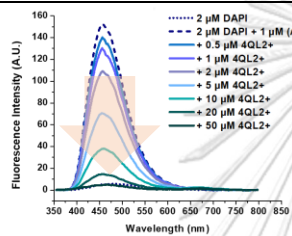


✓

4QL2+

DAPI

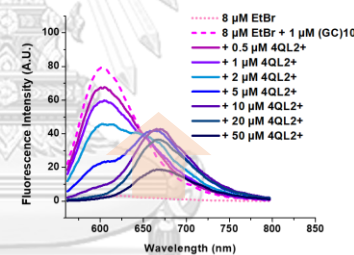
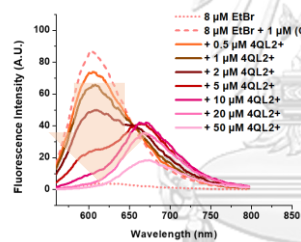
displacement



✓

EtBr

displacement



✓

^a The excitation wavelengths (λ_{ex}) of the indicators were 545 nm for EtBr, and 341 nm for DAPI, while the styryl dyes excitation wavelengths (λ_{ex}) were 480 nm for PY+ and PY2+(C4), 450 nm for BT2+(OMe), 565 nm for BY+ and BT2+(NEt₂), 548 nm for 4QL+ and 4QL2+. The DNA sequences used were (a) d(AT)₁₀ and (b) d(GC)₁₀. The assays were performed in 10 mM sodium phosphate buffer pH 7.0.

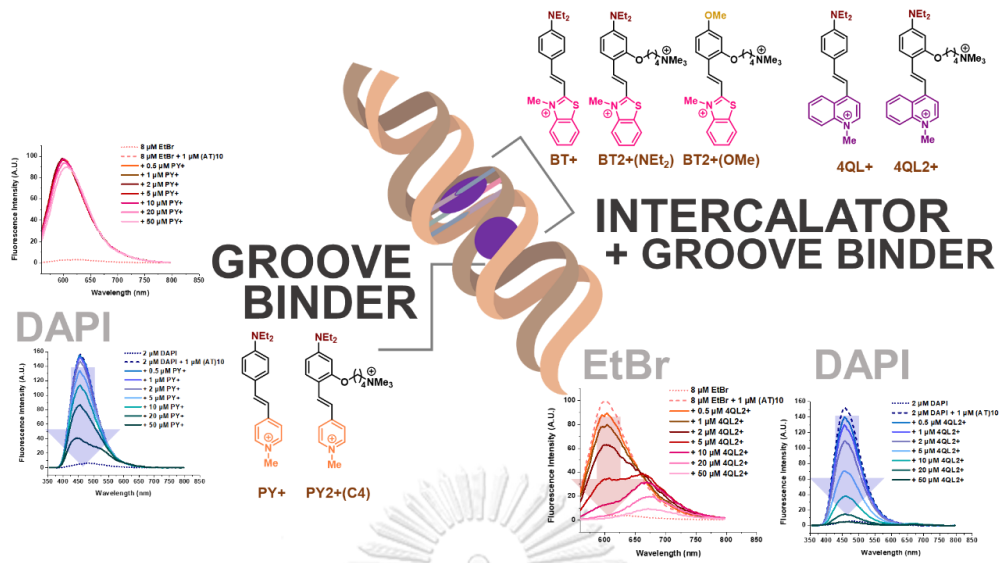


Figure 3.11 Summary of binding characteristics of cationic styryl dyes determining by fluorescence indication displacement assay

3.4 Binding studies using circular dichroism spectroscopy

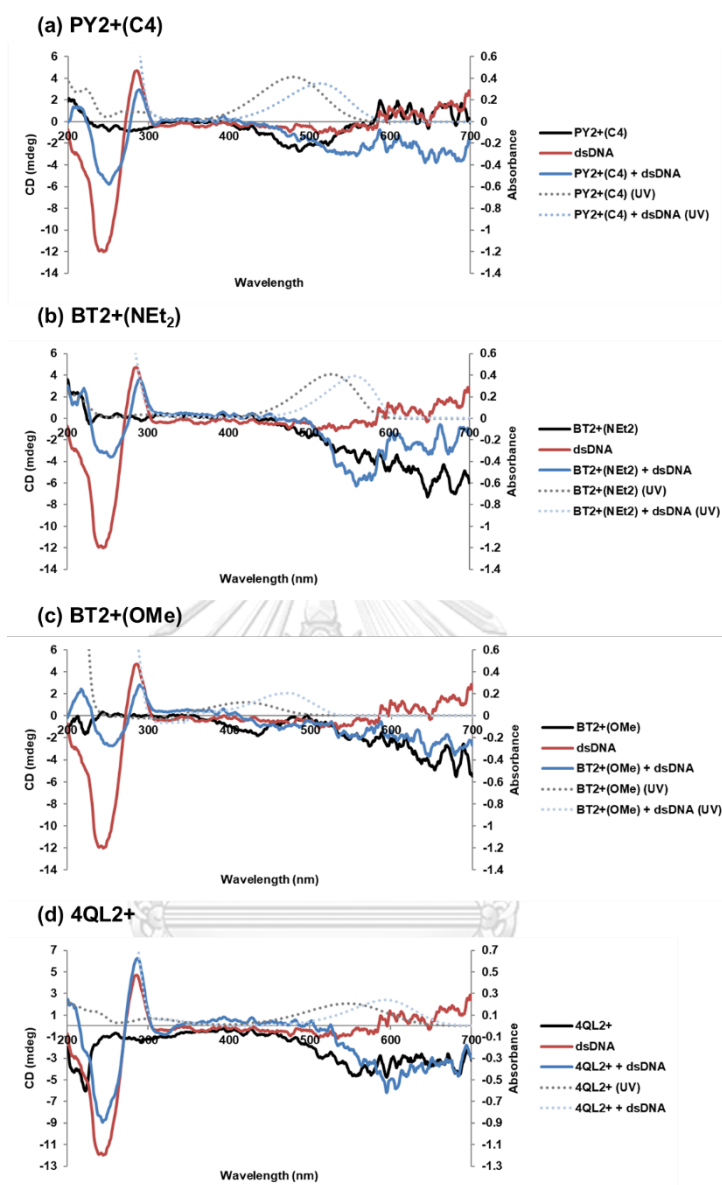


Figure 3.12 Circular dichroism (solid line) and absorption (dotted line) spectra of (a) PY2+(C4), (b) BT2+(NEt₂), (c) BT2+(OMe), (d) 4QL2+ in the presence and absence of dsDNA. Conditions: [Dye] = 10 μ M, [DNA (in bp)] = 150 μ M. CD Measurement: Accumulation = 16, scan rate = 500 nm/min. All experiments were performed in 10 mM sodium phosphate buffer pH 7.0.

Circular dichroism (CD) experiments were performed with the aim to gain more insights into the structural information of the dye bound to dsDNA. According to CD spectra in Figure 3.12, the free dsDNA showed a large positive peak at 273 nm and a negative peak at 243 nm, which is characteristic of the B-form of DNA.¹³ The positive band has been attributed to the stacking between base pairs, whereas the negative band was due to the helical structure of DNA.¹⁰⁷ The cationic styryl dyes used in this study were achiral and no CD spectrum should be expected. The CD spectra of dsDNA in the presence of the dyes clearly indicate that both base pair stacking and helicity of DNA change during the binding. The decreasing of the negative peak at 243 nm upon addition of the dye indicated untwisting of the DNA helix occurred when the dyes bound to the DNA. Moreover, the **BT2+** and **PY2+(C4)** dyes (Figures 3.12a – c) interfered with the base stacking, resulting in the decline of the positive peak at 273 nm. On the other hand, the **4QL2+** dye (Figure 3.12d) showed base stacking stabilization according to the slight increase of the signal at 273 nm which is in good agreement with the possible intercalative binding mode (*vide infra*, section 3.3). Unfortunately, the CD signals at the absorption wavelength of the dyes were difficult to interpret due to the extensive noise.

3.5 Comparison of DNA binding affinity between monocationic dyes and dicationic dyes

3.5.1 Double-stranded DNA titration

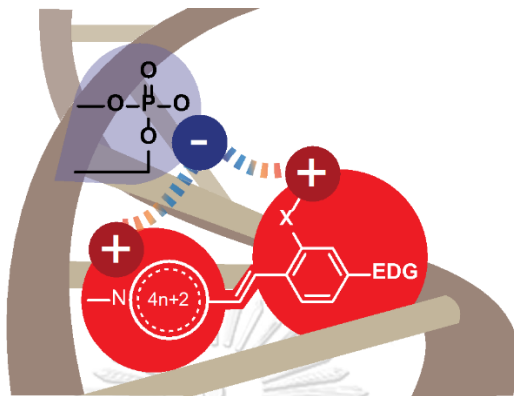


Figure 3.13 The proposed enhancement of electrostatic interaction between dicationic styryl dyes and DNA

The central idea of this work is to enhance the binding interaction between the cationic styryl dyes and DNA by the introduction of an additional positively charged alkoxy sidechain to the dye molecules. The extra positive charge in the dye molecule is expected to increase the electrostatic interaction with the negative charges from the DNA phosphate backbone (Figure 3.13). To determine whether the introduction of an additional positive charge to the dye molecules could improve the binding of the dye with DNA which might be responsible for the observed improvement of color/fluorescence response, the optical properties of the dyes **PY2+(C4)**, **4QL2+**, and **BT2+(NEt₂)** in the absence and presence of dsDNA were compared with those of **PY+**, **4QL+** and **BT+**. As illustrated in Figures 3.14a – c, both UV-visible and fluorescence spectra showed that all dicationic styryl dyes bearing two positive charges in the molecule showed a more obvious response to DNA compared to the corresponding monocationic dyes with only one positive charge in terms of both absorption and fluorescence change. The most dramatic changes were observed in the case of **PY+** and **PY2+(C4)** dyes followed by the **BT+** and

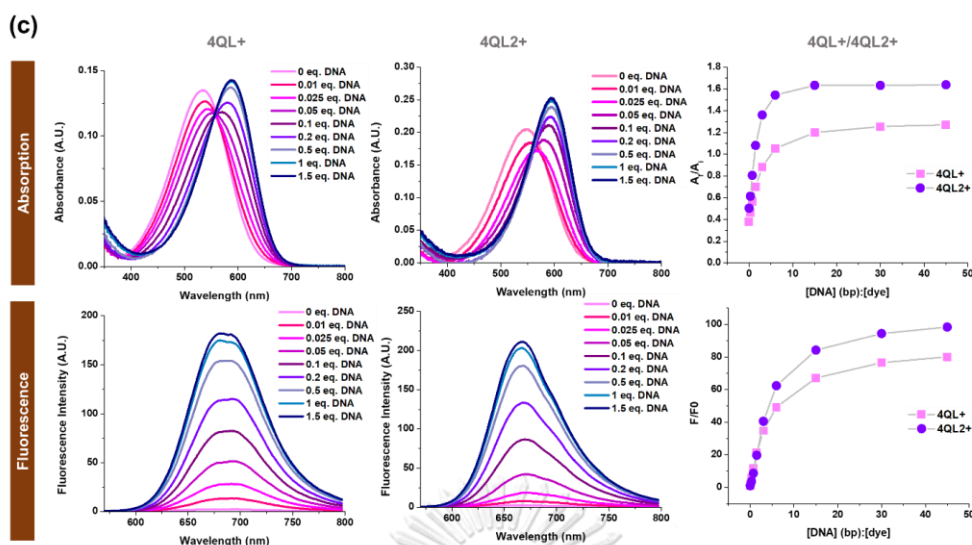


Figure 3.14 UV-vis and fluorescence titration with DNA (3 – 450 μM , in bp) and plot of relative change of maximum absorption (expressed as A_f/A_i , which referred to the ratios between the absorption maxima of the free dye (A_i) and of the DNA-bound dye (A_f)) and maximum fluorescence emission (expressed as F/F_0) (c) vs. concentration ratio of DNA (bp) and the dyes **PY+**/**PY2+(C4)** (a), **BT+**/**BT2+(NEt₂)** (b), **4QL+**/**4QL2+** (c). Conditions: [Dye] = 10 μM , [DNA (in bp)] = 450 μM , except for [BT+] = [BT2+(NEt₂)] = 1 μM , [DNA] = 1.5 μM for fluorescent measurement, **BT2+(OMe)** λ_{ex} = 450 nm, **PY+**, **PY2+(C4)** λ_{ex} = 480 nm, **BT+**, **BT2+(NEt₂)** λ_{ex} = 565 nm, **4QL+**, **4QL2+** λ_{ex} = 548 nm in 10 mM sodium phosphate buffer pH 7.0.

3.5.2 Ionic strength dependence quenching of cationic styryl dyes bound to dsDNA

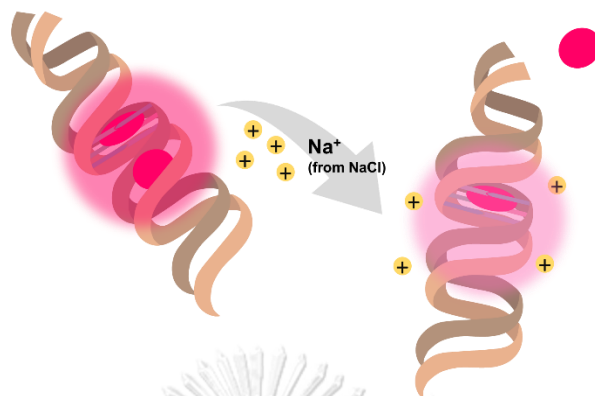


Figure 3.15 Salt displacement principle displaying ionic strength dependence quenching mechanism of cationic styryl dyes bound to dsDNA

The electrostatic interaction is expected to play an important role in enhancing the interaction between the cationic styryl dyes and dsDNA, thus it is expected that the binding strength should be sensitive to the ionic strength. To ascertain this, the ionic strength dependency of dye-DNA binding was investigated in the presence of NaCl as a strong electrolyte. Normally, the decrease in repulsive electrostatic interactions between the phosphate groups on the DNA backbones as the ionic strength increases contributes to the higher stability of the DNA duplexes.^{108, 109} On the other hand, the increase in salt concentration would prevent the positively charged dye from attaching to the DNA double helix.¹³ To evaluate the influence of ionic strength on the interaction of mono- and dicationic dyes with DNA, the dyes **BT+** and **BT2+(NEt₂)** which show the most significant fluorescence change in the presence of DNA were used in this study. The fluorescent intensity data obtained from the microplate reader at different NaCl concentrations was analyzed following the Stern-Volmer equation (equation 4).⁸¹

$$F_0/F = 1 + K_{SV}[Q] \quad (4)$$

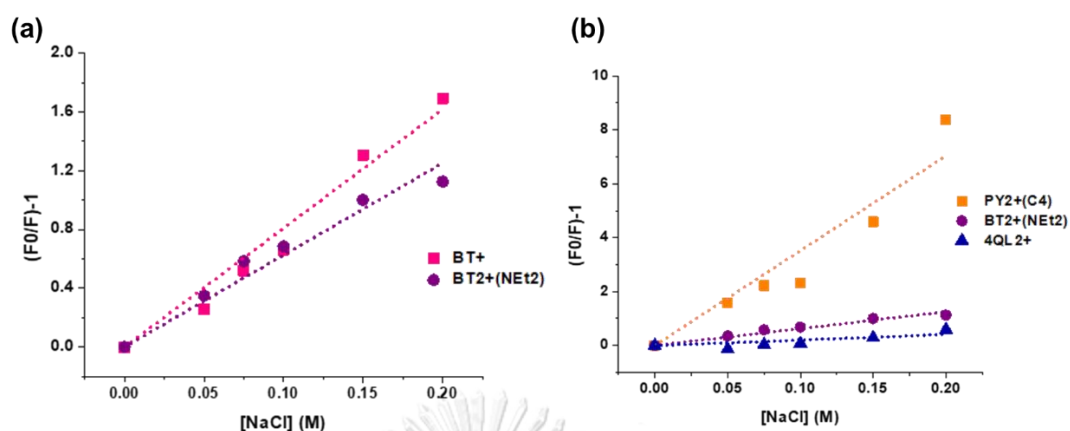


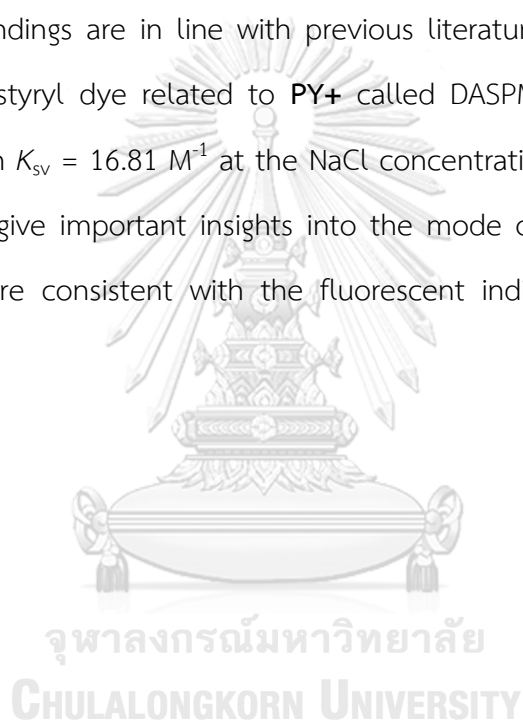
Figure 3.16 Quenching of the complexes of **BT+** and **BT₂+(NEt₂)** (a), **PY₂+(C₄)**, **BT₂+(NEt₂)**, and **4QL₂+** (b) (1 μM) with DNA (15 μM, in bp) in the presence of NaCl (50 mM – 200 mM).

Table 3.3 Quenching constants (K_{SV}) of the cationic styryl dyes

Dye	K_{SV} (M ⁻¹)
BT+	8.09
BT₂+(NEt₂)	6.26
PY₂+(C₄)	35.3
4QL₂+	2.05

As depicted in Table 3.3, the quenching constants (K_{SV}) were determined to be 8.09 and 6.26 M⁻¹ from the NaCl titration experiments of the dye **BT+** and **BT₂+(NEt₂)**, respectively (Figure 3.16a). The results revealed that the introduction of an additional positive charge to the dye molecules enhances the binding affinity with the DNA, leading to a more stable dye-DNA complex. The effect of ionic strength on the DNA binding of the dye **BT₂+(NEt₂)** as well as two other dicationic dyes, namely **PY₂+(C₄)** and **4QL₂+**, were also investigated at a higher NaCl concentration range. In

the presence of NaCl (50 – 200 mM), the observed quenching constants (K_{SV}) were 35.3, 6.26, and 2.05 M^{-1} for the dyes **PY2+(C4)**, **BT2+(NEt₂)**, and **4QL2+**, respectively (Figure 3.16b). Since the intercalation of the dye molecules between the DNA base stacks effectively protects the entrapped dye molecules, the fluorescence of the intercalated dye is not much affected.⁸¹ In contrast, the dye **PY2+(C4)** showed an order of magnitude larger K_{SV} value which is consistent with the fact that this dye only binds to the groove thus making it more susceptible to displacement and quenching. The findings are in line with previous literature,⁸¹ which showed that a pyridinium-based styryl dye related to **PY+** called DASPMI (Figure 1.10a) is a DNA groove binder with $K_{sv} = 16.81 M^{-1}$ at the NaCl concentration range of 10 – 300 mM. Thus, the results give important insights into the mode of binding of the dye-DNA complexes that are consistent with the fluorescent indicator displacement assay results.



3.5.3 Binding constant (K_b) and the number of dsDNA base pairs occupied by one bound dye molecule (n)

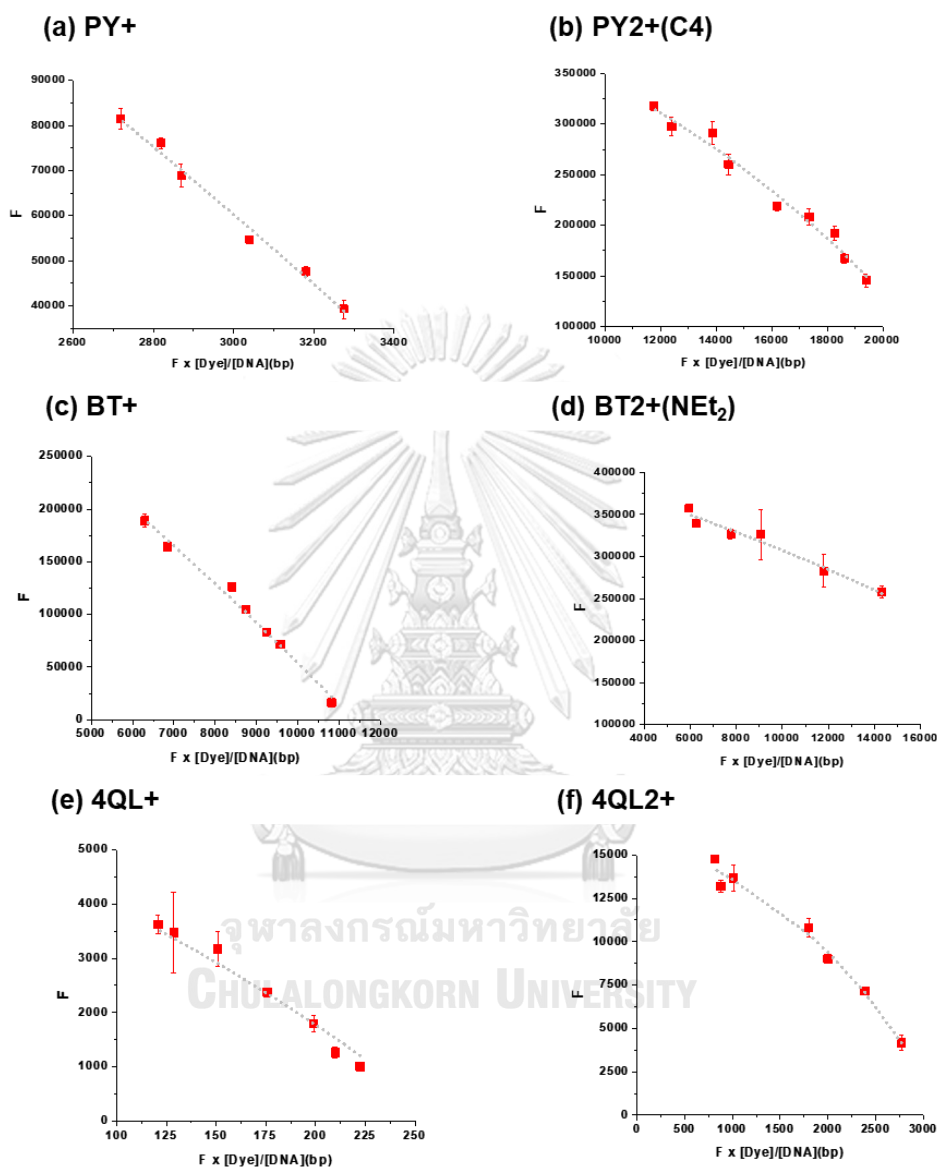


Figure 3.17 Plots of fluorescence intensity dependence on $F \times [Dye]/[DNA]$ (bp) ratio (square) and its approximation by the modified McGhee and von Hippel equation (equation 5) (dotted line) for **PY+** (a), **PY2+(C4)** (b), **BT+** (c), **BT2+(NEt₂)** (d), **4QL+** (e), **4QL2+** (f).

Table 3.4 Binding constant (K_b) and the number of base pairs in dsDNA occupied by one bound dye molecule (n) values of the synthesized styryl dyes^a

Dye	K_b ($\times 10^4$ M ⁻¹)	n
PY+	1.0	4.4
PY2+(C4)	14.1	4.0
BT+	3.5	2.5
BT2+(NEt ₂)	12.1	2.5
4QL+	7.0	2.8
4QL2+	24.5	2.1

^a Conditions: [Dye] = 2 μ M, [DNA (in bp)] = 0.3 – 3 μ M; all measurements were performed in 10 mM sodium phosphate buffer pH 7.0.

The binding constant (K_b) is a useful parameter to describe the binding affinity between DNA and its ligands. The binding constants were determined from the fluorescence titration curves in the linear ranges as determined from the plot of the relative change of maximum fluorescence emission vs. concentration ratio of DNA (bp) and dyes (Figures 3.17a – f). The data were analyzed according to the modified McGhee and von Hippel equation (equation 5).⁸⁸

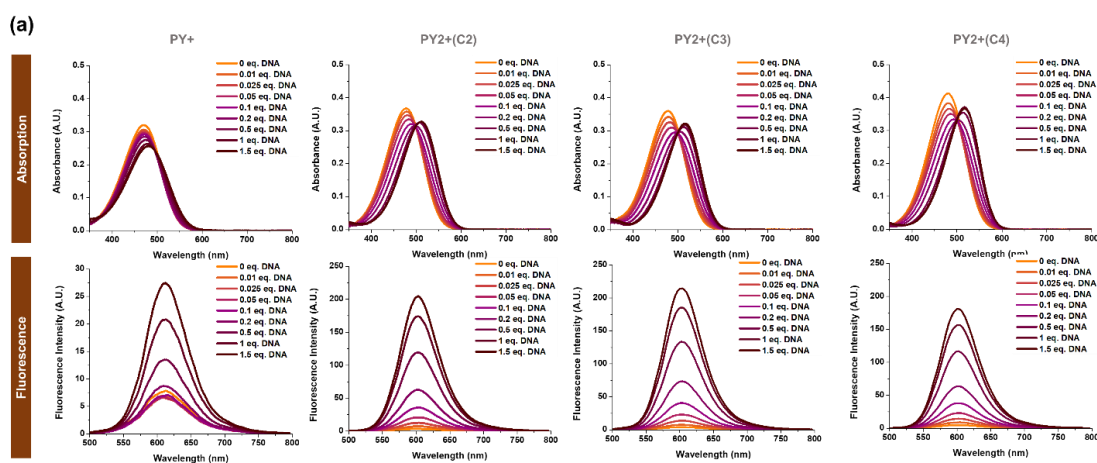
$$Y = F_{\max} - \frac{X}{C_{\text{dye}}K_b} \frac{(1 - [(n-1)\frac{X}{F_{\max}}])^{n-1}}{(1 - n\frac{X}{F_{\max}})^n} \quad (5)$$

where Y = fluorescence intensity at maximum emission wavelength (F) and $X = F \times C_{\text{dye}} / C_{\text{DNA}}$ (bp). Therefore, K_b , n and F_{\max} values can be calculated by non-linear curve fitting of the experimentally obtained data plotted as the dependence of Y on X .

According to the literature, DNA intercalators typically exhibit binding constants (K_b) of less than 10^7 M⁻¹.⁸⁸ Acridine orange (AO), thiazole orange (TO),¹¹⁰ and ethidium bromide¹¹¹ show the K_b values of 5.0×10^4 , 1×10^6 , and 1.5×10^5 M⁻¹,

respectively. Another parameter obtained from the equation is the binding site (n), which describes the number of base pairs required for the ligand molecule to occupy. From the results in Table 3.4, the small n values of **BT+**, **BT2+(NET₂)**, **4QL+**, and **4QL2+** indicate that the dye is likely to interact with DNA via intercalation. The larger n values of **PY+** (4.4) and **PY2+(C4)** (4.0) are more consistent with the groove-binding mode in which at least 3 base pairs would be required for the dye to occupy.⁸⁸ Consistent with the expectation, the larger binding constant of **BT2+(NET₂)** than **BT+** by an order of magnitude also confirms that the introduction of an additional positive charge improves the binding affinity of the dye towards DNA targets as proposed. The same conclusion can be drawn from the **4QL+/4QL2+** and **PY+/PY2+(C4)** pairs as well. Therefore, the obtained binding parameters (K_b and n) fully support the original hypothesis that the introduction of the positive charge to the styryl dye could improve its DNA binding affinity as reflected by the larger binding constants and better responsiveness of the dicationic dyes compared to the monocationic dyes. The acquired binding parameters of **BT+** ($K_b = 3.5 \times 10^4 \text{ M}^{-1}$, $n = 2.5$) were in accordance with another related dye that carries the $-\text{NMe}_2$ group as the aromatic substituent, in which the $K_b = 1.8 \times 10^4 \text{ M}^{-1}$ and $n = 3.4$ were reported.⁸⁸

3.5.4 Effect of linker length



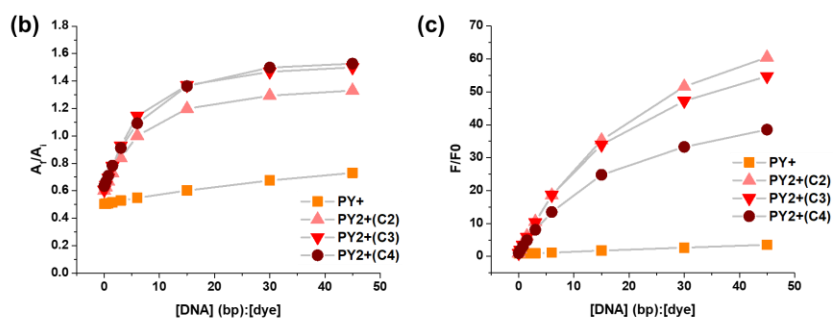


Figure 3.18 UV-vis and fluorescence titration with DNA (3 – 450 μM , in bp) (a) and plot of relative change of maximum absorption (expressed as A_f/A_i , which referred to the ratios between the absorption maxima of the free dye (A_i) and of the DNA-bound dye (A_f)) (b) and maximum fluorescence emission (expressed as F/F_0) (c) vs. concentration ratio of DNA (bp) and the dyes with different linker length (PY+, PY2+(C2), PY2+(C3) and PY2+(C4)). Conditions: [Dye] = 10 μM , [DNA (in bp)] = 3 - 450 μM , λ_{ex} = 480 nm in 10 mM sodium phosphate buffer pH 7.0.

The fluorescence and absorption properties of the monocationic dye PY+ and the dicationic dyes PY2+(C2), PY2+(C3), and PY2+(C4) bearing different linkers were studied to determine the effect of the length of the linker joining the positively charged quaternary ammonium group and the aromatic ring. In the presence of dsDNA, the PY2+(C2) and PY2+(C3) dyes exhibited the largest fluorescence response, as shown in Figure 3.18b. The PY2+(C4) dye showed a somewhat lower fluorescence response, but it was still significantly larger than the control PY+ dye. The findings reveal that the introduction of an additional positive charge improves the dye's fluorescence response to DNA and that the shorter linker length appeared to improve the fluorescence response better. However, when compared to the effect of introducing the positive charge, the effect of linker length was much less significant.

The results from the UV spectra in Figure 3.18c did not exactly follow the same trend as the fluorescence spectra when compared between dicationic styryl dyes with different linkers. In the presence of dsDNA, the dyes **PY2+(C2)** and **PY2+(C4)** showed the most red-shifted absorption spectra, followed by the dye **PY2+(C2)**. Nevertheless, when compared to the monocationic dye **PY+**, all dicationic dyes displayed considerably more noticeable absorption changes. Accordingly, the colorimetric responses also follow the same overall trend as fluorescence studies whereby the linker length had only minor effects on the dyes' responsiveness to DNA compared to the presence of an additional positive charge.

3.6 DNA sequence selectivity

All studies reported so far focused on only one “average” dsDNA sequence. To determine the possible sequence-dependent responsiveness of the dicationic styryl dyes, the studies were next performed with various DNA sequences to investigate the responsiveness of the developed dyes towards DNA with different base sequences. As shown in Table 2.1, an additional 8 ssDNA and dsDNA sequences were included in the study. This can be classified into ssDNA and dsDNA groups. The ssDNA group consisted of dA₂₀, dT₂₀, dC₂₀, and dG₂₀ to compare the intrinsic responsiveness of the dyes towards different nucleobases. In the dsDNA group, d(AT)₁₀, d(GC)₁₀, Block(AT), and Block(GC) were chosen as representative dsDNA with well-defined sequences. The sequences of the latter four DNA were self-complementary, hence all should form AT and GC rich duplexes with alternating purine/pyrimidine (d(AT)₁₀, d(GC)₁₀) or with short (5bp) purine/pyrimidine (Block(AT), Block(GC)) stretches.

In the preliminary screening experiments by direct visual observation under UV light, different dyes showed different responsiveness towards different DNA sequences (Figure 3.19). Most dyes showed more pronounced responsiveness

towards dsDNA over ssDNA, with the exception of dG₂₀ where secondary structures such as G-quadruplex could also form. The dyes with the diethylamino substituent [PY2+ and BT2+(NEt₂)] show a small preference for GC- over AT-rich DNA sequences, while the dyes with a methoxy substituent (BT2+(OMe)) showed more pronounced responsiveness towards AT-rich over GC-rich sequences. The quinoline dye 4QL2+ showed the smallest responsiveness, and the difference among different dsDNA sequences was small. Nevertheless, the selectivity between dsDNA over ssDNA follows the same trend as other dyes.

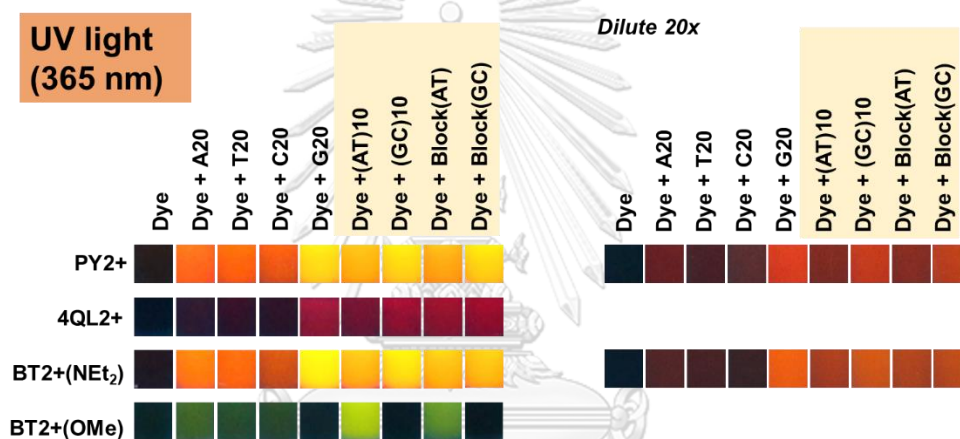


Figure 3.19 Preliminary visual screening of the responsiveness of the dyes towards different base sequence. Condition: [Dye] = 50 μ M, [dsDNA (bp)] = 100 μ M; all experiments were performed in 10 mM sodium phosphate buffer pH 7.0.

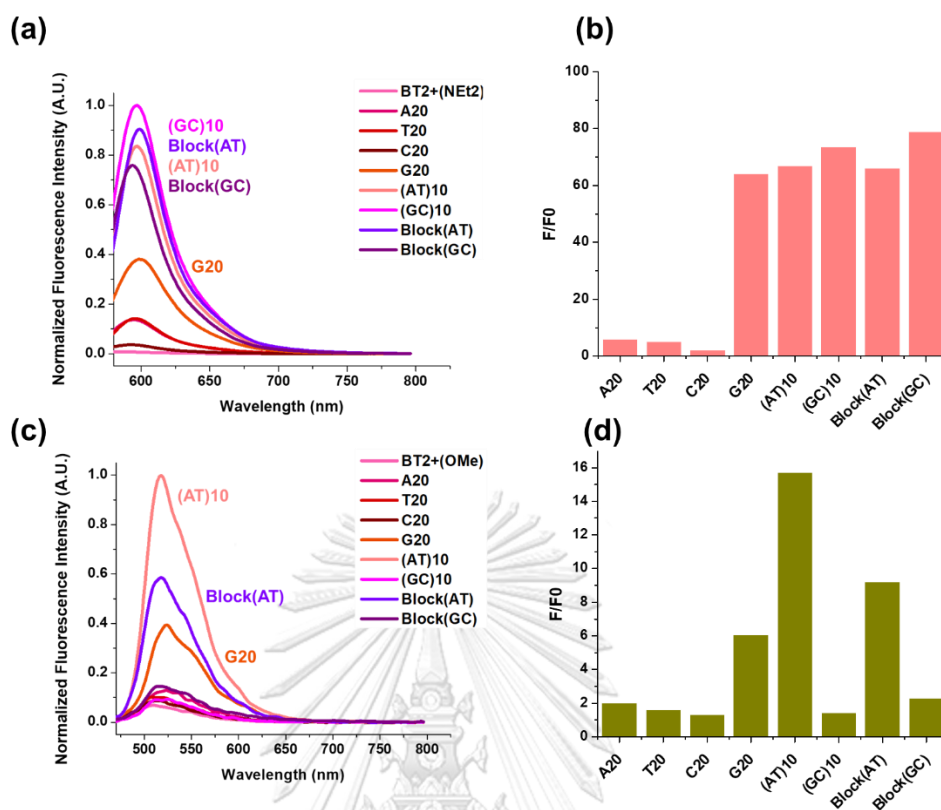


Figure 3.20 Normalized fluorescence spectra of **BT2+(NET₂)** (a) and **BT2+(OMe)** (c) towards different nucleobases DNA sequences and bar graphs represented responsiveness of **BT2+(NET₂)** (b) and **BT2+(OMe)** (d) towards different nucleobases DNA sequences using F/F_0 ratio. Condition: [Dye] = 1 μ M, [DNA (bp)] = 40 μ M, **BT2+(OMe)** λ_{ex} = 450 nm, **BT2+(NET₂)** λ_{ex} = 565 nm 10 mM sodium phosphate buffer pH 7.0.

Next, the two styryl dyes with the same BT2+ core but carrying different electron-donating substituents (**BT2+(NET₂)** and **BT2+(OMe)**) that show distinctive behaviors towards AT- and GC-rich DNA based on the visual screening results in Figure 3.20 were selected for more detailed spectroscopic studies. In line with the previous experiments (vide supra, section 3.2), the fluorescence spectra of **BT2+(NET₂)** dye bearing a strong electron-donating diethylamino substituent showed the emission maxima at a longer wavelength compared to **BT2+(OMe)** carrying the

weak electron-donating methoxy substituent. This is in agreement with the observed orange and green fluorescence for the dyes **BT2+(NEt₂)** and **BT2+(OMe)**, respectively. The nature of the electron-donating substituents not only affected the dye colors but also related to binding characteristics with DNAs. From the normalized fluorescence spectra in Figure 3.20, both dyes showed better responsiveness towards dsDNA over ssDNA (with the exception of dG₂₀ as mentioned earlier). In line with the visual screening experiments, the **BT2+(OMe)** showed good selectivity for AT-rich dsDNA sequences, whereby the fluorescence of the dye increased significantly only in the presence of d(AT)₁₀ and Block(AT) DNAs. In the case of dG₂₀ ssDNA, it should be noted that the fluorescence response of dyes towards this particular sequence is likely due to the formation of secondary structures in G-rich sequences such as the parallel G-quadruplex¹¹² that may interact with the dye differently when compared to typical ssDNA.

The availability of two dyes with different fluorescence emission wavelengths and distinctive base sequence selectivities could lead to some interesting applications in DNA sensing. It was proposed that a combination of two dyes – one responds to GC and AT in a non-discriminatory manner whereas the other only responds to AT – should allow the measurement of relative quantities of AT and CG bases in the amplified DNA mixture by measuring the ratio of the emission of the two dyes. This should give more reliable results than employing just one dye because the signal of only one of the dyes in the pair will change while the other remains constant, and hence can be used as a reference.

Preliminary experiments were carried out using a combination of the dyes **BT2+(NEt₂)** vs **BT2+(OMe)** for the detection of DNA with different AT/GC contents. In the absence of any DNA, the dye mixture exhibited low fluorescence when excited at the shorter of the two dyes' excitation wavelengths. In the presence of DNA, the

fluorescence of **BT2+(OMe)** was selectively enhanced in the presence of $d(AT)_{10}$. On the other hand, the fluorescence of **BT2+(NEt₂)** was enhanced with both $d(AT)_{10}$ and $d(GC)_{10}$ (Figure 3.21a). Unfortunately, the fluorescence spectra of the two dyes are not well-resolved. In subsequent studies, the non-selective dye was changed from **BT2+(NEt₂)** to **4QL2+**, which resulted in a much better-resolved fluorescence spectrum. The fluorescence emission of the **4QL2+** dye, on the other hand, was rather weak due to the low quantum yield together with the non-optimal excitation wavelength (Figure 3.21b). Accordingly, the ratios of the two dyes were adjusted by increasing the molar ratio of the **4QL2+** in the dye mixture to obtain a comparable response when excited at the **BT2+(OMe)** wavelength. At a molar ratio of **BT2+(OMe):4QL2+** = 1:3, both dyes exhibited almost the same level of fluorescence response in the presence of an equimolar mixture of $d(GC)_{10}$ and $d(AT)_{10}$. When the ratio of the two DNAs changed, it can be seen that the intensity of the orange signal at 670 nm was relatively constant, but the green signal at 530 nm changed according to the presence or absence of $d(AT)_{10}$ (Figure 3.21c). Naked eye observation in fluorescence mode revealed the same trend, thus this system is potentially useful for measuring of GC-rich DNA whereby the green signal which should be independent of the amount of GC-rich DNA can be used as a reference to provide a more reliable measurement than using just one dye. The possible application of this concept towards the identification of GC-rich trinucleotide repeats will be further investigated in collaboration with Dr. Chitanon Buranachai from Prince of Songkhla University.

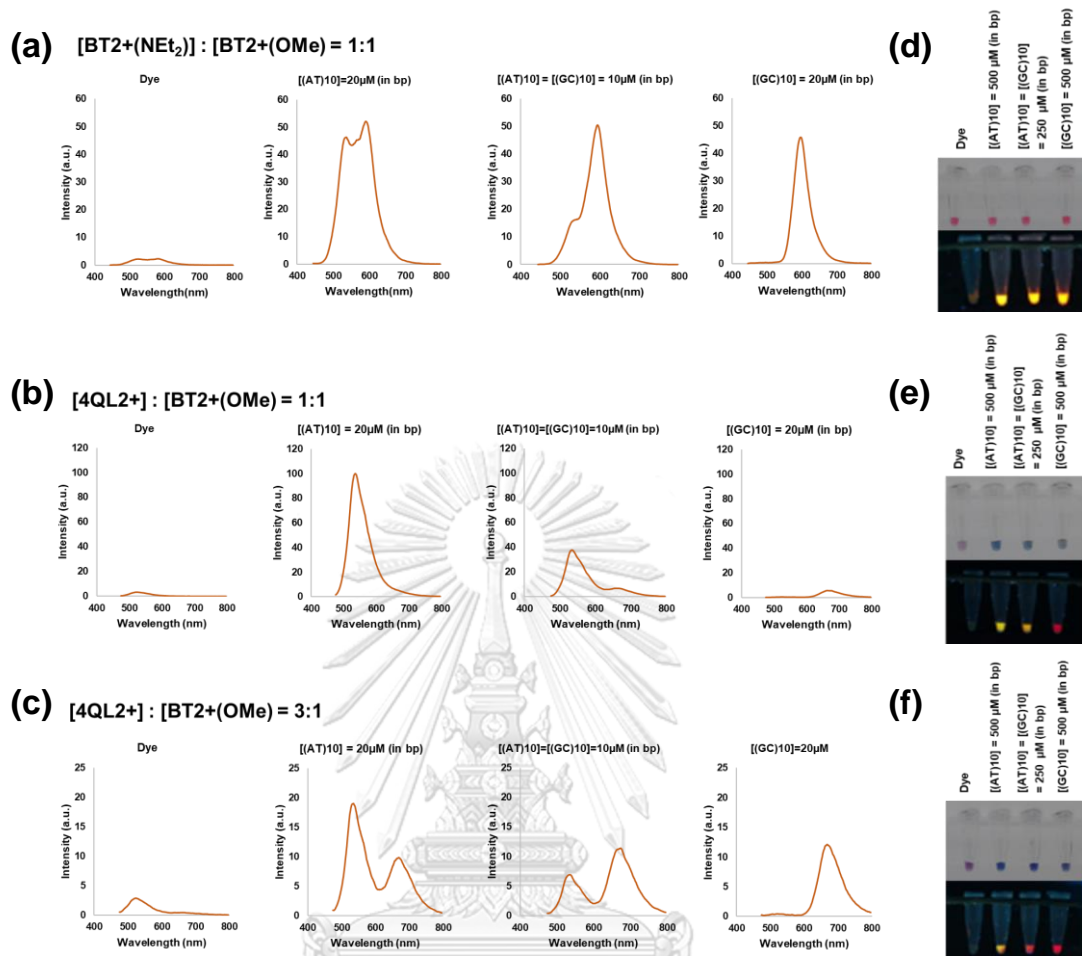


Figure 3.21 Fluorescent properties of the dyes mixture **BT2+(NEt₂)** and **BT2+(OMe)** (a),(d) or **4QL2+** and **BT2+(OMe)** (b), (c), (e) and (f) in the absence and presence of DNA mixture with different AT/CG compositions. Conditions: Fluorescence detection [dye] = 2 μ M (each) with the exception of [4QL2+] in (c) = 6 μ M, [DNA] = 20 μ M (total, in bp), λ_{ex} = 460 nm, Naked-eye detection dye = 50 μ M (each) with the exception of [4QL2+] in (f) = 150 μ M, [DNA] = 500 μ M (total, in bp), UV light = 365 nm.; All experiments were performed in 10 mM sodium phosphate buffer pH 7.0.

3.7 Docking simulation for DNA-dye interaction study

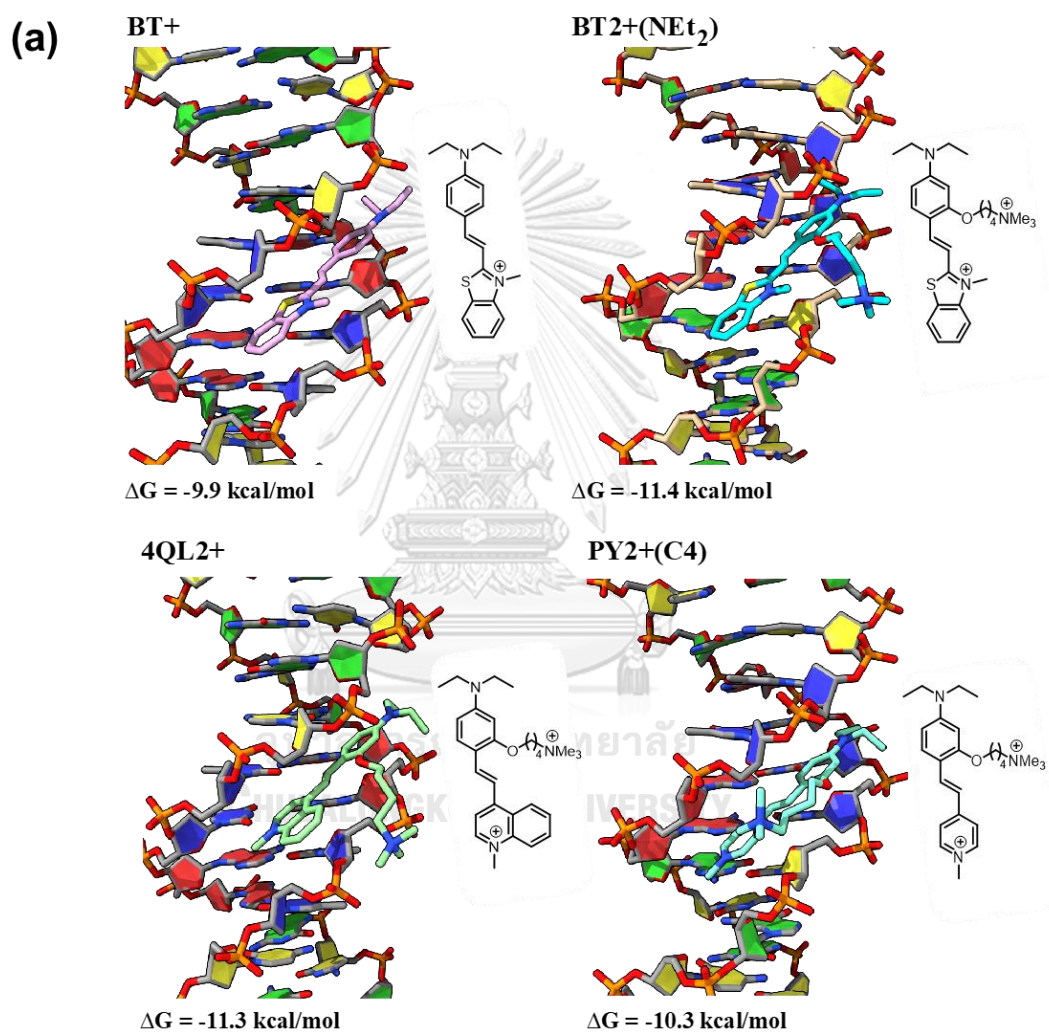
(This part of the work was performed by Dr. Jaru Taechalertrpaisarn from Department of Chemistry and Biochemistry, University of California, Santa Cruz, California, United States)

Molecular dockings of four styryl dyes carrying the $-\text{NEt}_2$ substituent (**BT+**, **BT2+(NEt₂)**, **PY2+(C4)**, and **4QL2+**) were performed with AutoDock 4.2.6⁹³ to further evaluate the binding affinity improvement of the dicationic styryl dyes toward dsDNA and their modes of binding. The dihedral angle between electron-rich aromatic and heteroaromatic moieties was fixed at 0° to enhance their ICT via donor-acceptor conjugation due to the increase in fluorescence intensity upon binding on DNA.

In the case of minor groove interaction, a crystal structure of the Drew-Dickerson DNA duplex (4C64)¹¹³ was used as a representative model. The electrostatic interaction of the quaternary amine sidechain to the phosphate backbone was shown by comparing binding energies of the monocationic (**BT+**; -9.9 kcal/mol) and dicationic dyes (**BT2+(NEt₂)**; -11.4 kcal/mol). Among the dicationic dyes, **BT2+(NEt₂)** and **PY2+(C4)** preferred to bind at the AT region, but **4QL2+** slightly altered its binding position toward the CG region to accommodate the larger quinoline ring (Figure 3.22a). **BT2+(NEt₂)** showed a slightly lower binding energy (-11.4 kcal/mol) than **4QL2+** (-11.3 kcal/mol) and **PY2+(C4)** (-10.3 kcal/mol). In all docking structures, the positively charged side chain can indeed interact with the phosphate backbone as proposed.

For the intercalative binding mode, an average NMR solution structure of a DNA complex with a dimeric intercalator dye TOTO (108D) was selected as the initial structure because of the close structural similarity between styryl dyes and thiazole orange.¹¹⁴ Similar to the minor groove interaction, the binding energy of **BT2+(NEt₂)** was more negative than **BT+** by approximately 1.6 kcal/mol (-9.0 vs -7.4 kcal/mol).

All three dicationic dyes fit into the intercalation site and their positive charged sidechains interacted with phosphate backbone similar to the minor-groove model (Figure 3.22b). The dye **4QL2+** showed a slightly lower binding energy (-9.5 kcal/mol) than **BT2+(NEt₂)** (-9.0 kcal/mol) and **PY2+(C4)** (-8.4 kcal/mol) possibly due to its favorable π - π stacking of quinoline to the nucleobases.



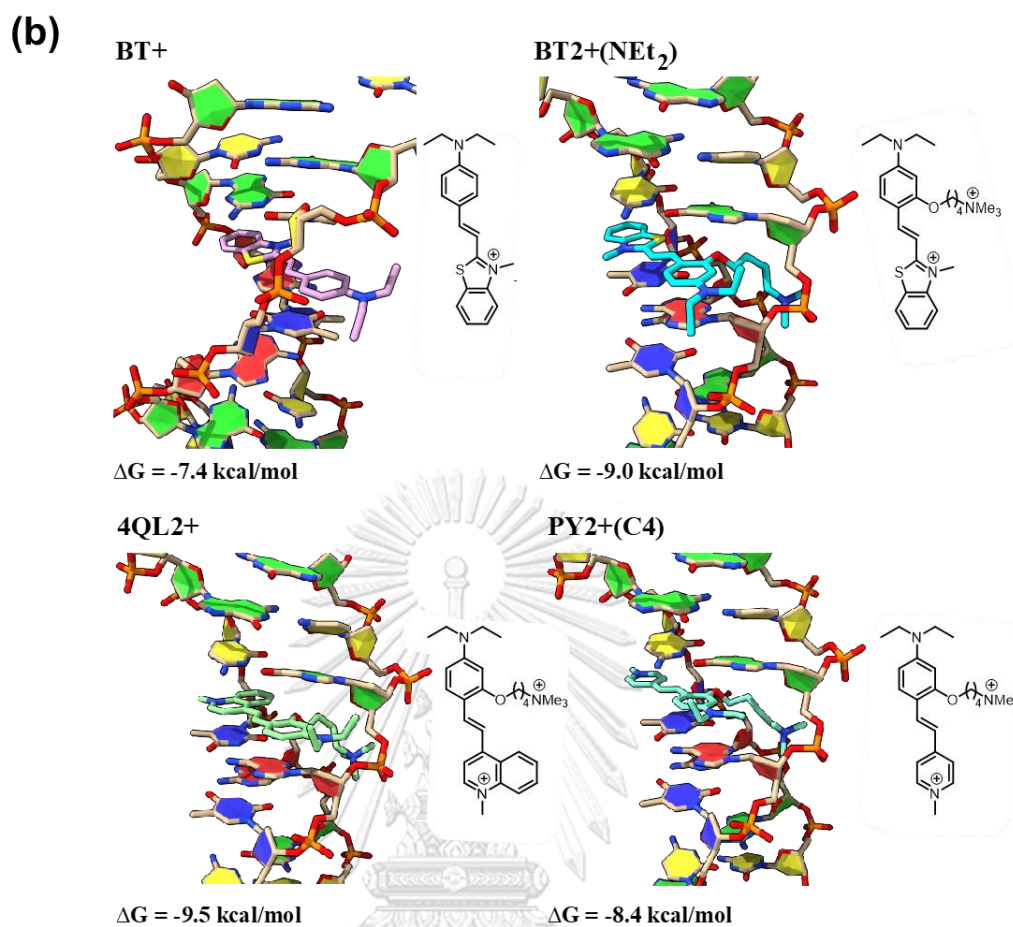


Figure 3.22 Molecular docking of **BT+**, **BT2+(NEt₂)**, **4QL2+** and **PY2+(C4)** on a minor-groove DNA (4C64) (a) and at an intercalative site of DNA (108D) (b)

Overall, styryl dyes are 2 kcal/mol more favorable to minor-groove interaction, supporting prior experimental results that **PY2+(C4)** serves as a groove binder. On the other hand, the strong negative binding energies of **BT2+(NEt₂)** and **4QL2+** in both minor groove and intercalative modes suggest that these dyes can act as both groove binders and intercalators. The more negative binding energies of dicationic styryl dyes compared to the corresponding monocationic styryl dyes support the hypothesis and experimental results that the introduction of the positively charged quaternary ammonium sidechain improves the DNA duplex binding affinity. When monocationic and dicationic dye structures are compared, the

only main difference is the additional positively charged sidechain. The DNA-bound dicationic dyes tended to lose more entropy due to the restriction of the alkoxy chain movement. However, the more negative binding energies in the case of dicationic dyes suggested the more favorable enthalpy, which can be explained by the compensation by the electrostatic interaction. This is also further shown by the proximity of the positively charged ammonium group and the negatively charged phosphate DNA backbone according to the docking models.

3.8 Limit of detection of cationic styryl dyes for DNA detection in fluorescence and colorimetric modes

Table 3.5 Comparison of the limit of detection of cationic styryl dyes for the determination of dsDNA by fluorescence and UV-visible spectrophotometry ^a

Dyes	Detection method			
	Fluorescence		Absorption	
	λ_{ex} (nm)/ λ_{em} (nm)	LOD (ng/mL)	A_f (nm)/ A_i (nm)	LOD (ng/mL)
PY+	480 / 600	276 (15.0 nM)	520 / 480	5918 (321 nM)
PY2+(C4)	480 / 600	35 (1.9 nM)	520 / 480	583 (32 nM)
BT+	565 / 600	4.1 (0.22 nM)	560 / 530	3213 (174 nM)
BT2+(NEt ₂)	565 / 600	1.2 (0.07 nM)	560 / 530	973 (53 nM)
4QL+	548 / 670	57 (3.1 nM)	600 / 550	1666 (90 nM)
4QL2+	548 / 670	50 (2.7 nM)	600 / 550	433 (23.5 nM)

^a Conditions: [Dye] = 2 μM , [DNA (in bp)] = 0.3 – 3 μM ; all measurements were performed in 10 mM sodium phosphate buffer pH 7.0.

The responsiveness of mono- and dicationic styryl dyes towards dsDNA in the low concentration ranges was next investigated. For the fluorescence method, the maximum fluorescence intensities of the dye at a fixed concentration and at least five DNA concentrations were used to construct the calibration curve. For the

absorption method, the A_f/A_i ratios, which reflected the relative change of the maximum absorption (similar to Figure 3.14), as determined from the absorption spectra of the dye in the presence of excess DNA at a fixed dye concentration and various concentrations of DNA were used. Based on the $(3 \times SD)/\text{slope}$ of the calibration curve, the limits of detection (LODs) were determined as shown in Table 3.5. All dicationic dyes showed lower LODs than the corresponding monocationic styryl dyes with the same heteroaromatic core structures. **BT2+(NEt₂)** was the most responsive dicationic styryl dye, exhibiting higher sensitivity than the existing commercially DNA fluorescent staining dyes including ethidium bromide (10 – 33 ng/mL),^{115, 116} Hoechst 33258 (10 ng/mL),¹¹⁷ and 4-Di-1-ASP (5 ng/mL).⁴⁴ Moreover, the sensitivity of **BT2+(NEt₂)** for the DNA detection was comparable with the bis-cyanine dyes including TOTO and YOYO (0.5 ng/mL), which revealed the potential of the developed dicationic styryl dye considering its more simple structure when compared to the previously reported sophisticated dimeric dyes. An application of **BT2+(NMe₂)** for the fluorescence detection of amplified pathogenic bacterial DNA have been recently demonstrated in a previous study by Srimongkol et al.⁹⁰

In terms of colorimetric detection of dsDNA, poorer sensitivity than fluorescence detection was observed for all cationic styryl dyes studied (Table 3.5). Nevertheless, the simplicity of the colorimetric assay is highly attractive for the point-of-care DNA detection that is more convenient to perform than the fluorescence assay, at the expense of sensitivity. Until now, there is only a limited collection of commercially available colorimetric dyes for DNA assays. When compared to the leuco-triphenylmethane dyes (LCV) that have recently been introduced as a colorimetric dye for the detection of DNA with a relatively high LOD of 7,100 ng/mL,²⁶ the dicationic styryl dyes **PY2+(C4)**, **BT2+(NEt₂)**, and **4QL2+** showed far better LODs thus offering more sensitive colorimetric DNA detection (LODs in the

range of 400 – 1,000 ng/mL). Moreover, the detection limits of the dicationic dyes for the colorimetric detection of DNA were better than the corresponding monocationic dye and were comparable with the unmodified gold nanoparticle-PNA platform (50 nM or less).²⁹ The dye **4QL2+** which showed the most pronounced spectral shift in the presence of dsDNA was the most sensitive dye for the dsDNA assay, giving the LOD of 23.5 nM. These results suggest that the introduction of the additional positive charge to the dye molecule improved the DNA detection sensitivity in both the fluorescence and colorimetric assays. Consequently, these new dicationic styryl dyes are suitable for the fluorescence and colorimetric detection of nucleic acid targets in various applications.¹¹⁸

3.9 Applications of dicationic styryl dyes in cell imaging

(This part of the work was performed by Mr. Kriangsak Faikhruea under supervision of Dr. Chanat Aonbangkhaen)

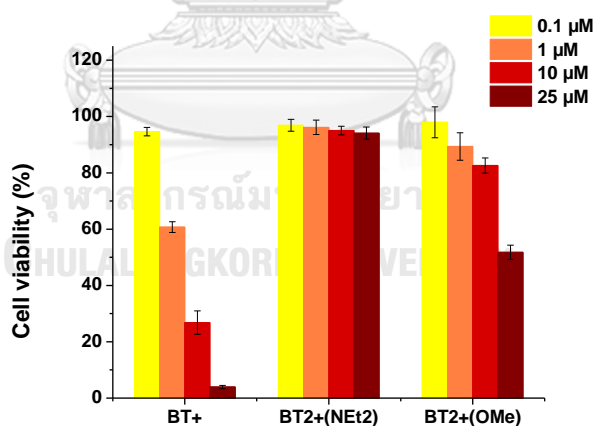


Figure 3.23 Cytotoxicity study of **BT+**, **BT2+(NEt₂)** and **BT2+(OMe)** by MTT assay (HeLa cells, 1×10^4 cells per plate, 24 h incubation)

To evaluate the suitability of the dicationic styryl dyes for cellular nucleic acids imaging, HeLa cells were stained with the dyes **BT2+(NEt₂)** and **BT2+(OMe)**.

Interestingly, the dicationic dyes appeared to be less cytotoxic when compared to the monocationic dye (**BT+**) at the same concentrations. The cells appeared healthy at dye concentrations in the high micromolar range. MTT assays confirmed that the cell viability was not affected when treating the cells with either dye at a concentration up to 25 μM for 24 h (Figure 3.23).

Next, live cell staining and imaging experiments were performed using the same HeLa cells as a model. Co-staining with DAPI, which selectively stains cellular nuclei,¹¹⁹ was performed in all cell staining experiments. The dye **BT2+(NEt₂)** stained several parts of the whole cell, resulting in a high fluorescent signal all over the cells, but the brightest area appeared in the nucleoli regions which serve as the site for ribosome synthesis and RNA assembly.¹²⁰ The ability to stain nucleoli and chromosomes of the monocationic dye **BT+** has recently been reported.⁷¹ Based on the structural similarity between **BT+** and **BT2+(NEt₂)**, we proposed that **BT2+(NEt₂)** might bind to the same target(s) as the **BT+** dye. However, the ability of **BT2+(NEt₂)** to stain other locations in the cells suggests that it may also bind to several other kinds of cellular nucleic acids including mitochondrial DNA, ribosomal RNA, other cytoplasmic nucleic acids, and nucleic acids in the nucleus.

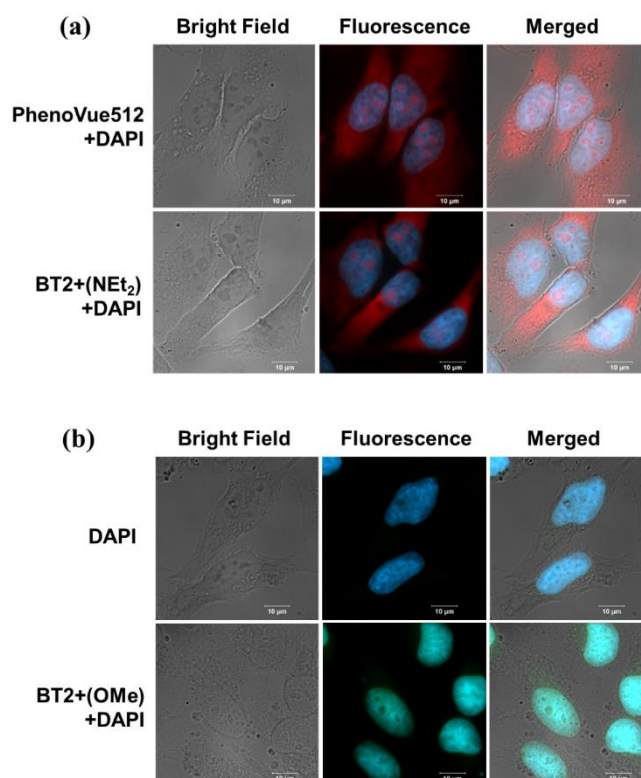


Figure 3.24 Fluorescence image analysis of HeLa cells treated with indicated compound at of PhenoVue512 (500nM) and **BT2+(NEt₂)** (20 μM) (a), DAPI (0.2 μg/mL) and **BT2+(OMe)** (200 μM) (b). Cells (5×10^4 cells/well) were incubated for 18 h in complete media (DMEM with 10% fetal bovine serum and 1% penicillin) prior to imaging. Excitation wavelengths of 561 nm was used for **BT2+(NEt₂)** and PhenoVue512 (500 nM) and 488 nm was used for **BT2+(OMe)** and DAPI. In all cases, co-staining with DAPI to visualize the nuclei was performed. Scale bars = 10 μm.

To verify this hypothesis, a staining experiment with PhenoVue512, a nucleic acid stain displaying a higher fluorescence response when complexed with RNA compared to DNA that can be used for nucleoli staining, was performed in comparison. The result in Figure 3.24a showed the similar cell staining behaviors of PhenoVue512 and **BT2+(NEt₂)**. Also, **BT2+(NEt₂)** staining showed higher fluorescence

intensity with nucleoli area than in other parts of nuclei. Although the RNA binding behavior of **BT2+(NEt₂)** is currently uninvestigated, these results suggested that the dye may bind to secondary structures of rRNA that are partly double-stranded. Other parts of the nuclei were not stained by this dye. In another recent study on a series of dyes related to **4QL+**, it was reported that the histones forming the nucleosomes on cellular DNA hindered the dye binding, thus resulting in a lower fluorescent response.⁶⁵ Collectively, the results indicated that **BT2+(NEt₂)** can stain several cellular nucleic acids, especially RNA in the nucleoli.

It should be noted that the **BT2+(OMe)** dye responded selectively to AT-rich DNA similar to DAPI (Section 3.6). Interestingly, they also share the same cell nuclei staining characteristics (Figure 3.24b). Consequently, the dye showed a different staining behavior, whereby the staining was limited to the nuclei of the cells and completely co-localized with DAPI, suggesting that they similarly stain DNA in the nuclei.

3.10 Mercury(II) detection platform based on cationic styryl dyes and DNA aptamer

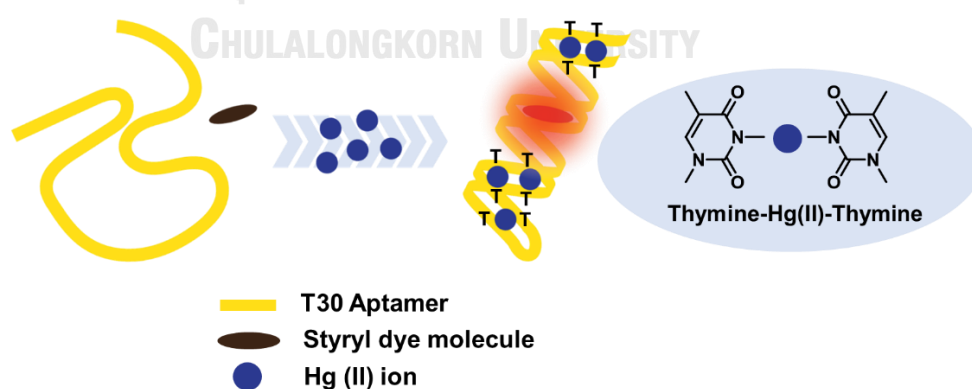


Figure 3.25 Detection platform for mercury(II) ions based on cationic styryl dyes and dT₃₀ DNA aptamer

Aptamers are short oligonucleotides (DNA or RNA) designed to specifically bind to a target molecule of interest (“ligand”) through myriads of non-covalent interactions, including electrostatic, hydrophobic, π - π stacking, and hydrogen bonding interactions. Taking the advantage of the dicationic styryl dye that is responsive towards dsDNA over ssDNA, an aptamer-based assay of Hg(II) was developed in this study. The working principle relied on the specific interaction between the thymine nucleobase in the DNA strands and mercury(II) ions¹²¹ which can form a stable T-Hg(II)-T base pair. In the absence of the mercury(II) ion, the single-stranded T-rich DNA sequence (Hg(II) aptamer) should adopt a random-coiled structure that cannot form stable complexes with the dye thus low fluorescence is to be expected. However, in the presence of mercury(II) ions, the formation of thymine-Hg(II)-thymine complexes should result in the folding or association of the aptamer into dsDNA-like structures that allow the dye to bind and give a fluorescence response. Such principle has been demonstrated in several examples employing commercially available nucleic acid stains¹²² or gold nanoparticles.^{123, 124} In this study, the cationic styryl dyes that show excellent fluorescent response towards dsDNA were proposed as an alternative dye for the aptamer-based detection of mercury(II) ion (Figure 3.25).

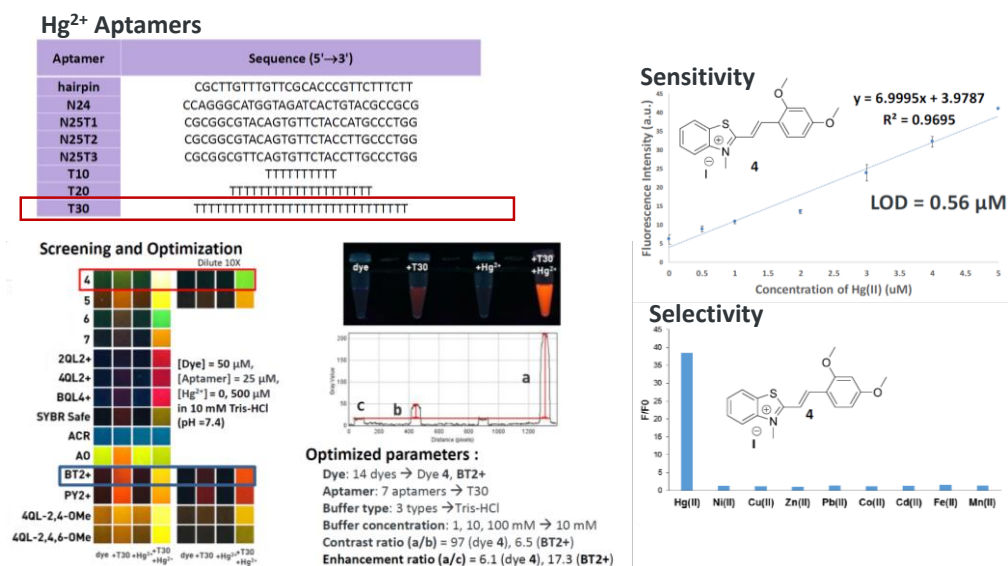


Figure 3.26 The styryl dye-aptamer based mercury(II) detection platform developed by Tiarpattaradilok ⁹⁴

Some preliminary experiments have been conducted by Ms. Duangkamol Tiarpattaradilok.⁹⁴ The findings as summarized in Figure 3.26 suggested that the combination of dT₃₀ as the Hg(II) aptamer and a monocationic styryl dye 2-(2',4'-dimethoxy)styryl)-3-methylbenzothiazol-3-ium iodide (BT+(2,4-OMe)) in Tris-HCl buffer (pH 7.4) yielded the best distinction between the free and mercury-bound aptamers. Screening experiments with various metal ions to determine the selectivity confirmed that the fluorescence response was indeed highly selective for the mercury(II) ion. However, although the calibration curve between Hg(II) concentration and fluorescence signal showed a good linear correlation ($r^2 = 0.9695$) over the range of 0 – 5 μM Hg(II), the limit of detection (LOD) was rather poor (560 nM or 0.56 μM).

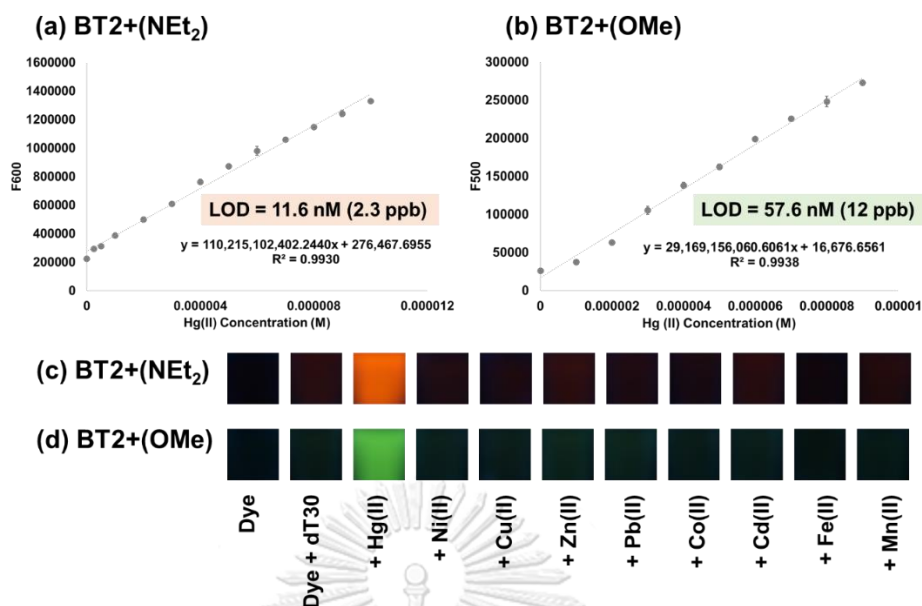


Figure 3.27 Calibration curves and LODs for the developed mercury(II) detection platform based on dT₃₀ aptamer and cationic styryl dyes **BT2+(NEt₂)** (a) and **BT2+(OMe)** (b). Condition: [dye] = 2 μ M, [dT₃₀] = 1 μ M, [Hg(II)] = 0 – 10 μ M. Screening experiments with various metal ions to determine the selectivity of the developed platform for **BT2+(NEt₂)** (c) and **BT2+(OMe)** (d). Condition: [dye] = 50 μ M, [dT₃₀] = 25 μ M, [metal (II)] = 500 μ M, observed under UV illumination (365 nm); all measurements were performed in 10 mM Tris-HCl buffer pH 7.4.

In this study, the monocationic styryl dye **BT+(2,4-OMe)** previously used in Tiarpattaradilok's work⁹⁴ was replaced with the dicationic benzothiazolium-based styryl dyes **BT2+(NEt₂)** and **BT2+(OMe)** under the same conditions with the aim to improve the sensitivity further. Indeed, the dye **BT2+(NEt₂)** which is the most sensitive dye for DNA detection according to this study showed a satisfactory detection limit towards mercury(II) ion with an LOD of 11.6 nM (2.3 ppb) over the range of 0 – 10 μ M Hg(II). The obtained detection limit is sufficient to measure Hg(II) in industrial wastewaters according to Thailand Ministry of Industry's Industrial Wastewaters Standard¹²⁵ which stated that the level of Hg(II) must not exceed 0.005

mg/L (5 ppb or 25 nM). The dicationic styryl dye **BT2+(OMe)** with methoxy substituents showed a somewhat higher detection limit at 57.6 nM (12 ppb), which was still 10 times more sensitive than the corresponding methoxy-substituted monocationic styryl dye **BT+(2,4-OMe)**. The results confirmed that the introduction of more positive charges to the styryl dye molecule could improve the sensitivity for the aptamer-based detection of small molecules such as Hg(II) in addition to the detection of DNA.

It should be noted that the obtained calibration curves are not perfectly linear. In the presence of a low concentration of Hg(II), between 0 – 2 equiv. of Hg(II) compared to the aptamer strand concentration, the fluorescence was only modestly increased, resulting in a less steep slope. Beyond this point, a steeper slope was obtained when the Hg(II) concentration was increased. This suggests that at low concentrations of Hg(II), the aptamer was not yet properly folded leading to low fluorescence enhancement. At higher Hg(II) concentration, the dsDNA-like structure of Hg(II)-bound aptamer was formed, resulting in a greater fluorescence response. The same pattern was also observed in the preliminary experiments from Tiarpattaradilok work.⁹⁴ Furthermore, the fluorescence response was demonstrated to be selective to only the mercury(II) ion, as determined by screening studies with several metal ions (Figures 3.27c – d), which confirmed the high performance of the developed platform.

CHAPTER IV

CONCLUSION

In this dissertation, new dicationic styryl dyes carrying the pyridinium (**PY2+(C2)**, **PY2+(C3)**, and **PY2+(C4)**), benzothiazolium (**BT2+(NEt₂)**), and quinolinium (**4QL2+**) heteroaromatic cores connected to an aromatic ring bearing the -NEt₂ group as the electron-donating substituent through a vinylene linker have been developed. The key molecular design was the incorporation of a positively charged modifier to the aromatic ring part with the aim to improve the binding affinity to DNA through electrostatic interactions with the negatively charged phosphate backbone. It was proposed that such enhanced electrostatic interaction should improve the DNA responsiveness of the dyes compared with the previously known monocationic dyes (**PY+**, **BT+**, and **4QL+**) without the positively charged groups. The additional positive charge was introduced to the dye molecules via a quaternary ammonium group (-NMe₃⁺) attached to the electron-rich aromatic ring via a flexible alkoxy linker. To further investigate the effect of heteroaromatic moieties, **2QL2+**, **TMIN2+**, and **AD2+** were also designed with the same aromatic part. Moreover, the effect of substituent on the aromatic ring was investigated by comparing the dyes carrying a strong electron-donating substituent (-NEt₂) (**BT2+(NEt₂)**) to a weak electron-donating aromatic substituent (-OMe) in the dye **BT2+(OMe)**.

The equivalent pairs of monocationic and dicationic styryl dyes were compared in terms of optical characteristics, DNA binding interaction, and responsiveness in colorimetric and fluorescence mode. All dyes exhibited weak emission in the free state because of the rapid rotation of the central C=C leading to non-emissive relaxation pathways. However, strong fluorescence enhancement (up to 126 times for **BT2+(NEt₂)**) and a bathochromic shift of the absorption spectra (up to 48 nm for **4QL2+**) are observed in the presence of dsDNA with good selectivity

over other types of molecules including proteins and other anionic polymers. In agreement with the proposed design, the dicationic dyes consistently provided higher binding affinity towards dsDNA and more pronounced fluorescence and colorimetric responses than the monocationic dyes. In comparison to the additional positive charge, the length of the linker joining the trimethylammonium group and the aromatic ring showed a relatively minor influence on the optical responsiveness of the dyes towards DNA.

Screening of the dicationic styryl dyes with various DNA sequences revealed that most of the dyes showed better responsiveness towards dsDNAs over ssDNAs (except for dG₂₀ which could form secondary structures like G-quadruplexes). Serendipitously, the **BT2+(OMe)** showed good selectivity for AT-rich dsDNA sequences. This could lead to some potential DNA sensing applications that rely on the use of two dyes displaying different fluorescence emission wavelengths and unique base sequence selectivity. A preliminary investigation of the possibility of using a dye mixture, one that responds to GC nucleobases non-discriminatorily and the other that exclusively responds to AT nucleobases, to determine the relative amounts of AT and CG bases in a DNA mixture by taking the two dyes' emission ratios was successfully demonstrated.

From the study of the binding interaction between the dyes and DNA, both experimental investigation and theoretical calculation by docking experiments supported that the styryl dyes mainly bound to the DNA minor groove. According to the dye displacement titration and binding parameters determination, the benzothiazolium- and quinolinium-based styryl dyes were proposed to bind to DNA as groove binders and intercalators, whereas the pyridinium-based styryl dyes only act as a groove binder. With detection limits (LODs) between 1.2 and 50 ng/mL in the fluorescence mode and 400 and 1,000 ng/mL in the colorimetric mode, these dicationic dyes exhibited superior sensitivity for the detection of DNA to the

corresponding monocationic dyes and compare favorably with many existing commercial nucleic acid stains.

In terms of applications, the dicationic styryl dyes **BT2+(NEt₂)** and **BT2+(OMe)** were demonstrated as live-cell staining dyes which showed good cell permeability with low cytotoxicity. Also, the use of the dicationic styryl dyes **BT2+(NEt₂)** and **BT2+(OMe)** was shown to enhance the performance of the aptamer-based mercury(II) detection platform by providing an order of magnitude better detection limits when compared to the corresponding monocationic dyes while still maintaining excellent selectivity.



REFERENCES

1. Watson, J. D.; Crick, F. H. C., Molecular Structure of Nucleic Acids: A Structure for Deoxyribose Nucleic Acid. *Nature* **1953**, *171* (4356), 737-738.
2. Kulkarni, J. A.; Witzigmann, D.; Thomson, S. B.; Chen, S.; Leavitt, B. R.; Cullis, P. R.; van der Meel, R., The current landscape of nucleic acid therapeutics. *Nat. Nanotechnol.* **2021**, *16* (6), 630-643.
3. Gunn, P.; Walsh, S.; Roux, C., The nucleic acid revolution continues – will forensic biology become forensic molecular biology? *Front. genet.* **2014**, *5* (44).
4. Jingui, F.; Xudong, Z.; Chen, W.; Lingfei, S., Applications of DNA Technologies in Agriculture. *Curr Genomics* **2016**, *17* (4), 379-386.
5. Dooley, J. S. G., Nucleic acid probes for the food industry. *Biotechnol. Adv.* **1994**, *12* (4), 669-677.
6. Stains, labels and detection strategies for nucleic acids assays. *Ann. Clin. Biochem.* **2002**, *39* (2), 114-129.
7. Nolan, T.; Hands, R. E.; Bustin, S. A., Quantification of mRNA using real-time RT-PCR. *Nature Protocols* **2006**, *1* (3), 1559-1582.
8. Tie, L.; Xiao, H.; Wu, D.-l.; Yang, Y.; Wang, P., A brief guide to good practices in pharmacological experiments: Western blotting. *Acta Pharmacol. Sin.* **2021**, *42* (7), 1015-1017.
9. Maddox, J., Understanding gel electrophoresis. *Nature* **1990**, *345* (6274), 381-381.
10. Stellwagen, N. C., Electrophoresis of DNA in agarose gels, polyacrylamide gels and in free solution. *ELECTROPHORESIS* **2009**, *30* (S1), S188-S195.
11. Tost, J.; Gut, I. G., DNA analysis by mass spectrometry—past, present and future. *J. Mass Spectrom.* **2006**, *41* (8), 981-995.
12. Almaqwashi, A. A.; Zhou, W.; Naufer, M. N.; Riddell, I. A.; Yilmaz, Ö. H.; Lippard, S. J.; Williams, M. C., DNA Intercalation Facilitates Efficient DNA-Targeted Covalent Binding of Phenanthriplatin. *J. Am. Chem. Soc.* **2019**, *141* (4), 1537-1545.
13. Mohammad, M.; Al Rasid Gazi, H.; Pandav, K.; Pandya, P.; Islam, M. M.,

- Evidence for Dual Site Binding of Nile Blue A toward DNA: Spectroscopic, Thermodynamic, and Molecular Modeling Studies. *ACS Omega* **2021**, *6* (4), 2613-2625.
14. Yarmoluk, S. M.; Kovalska, V. B.; Volkova, K. D., Optimized Dyes for Protein and Nucleic Acid Detection. In *Advanced Fluorescence Reporters in Chemistry and Biology III: Applications in Sensing and Imaging*, Demchenko, A. P., Ed. Springer Berlin Heidelberg: Berlin, Heidelberg, 2011; pp 161-199.
 15. Sánchez, M. I.; Martínez-Costas, J.; Gonzalez, F.; Bermudez, M. A.; Vázquez, M. E.; Mascareñas, J. L., In Vivo Light-Driven DNA Binding and Cellular Uptake of Nucleic Acid Stains. *ACS Chem. Biol.* **2012**, *7* (7), 1276-1280.
 16. Ma, Y.; Zhang, G.; Pan, J., Spectroscopic Studies of DNA Interactions with Food Colorant Indigo Carmine with the Use of Ethidium Bromide as a Fluorescence Probe. *J. Agric. Food Chem.* **2012**, *60* (43), 10867-10875.
 17. Huang, J.; Wang, Z.; Kim, J.-K.; Su, X.; Li, Z., Detecting Arbitrary DNA Mutations Using Graphene Oxide and Ethidium Bromide. *Anal. Chem.* **2015**, *87* (24), 12254-12261.
 18. Haines, A. M.; Tobe, S. S.; Kobus, H. J.; Linacre, A., Properties of Nucleic Acid Staining Dyes Used In Gel Electrophoresis. *ELECTROPHORESIS* **2015**, *36* (6), 941-944.
 19. Zhussupova, A., *PCR-diagnostics*. Litres: 2022.
 20. Stone, A. L.; Bradley, D. F., Aggregation of Acridine Orange Bound to Polyanions: The Stacking Tendency of Deoxyribonucleic Acids. *J. Am. Chem. Soc.* **1961**, *83* (17), 3627-3634.
 21. *Acridine Orange hydrochloride hydrate*; SDS No.318337[Online]; Sigma-Aldrich: SINGAPORE, April 14, 2022. <https://www.sigmaaldrich.com/TH/en/sds/sial/318337> (accessed June 18, 2022).
 22. Wang, M.; Dilek, I.; Armitage, B. A., Electrostatic Contributions to Cyanine Dye Aggregation on Peptide Nucleic Acid Templates. *Langmuir* **2003**, *19* (16), 6449-6455.
 23. Komiyama, M.; Ye, S.; Liang, X.; Yamamoto, Y.; Tomita, T.; Zhou, J. M.; Aburatani, H., PNA for one-base differentiating protection of DNA from nuclease and its use for SNPs detection. *J. Am. Chem. Soc.* **2003**, *125* (13), 3758-62.
 24. Dong, J.; Chen, G.; Wang, W.; Huang, X.; Peng, H.; Pu, Q.; Du, F.; Cui, X.; Deng, Y.; Tang, Z., Colorimetric PCR-Based microRNA Detection Method Based on Small Organic Dye and Single Enzyme. *Anal. Chem.* **2018**, *90* (12), 7107-7111.

25. Seifert, J. L.; Connor, R. E.; Kushon, S. A.; Wang, M.; Armitage, B. A., Spontaneous Assembly of Helical Cyanine Dye Aggregates on DNA Nanotemplates. *J. Am. Chem. Soc.* **1999**, *121* (13), 2987-2995.
26. Miyamoto, S.; Sano, S.; Takahashi, K.; Jikihara, T., Method for Colorimetric Detection of Double-Stranded Nucleic Acid Using Leuco Triphenylmethane Dyes. *Anal. Biochem.* **2015**, *473*, 28-33.
27. Roy, S.; Mohd-Naim, N. F.; Safavieh, M.; Ahmed, M. U., Colorimetric Nucleic Acid Detection on Paper Microchip Using Loop Mediated Isothermal Amplification and Crystal Violet Dye. *ACS Sensors* **2017**, *2* (11), 1713-1720.
28. Rycenga, M.; Cobley, C. M.; Zeng, J.; Li, W.; Moran, C. H.; Zhang, Q.; Qin, D.; Xia, Y., Controlling the Synthesis and Assembly of Silver Nanostructures for Plasmonic Applications. *Chem. Rev.* **2011**, *111* (6), 3669-3712.
29. Li, H.; Rothberg, L., Colorimetric Detection of DNA Sequences based on Electrostatic Interactions with Unmodified Gold Nanoparticles. *Proc. Natl. Acad. Sci. U.S.A.* **2004**, *101* (39), 14036-14039.
30. Franco, R.; Pedrosa, P.; Carlos, F. F.; Veigas, B.; Baptista, P. V., Gold Nanoparticles for DNA/RNA-Based Diagnostics. In *Handbook of Nanoparticles*, Aliofkhazraei, M., Ed. Springer International Publishing: Cham, 2016; pp 1339-1370.
31. Thaxton, C. S.; Georganopoulou, D. G.; Mirkin, C. A., Gold nanoparticle probes for the detection of nucleic acid targets. *Clin. Chim. Acta* **2006**, *363* (1), 120-126.
32. Faikhruea, K.; Choopara, I.; Somboonna, N.; Assavalapsakul, W.; Kim, B. H.; Vilaivan, T., Enhancing Peptide Nucleic Acid–Nanomaterial Interaction and Performance Improvement of Peptide Nucleic Acid-Based Nucleic Acid Detection by Using Electrostatic Effects. *ACS Appl. Bio Mater.* **2022**, *5* (2), 789-800.
33. Kabatc, J.; Jędrzejewska, B.; Orliński, P.; Paćzkowski, J., The Synthesis and the Solvent and Substituent Effect on the Spectroscopic Characteristic of 3-Ethyl-2-(p-Substitued Styryl)Benzothiazolium Iodides. *Spectrochim. Acta A Mol. Biomol. Spectrosc.* **2005**, *62* (1), 115-125.
34. Ziarani, G. M.; Moradi, R.; Lashgari, N.; Kruger, H. G., Chapter 8 - Cyanine Dyes. In *Metal-Free Synthetic Organic Dyes*, Ziarani, G. M.; Moradi, R.; Lashgari, N.; Kruger, H. G.,

Eds. Elsevier: 2018; pp 127-152.

35. Ren, C.-B.; Wang, J.-J.; Qin, C.-X.; Wang, K.; Gao, Q.; Cheng, S.; Dai, L.-X.; Chen, G.-Q., Research Progress in Hemicyanine-Based Polymers. *Des. Monomers Polym.* **2011**, *14* (6), 541-558.
36. Cho, Y.; An, H. J.; Kim, T.; Lee, C.; Lee, N. K., Mechanism of Cyanine5 to Cyanine3 Photoconversion and Its Application for High-Density Single-Particle Tracking in a Living Cell. *J. Am. Chem. Soc.* **2021**, *143* (35), 14125-14135.
37. Daehne, S.; Resch-Genger, U.; Wolfbeis, O. S., *Near-infrared dyes for high technology applications*. Springer Science & Business Media: 1998; Vol. 52.
38. Xu, Y.; Liu, Y.; Qian, X., Novel cyanine dyes as fluorescent pH sensors: PET, ICT mechanism or resonance effect? *J. Photochem. Photobiol* **2007**, *190* (1), 1-8.
39. Choi, H. S.; Nasr, K.; Alyabyev, S.; Feith, D.; Lee, J. H.; Kim, S. H.; Ashitate, Y.; Hyun, H.; Patonay, G.; Strekowski, L.; Henary, M.; Frangioni, J. V., Synthesis and In Vivo Fate of Zwitterionic Near-Infrared Fluorophores. *Angew. Chem. Int. Ed.* **2011**, *50* (28), 6258-6263.
40. Li, J.; Gan, F., Dynamic storage performance of two cyanine dye films and optimization design for a recordable compact disk. *Appl. Opt.* **2000**, *39* (20), 3525-3530.
41. Hirche, C.; Murawa, D.; Mohr, Z.; Kneif, S.; Hünerbein, M., ICG fluorescence-guided sentinel node biopsy for axillary nodal staging in breast cancer. *Breast Cancer Res. Treat.* **2010**, *121* (2), 373-378.
42. Haugland, R. P., Handbook of fluorescent probes and research chemicals. *Molecular Probes*, Eugene **1996**, 8.
43. Deligeorgiev, T. G.; Zaneva, D. A.; Kim, S. H.; Sabnis, R. W., Preparation of monomethine cyanine dyes for nucleic acid detection. *Dyes Pigm.* **1998**, *37* (3), 205-211.
44. Zhu, C.-Q.; Zhuo, S.-J.; Zheng, H.; Chen, J.-L.; Li, D.-H.; Li, S.-H.; Xu, J.-G., Fluorescence Enhancement Method for the Determination of Nucleic Acids Using Cationic Cyanine as a Fluorescence Probe. *Analyst* **2004**, *129* (3), 254-258.
45. Kretschy, N.; Sack, M.; Somoza, M. M., Sequence-Dependent Fluorescence of Cy3- and Cy5-Labeled Double-Stranded DNA. *Bioconjug. Chem.* **2016**, *27* (3), 840-848.
46. Duthie, R. S.; Kalve, I. M.; Samols, S. B.; Hamilton, S.; Livshin, I.; Khot, M.;

- Nampalli, S.; Kumar, S.; Fuller, C. W., Novel Cyanine Dye-Labeled Dideoxynucleoside Triphosphates for DNA Sequencing. *Bioconjug. Chem.* **2002**, *13* (4), 699-706.
47. Agbavwe, C.; Somoza, M. M., Sequence-Dependent Fluorescence of Cyanine Dyes on Microarrays. *PLOS ONE* **2011**, *6* (7), e22177.
48. Evenson, W. E.; Boden, L. M.; Muzikar, K. A.; O'Leary, D. J., ¹H and ¹³C NMR Assignments for the Cyanine Dyes SYBR Safe and Thiazole Orange. *J. Org. Chem.* **2012**, *77* (23), 10967-10971.
49. Vasilev, A. A.; Kandinska, M. I.; Stoyanov, S. S.; Yordanova, S. B.; Sucunza, D.; Vaquero, J. J.; Castaño, O. D.; Balushev, S.; Angelova, S. E., Halogen-containing thiazole orange analogues – new fluorogenic DNA stains. *Beilstein J. Org. Chem.* **2017**, *13*, 2902-2914.
50. Nygren, J.; Svanvik, N.; Kubista, M., The interactions between the fluorescent dye thiazole orange and DNA. *Biopolymers* **1998**, *46* (1), 39-51.
51. Lee, L. G.; Chen, C.-H.; Chiu, L. A., Thiazole orange: A new dye for reticulocyte analysis. *Cytometry* **1986**, *7* (6), 508-517.
52. Zhang, L.; Liu, X.; Lu, S.; Liu, J.; Zhong, S.; Wei, Y.; Bing, T.; Zhang, N.; Shanguan, D., Thiazole Orange Styryl Derivatives as Fluorescent Probes for G-Quadruplex DNA. *ACS Appl. Bio Mater.* **2020**, *3* (5), 2643-2650.
53. Hövelmann, F.; Seitz, O., DNA Stains as Surrogate Nucleobases in Fluorogenic Hybridization Probes. *Acc. Chem. Res.* **2016**, *49* (4), 714-723.
54. Vilaivan, T., Fluorogenic PNA probes. *Beilstein J. Org. Chem.* **2018**, *14*, 253-281.
55. Ditmangklo, B.; Boonlua, C.; Suparpprom, C.; Vilaivan, T., Reductive Alkylation and Sequential Reductive Alkylation-Click Chemistry for On-Solid-Support Modification of Pyrrolidinyl Peptide Nucleic Acid. *Bioconjugate Chem.* **2013**, *24* (4), 614-625.
56. Deligeorgiev, T.; Vasilev, A.; Kaloyanova, S.; Vaquero, J. J., Styryl Dyes – Synthesis and Applications During the Last 15 Years. *Color. Technol.* **2010**, *126* (2), 55-80.
57. Heilbron, I. M.; Walker, G. H.; Buck, J. S., XCVIII.—Styrylbenzopyrylium Salts. Part V. Distyryl Derivatives of 7-Hydroxy-2 : 4-Dimethylbenzopyrylium Chloride. *J. Chem. Soc., Trans* **1925**, *127* (0), 690-696.
58. Vasilev, A.; Deligeorgiev, T.; Gadjev, N.; Kaloyanova, S.; Vaquero, J. J.; Alvarez-

- Builla, J.; Baeza, A. G., Novel Environmentally Benign Procedures for the Synthesis of Styryl Dyes. *Dyes Pigm.* **2008**, *77* (3), 550-555.
59. O'Regan, B.; Grätzel, M., A Low-Cost, High-Efficiency Solar Cell Based On Dye-Sensitized Colloidal TiO₂ Films. *Nature* **1991**, *353* (6346), 737-740.
60. Fedorova, O. A.; Andryukhina, E. N.; Fedorov, Y. V.; Panfilov, M. A.; Alfimov, M. V.; Jonusauskas, G.; Grelard, A.; Dufourc, E., Supramolecular Assemblies of Crown-Containing 2-Styrylbenzothiazole with Amino Acids. *Org. Biomol. Chem.* **2006**, *4* (6), 1007-1013.
61. Gust, D.; Moore, T. A., Mimicking Photosynthesis. *Science* **1989**, *244* (4900), 35.
62. Krieg, R.; Eitner, A.; Günther, W.; Halbhuber, K. J., Optimization of Heterocyclic 4-Hydroxystyryl Derivatives for Histological Localization of Endogenous and Immunobound Peroxidase Activity. *Biotech. Histochem.* **2007**, *82* (4-5), 235-262.
63. Gwon, S.-Y.; Rao, B. A.; Kim, H.-S.; Son, Y.-A.; Kim, S.-H., Novel Styrylbenzothiazolium Dye-Based Sensor for Mercury, Cyanide and Hydroxide Ions. *Spectrochim. Acta A Mol. Biomol. Spectrosc.* **2015**, *144*, 226-234.
64. Krieg, R.; Eitner, A.; Halbhuber, K.-J., Tailoring and Histochemical Application of Fluorescent Homo-Dimeric Styryl Dyes Using Frozen Sections: From Peroxidase Substrates to New Cytochemical Probes for Mast Cells, Keratin, Cartilage and Nucleic Acids. *Acta Histochem.* **2011**, *113* (7), 682-702.
65. Saady, A.; Varon, E.; Jacob, A.; Shav-Tal, Y.; Fischer, B., Applying Styryl Quinolinium Fluorescent Probes for Imaging of Ribosomal RNA in Living Cells. *Dyes Pigm.* **2020**, *174*, 107986.
66. Przhonska, O. V.; Webster, S.; Padilha, L. A.; Hu, H.; Kachkovski, A. D.; Hagan, D. J.; Van Stryland, E. W., Two-Photon Absorption in Near-IR Conjugated Molecules: Design Strategy and Structure–Property Relations. In *Advanced Fluorescence Reporters in Chemistry and Biology I: Fundamentals and Molecular Design*, Demchenko, A. P., Ed. Springer Berlin Heidelberg: Berlin, Heidelberg, 2010; pp 105-147.
67. Haidekker, M. A.; Nipper, M.; Mustafic, A.; Lichlyter, D.; Dakanali, M.; Theodorakis, E. A., Dyes with Segmental Mobility: Molecular Rotors. In *Advanced Fluorescence Reporters in Chemistry and Biology I: Fundamentals and Molecular Design*, Demchenko, A. P., Ed. Springer Berlin Heidelberg: Berlin, Heidelberg, 2010; pp

267-308.

68. Lee, J. W.; Jung, M.; Rosania, G. R.; Chang, Y.-T., Development of Novel Cell-Permeable DNA Sensitive Dyes Using Combinatorial Synthesis and Cell-Based Screening. *Chem. Commun.* **2003**, (15), 1852-1853.
69. Li, Q.; Kim, Y.; Namm, J.; Kulkarni, A.; Rosania, G. R.; Ahn, Y.-H.; Chang, Y.-T., RNA-Selective, Live Cell Imaging Probes for Studying Nuclear Structure and Function. *Chem. Biol.* **2006**, *13* (6), 615-623.
70. Bohländer, P. R.; Wagenknecht, H.-A., Synthesis and Evaluation of Cyanine–Styryl Dyes With Enhanced Photostability for Fluorescent DNA Staining. *Org. Biomol. Chem.* **2013**, *11*, 7458-7462.
71. Wang, K.-N.; Chao, X.-J.; Liu, B.; Zhou, D.-J.; He, L.; Zheng, X.-H.; Cao, Q.; Tan, C.-P.; Zhang, C.; Mao, Z.-W., Red fluorescent probes for real-time imaging of the cell cycle by dynamic monitoring of the nucleolus and chromosome. *Chem. Commun.* **2018**, *54* (21), 2635-2638.
72. Schwartz, J. W.; Blakely, R. D.; DeFelice, L. J., Binding and Transport in Norepinephrine Transporters: REAL-TIME, SPATIALLY RESOLVED ANALYSIS IN SINGLE CELLS USING A FLUORESCENT SUBSTRATE*. *J. Biol. Chem.* **2003**, *278* (11), 9768-9777.
73. Feng, G.; Luo, X.; Lu, X.; Xie, S.; Deng, L.; Kang, W.; He, F.; Zhang, J.; Lei, C.; Lin, B.; Huang, Y.; Nie, Z.; Yao, S., Engineering of Nucleic Acids and Synthetic Cofactors as Holo Sensors for Probing Signaling Molecules in the Cellular Membrane Microenvironment. *Angew. Chem. Int. Ed.* **2019**, *58* (20), 6590-6594.
74. Ditmangklo, B.; Taechalertpaisarn, J.; Siriwong, K.; Vilaivan, T., Clickable styryl dyes for fluorescence labeling of pyrrolidinyl PNA probes for the detection of base mutations in DNA. *Org. Biomol. Chem.* **2019**, *17* (45), 9712-9725.
75. Abeywickrama, C. S.; Wijesinghe, K. J.; Stahelin, R. V.; Pang, Y., Lysosome imaging in cancer cells by pyrene-benzothiazolium dyes: An alternative imaging approach for LAMP-1 expression based visualization methods to avoid background interference. *Bioorg. Chem.* **2019**, *91*, 103144.
76. Dahal, D.; Pokhrel, S.; McDonald, L.; Bertman, K.; Paruchuri, S.; Konopka, M.; Pang, Y., NIR-Emitting Hemicyanines with Large Stokes' Shifts for Live Cell Imaging: from Lysosome to Mitochondria Selectivity by Substituent Effect. *ACS Appl. Bio Mater.* **2019**,

2 (9), 4037-4043.

77. Kovalska, V. B.; Kryvorotenko, D. V.; Balanda, A. O.; Losytsky, M. Y.; Tokar, V. P.; Yarmoluk, S. M., Fluorescent Homodimer Styrylcyanines: Synthesis and Spectral-Luminescent Studies in Nucleic Acids and Protein Complexes. *Dyes Pigm.* **2005**, *67* (1), 47-54.

78. Mahmood, T.; Paul, A.; Ladame, S., Synthesis and Spectroscopic and DNA-Binding Properties of Fluorogenic Acridine-Containing Cyanine Dyes. *J. Org. Chem.* **2010**, *75* (1), 204-207.

79. Tokar, V. P.; Losytsky, M. Y.; Kovalska, V. B.; Kryvorotenko, D. V.; Balanda, A. O.; Prokopets, V. M.; Galak, M. P.; Dmytruk, I. M.; Yashchuk, V. M.; Yarmoluk, S. M., Fluorescence of Styryl Dyes-DNA Complexes Induced by Single- and Two-Photon Excitation. *J. Fluoresc.* **2006**, *16* (6), 783-791.

80. 2-[4-(Dimethylamino)styryl]-1-methylpyridinium iodide.
<https://www.sigmaaldrich.com/TH/en/product/aldrich/280135> (accessed June 18, 2022).

81. Sahoo, D.; Bhattacharya, P.; Chakravorti, S., Quest for Mode of Binding of 2-(4-(Dimethylamino)styryl)-1-Methylpyridinium Iodide With Calf Thymus DNA. *J. Phys. Chem. B* **2010**, *114* (5), 2044-2050.

82. Ramadass, R.; Bereiter-Hahn, J., Photophysical Properties of DASPMI as Revealed by Spectrally Resolved Fluorescence Decays. *J. Phys. Chem. B* **2007**, *111* (26), 7681-7690.

83. Manna, A.; Chakravorti, S., Modification of a Styryl Dye Binding Mode with Calf Thymus DNA in Vesicular Medium: From Minor Groove to Intercalative. *J. Phys. Chem. B* **2012**, *116* (17), 5226-5233.

84. Berdnikova, D. V.; Sosnin, N. I.; Fedorova, O. A.; Ihmels, H., Governing the DNA-binding mode of styryl dyes by the length of their alkyl substituents – from intercalation to major groove binding. *Org. Biomol. Chem.* **2018**, *16* (4), 545-554.

85. Ustimova, M. A.; Fedorov, Y. V.; Tsvetkov, V. B.; Tokarev, S. D.; Shepel, N. A.; Fedorova, O. A., Helical aggregates of bis(styryl) dyes formed by DNA templating. *J. Photochem. Photobiol. A: Chem.* **2021**, *418*, 113378.

86. Lee, J. W.; Jung, M.; Rosania, G. R.; Chang, Y.-T., Development of Novel Cell-Permeable DNA Sensitive Dyes Using Combinatorial Synthesis and Cell-Based Screening.

Chem. Commun. **2003**, (15), 1852-1853.

87. Kovalska, V. B.; Kocheshev, I. O.; Kryvorotenko, D. V.; Balanda, A.; Yarmoluk, S. M., Studies on the Spectral-Luminescent Properties of the Novel Homodimer Styryl Dyes in Complexes with DNA. *J Fluoresc* **2005**, *15* (3), 215-219.

88. Akbay, N.; Losytskyy, M. Y.; Kovalska, V. B.; Balanda, A. O.; Yarmoluk, S. M., The Mechanism of Benzothiazole Styrylcyanine Dyes Binding With dsDNA: Studies by Spectral-Luminescent Methods. *J. Fluoresc.* **2008**, *18* (1), 139-147.

89. Wang, X.; Wang, C.; Yu, W.; Zhou, Y.; Zhao, X.; Fang, Q.; Jiang, M., Two-Photon Absorption of Styryl-Quinolinium, -Pyridinium, and -Barbituric Acid Derivatives, and Intramolecular Charge Transfer. *Can. J. Chem.* **2001**, *79* (2), 174-182.

90. Srimongkol, G.; Ditmangklo, B.; Choopara, I.; Thaniyavarn, J.; Dean, D.; Kokpol, S.; Vilaivan, T.; Somboonna, N., Rapid Colorimetric Loop-Mediated Isothermal Amplification for Hypersensitive Point-of-Care Staphylococcus aureus Enterotoxin a Gene Detection in Milk and Pork Products. *Sci. Rep.* **2020**, *10* (1), 7768.

91. Brouwer, A. M., Standards for Photoluminescence Quantum Yield Measurements in Solution (IUPAC Technical Report). *Pure Appl. Chem.* **2011**, *83* (12), 2213-2228.

92. Lippert, E., Dipolmoment und Elektronenstruktur von angeregten Molekülen. *Zeitschrift für Naturforschung A* **1955**, *10* (7), 541-545.

93. Morris, G. M.; Huey, R.; Lindstrom, W.; Sanner, M. F.; Belew, R. K.; Goodsell, D. S.; Olson, A. J., AutoDock4 and AutoDockTools4: Automated Docking With Selective Receptor Flexibility. *J. Comput. Chem.* **2009**, *30* (16), 2785-2791.

94. Tiarpattaradilok, D.; Vilaivan, T., The Detection of Small Molecule Target by Styryl Dye and Aptamer. *Senior Project, Chulalongkorn University* **2018**.

95. Abu-Shanab, F. A.; Wakefield, B. J.; Elnagdi, M. H., Methylpyridines and Other Methylazines As Precursors to Bicycles and Polycycles. In *Adv. Heterocycl. Chem.*, Katritzky, A. R., Ed. Academic Press: 1997; Vol. 68, pp 181-221.

96. Shi, M.; Ding, C.; Dong, J.; Wang, H.; Tian, Y.; Hu, Z., A Novel Europium(III) Complex With Versatility in Excitation Ranging From Infrared to Ultraviolet. *Phys. Chem. Chem. Phys.* **2009**, *11* (25), 5119-5123.

97. Berdnikova, D. V.; Fedorova, O. A.; Tulyakova, E. V.; Li, H.; Kölsch, S.; Ihmels, H., Interaction of Crown Ether-Annelated Styryl Dyes With Double-Stranded DNA.

Photochem. Photobiol. **2015**, *91* (3), 723-731.

98. Reichardt, C., Solvatochromic Dyes as Solvent Polarity Indicators. *Chem. Rev.* **1994**, *94* (8), 2319-2358.

99. Reichardt, C., Polarity of ionic liquids determined empirically by means of solvatochromic pyridinium N-phenolate betaine dyes. *Green Chem.* **2005**, *7* (5), 339-351.

100. Cerón-Carrasco, J. P.; Jacquemin, D.; Laurence, C.; Planchat, A.; Reichardt, C.; Sraïdi, K., Solvent Polarity Scales: Determination of New ET(30) Values for 84 Organic Solvents. *J. Phys. Org. Chem.* **2014**, *27* (6), 512-518.

101. Nigam, S.; Rutan, S., Principles and Applications of Solvatochromism. *Appl. Spectrosc.* **2001**, *55* (11), 362A-370A.

102. Isborn, C. M.; Luehr, N.; Ufimtsev, I. S.; Martínez, T. J., Excited-State Electronic Structure with Configuration Interaction Singles and Tamm–Dancoff Time-Dependent Density Functional Theory on Graphical Processing Units. *J. Chem. Theory Comput.* **2011**, *7* (6), 1814-1823.

103. Stsiapura, V. I.; Kurhuzenkau, S. A.; Kuzmitsky, V. A.; Bouganov, O. V.; Tikhomirov, S. A., Solvent Polarity Effect on Nonradiative Decay Rate of Thioflavin T. *J. Phys. Chem. A* **2016**, *120* (28), 5481-5496.

104. Patil, O., Ground and Excited State Dipole Moments of a Dye. *Int. Sci. Res. Organ. J.* **2016**, *08*, 55-59.

105. Tse, W. C.; Boger, D. L., A Fluorescent Intercalator Displacement Assay for Establishing DNA Binding Selectivity and Affinity. *Curr. Protoc. Nucleic Acid Chem.* **2005**, *20* (1), 8.5.1-8.5.11.

106. Szumilak, M.; Merecz, A.; Strek, M.; Stanczak, A.; Inglot, T. W.; Karwowski, B. T., DNA Interaction Studies of Selected Polyamine Conjugates. *Int. J. Mol. Sci.* **2016**, *17* (9), 1560.

107. Masum, A. A.; Chakraborty, M.; Pandya, P.; Halder, U. C.; Islam, M. M.; Mukhopadhyay, S., Thermodynamic Study of Rhodamine 123-Calf Thymus DNA Interaction: Determination of Calorimetric Enthalpy by Optical Melting Study. *J. Phys. Chem. B* **2014**, *118* (46), 13151-13161.

108. Kastenholz, M. A.; Schwartz, T. U.; Hünenberger, P. H., The Transition Between

the B and Z Conformations of DNA Investigated by Targeted Molecular Dynamics Simulations With Explicit Solvation. *Biophys. J.* **2006**, *91* (8), 2976-2990.

109. Modukuru, N. K.; Snow, K. J.; Perrin, B. S.; Thota, J.; Kumar, C. V., Contributions of a Long Side Chain to the Binding Affinity of an Anthracene Derivative to DNA. *J. Phys. Chem. B* **2005**, *109* (23), 11810-11818.

110. Rye, H. S.; Quesada, M. A.; Peck, K.; Mathies, R. A.; Glazer, A. N., High-sensitivity two-color detection of double-stranded DNA with a confocal fluorescence gel scanner using ethidium homodimer and thiazole orange. *Nucleic Acids Res.* **1991**, *19* (2), 327-333.

111. Rye, H. S.; Dabora, J. M.; Quesada, M. A.; Mathies, R. A.; Glazer, A. N., Fluorometric Assay Using Dimeric Dyes for Double- and Single-Stranded DNA and RNA with Picogram Sensitivity. *Anal. Biochem.* **1993**, *208* (1), 144-150.

112. Frasson, I.; Pirota, V.; Richter, S. N.; Doria, F., Multimeric G-quadruplexes: A review on their biological roles and targeting. *Int. J. Biol. Macromol.* **2022**, *204*, 89-102.

113. Lercher, L.; McDonough, M. A.; El-Sagheer, A. H.; Thalhammer, A.; Kriaucionis, S.; Brown, T.; Schofield, C. J., Structural Insights Into How 5-Hydroxymethylation Influences Transcription Factor Binding. *Chem. Commun.* **2014**, *50* (15), 1794-1796.

114. Cunningham, P. D.; Bricker, W. P.; Diaz, S. A.; Medintz, I. L.; Bathe, M.; Melinger, J. S., Optical Determination of the Electronic Coupling and Intercalation Geometry of Thiazole Orange Homodimer in DNA. *J. Chem. Phys.* **2017**, *147* (5), 055101.

115. Yguerabide, J.; Ceballos, A., Quantitative Fluorescence Method for Continuous Measurement of DNA Hybridization Kinetics Using a Fluorescent Intercalator. *Anal. Biochem.* **1995**, *228* (2), 208-220.

116. Le Pecq, J.-B.; Paoletti, C., A new fluorometric method for RNA and DNA determination. *Anal. Biochem.* **1966**, *17* (1), 100-107.

117. Labarca, C.; Paigen, K., A simple, rapid, and sensitive DNA assay procedure. *Anal. Biochem.* **1980**, *102* (2), 344-352.

118. Somboonna, N.; Vilaivan, T.; Junpra-ob, S.; Supabowornsathit, K.; Ditmangklo, B. A method for the detection of pathogens in foods and drinks by loop-mediated isothermal amplification technique in combination with double stranded DNA staining dyes. *Thai Petty Patent Application No. 11926300006 (20 Sep 2019)*.

119. Latt, S. A.; Stetten, G.; Juergens, L. A.; Willard, H. F.; Scher, C. D., Recent developments in the detection of deoxyribonucleic acid synthesis by 33258 Hoechst fluorescence. *J. Histochem. Cytochem.* **1975**, *23* (7), 493-505.
120. Yusupov, M. M.; Yusupova, G. Z.; Baucom, A.; Lieberman, K.; Earnest, T. N.; Cate, J. H. D.; Noller, H. F., Crystal Structure of the Ribosome at 5.5 Å Resolution. *Science* **2001**, *292* (5518), 883-896.
121. Chen, S.-H.; Wang, Y.-S.; Chen, Y.-S.; Tang, X.; Cao, J.-X.; Li, M.-H.; Wang, X.-F.; Zhu, Y.-F.; Huang, Y.-Q., Dual-channel detection of metallothioneins and mercury based on a mercury-mediated aptamer beacon using thymidine–mercury–thymidine complex as a quencher. *Spectrochim. Acta, Part A* **2015**, *151*, 315-321.
122. Zhai, K.; Liu, Y.; Xiang, D.; Guo, G.; Wan, T.; Hu, H., Dual color fluorescence quantitative detection of mercury in soil with graphene oxide and dye-labeled nucleic acids. *Anal. Methods* **2015**, *7* (9), 3827-3832.
123. Luo, F.; Zheng, L.; Chen, S.; Cai, Q.; Lin, Z.; Qiu, B.; Chen, G., An aptamer-based fluorescence biosensor for multiplex detection using unmodified gold nanoparticles. *Chem. Commun.* **2012**, *48* (51), 6387-6389.
124. Ma, N.; Ren, X.; Wang, H.; Kuang, X.; Fan, D.; Wu, D.; Wei, Q., Ultrasensitive Controlled Release Aptasensor Using Thymine–Hg²⁺–Thymine Mismatch as a Molecular Switch for Hg²⁺ Detection. *Anal. Chem.* **2020**, *92* (20), 14069-14075.
125. Thailand Ministry of Industry's Industrial Wastewaters Standard, Article of specific chemicals (Mercury). 2012; Vol. 3, p 21.



APPENDIX

จุฬาลงกรณ์มหาวิทยาลัย
CHULALONGKORN UNIVERSITY

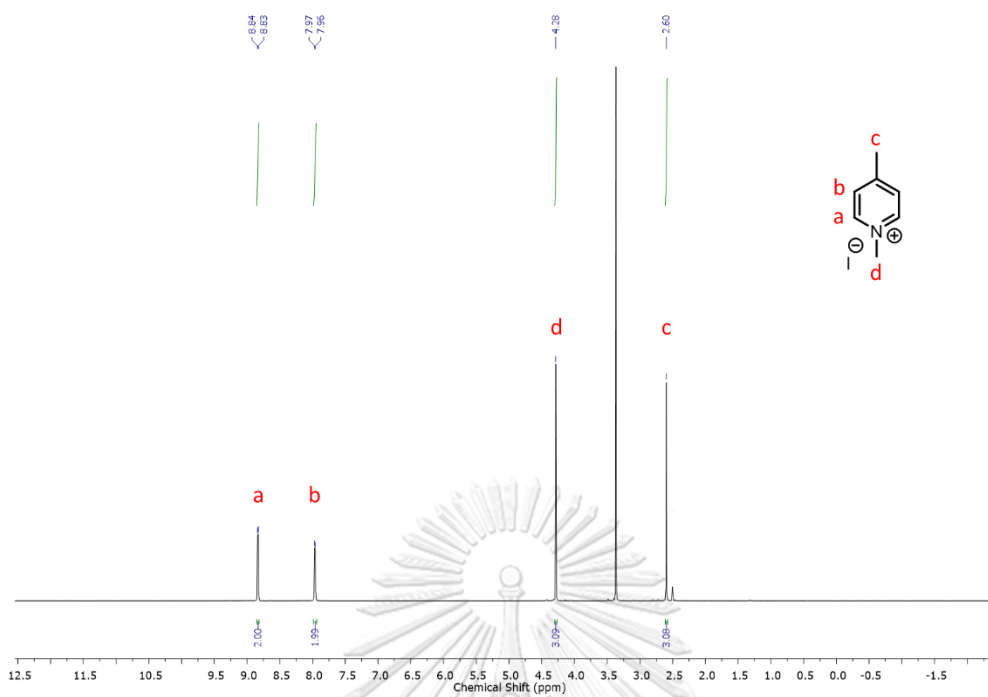


Figure A1 ^1H (500 MHz, $\text{DMSO-}d_6$) NMR spectrum of 1,4-dimethylpyridin-1-ium iodide

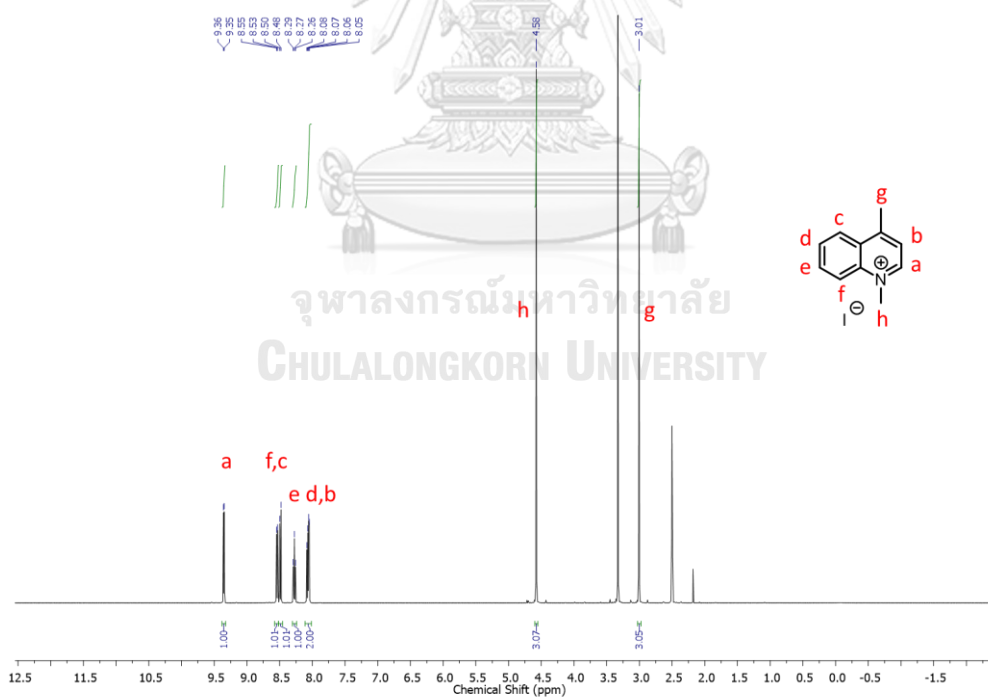


Figure A2 ^1H (500 MHz, $\text{DMSO-}d_6$) NMR spectrum of 1,4-dimethylquinolin-1-ium iodide

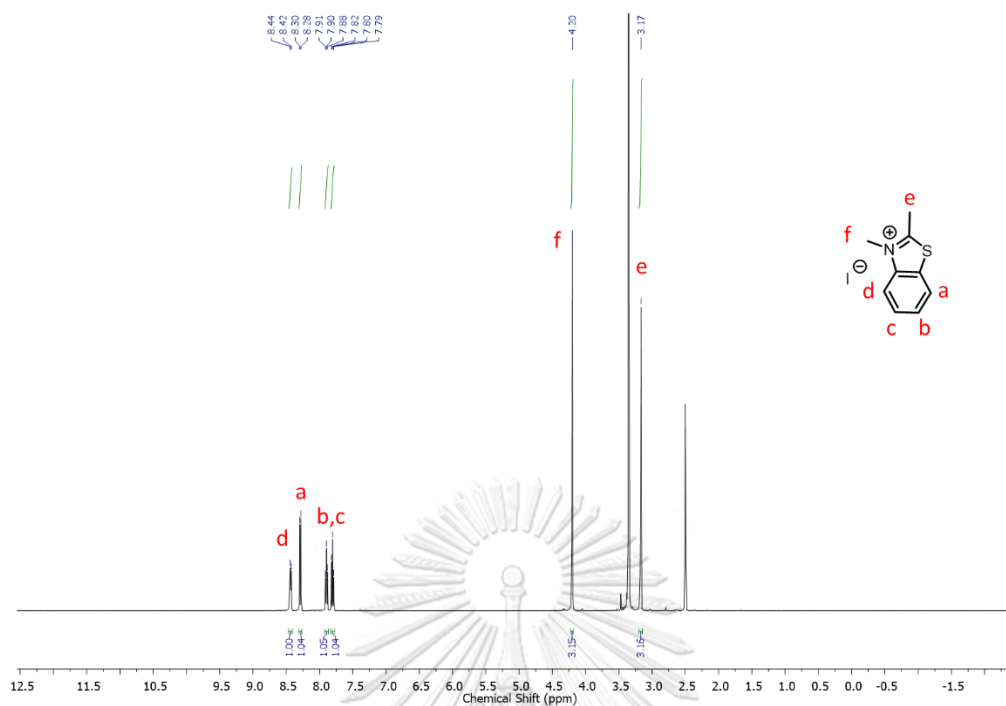


Figure A3 ^1H (500 MHz, $\text{DMSO-}d_6$) NMR spectrum of 2,3-dimethylbenzo[d]thiazol-3-ium iodide

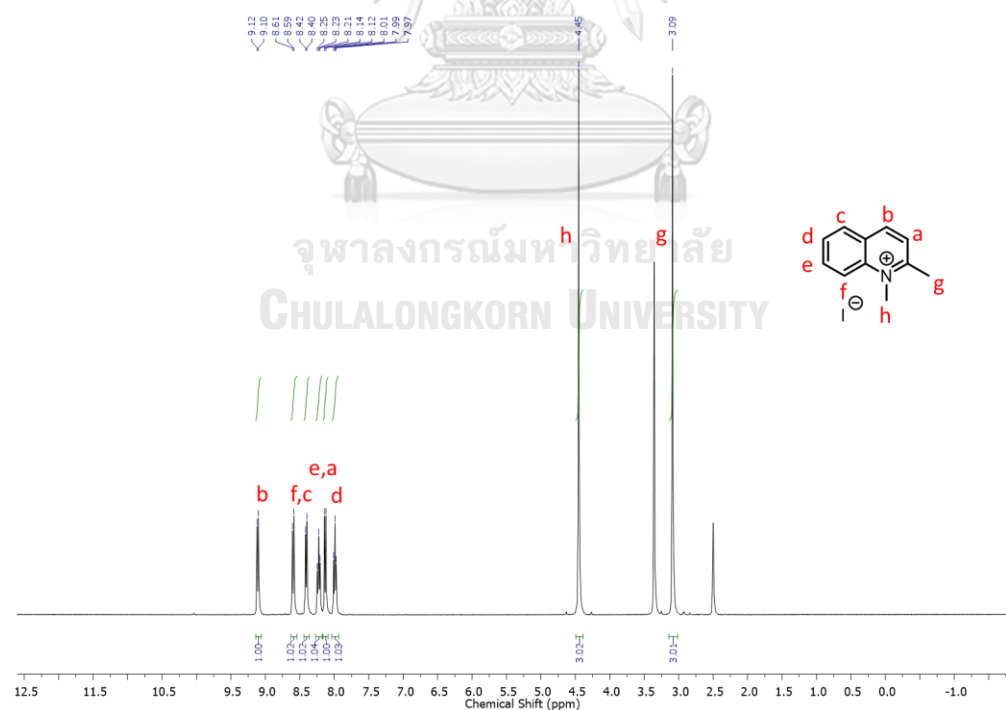


Figure A4 ^1H (500 MHz, $\text{DMSO-}d_6$) NMR spectrum of 1,2-dimethylquinolin-1-ium iodide

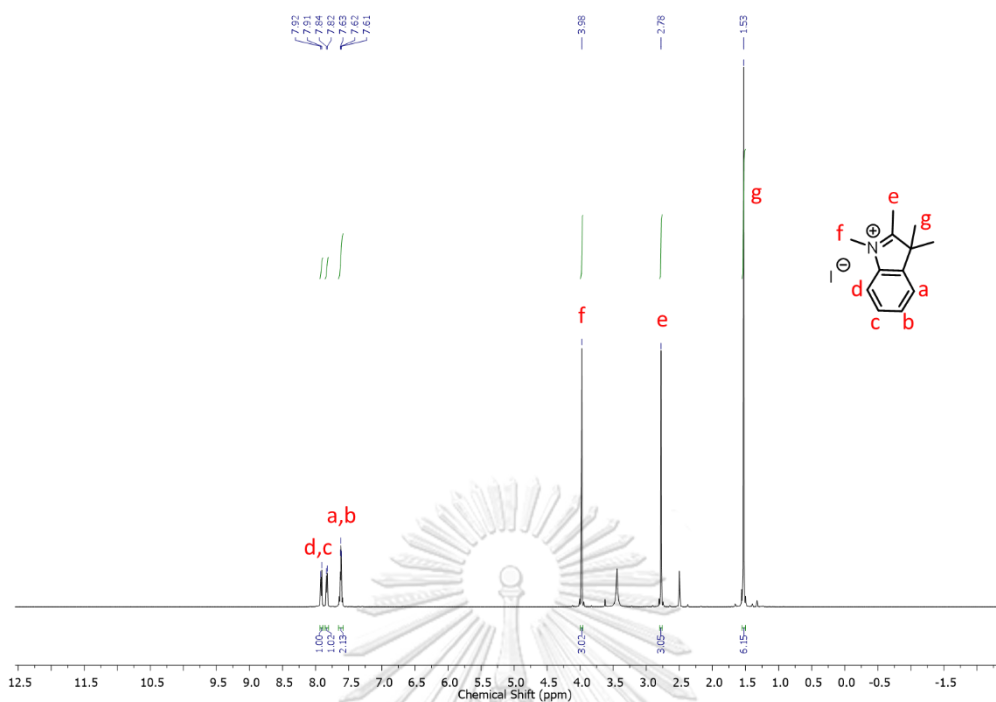


Figure A5 ^1H (500 MHz, $\text{DMSO-}d_6$) NMR spectrum of 1,2,3,3-tetramethyl-3*H*-indol-1-ium iodide

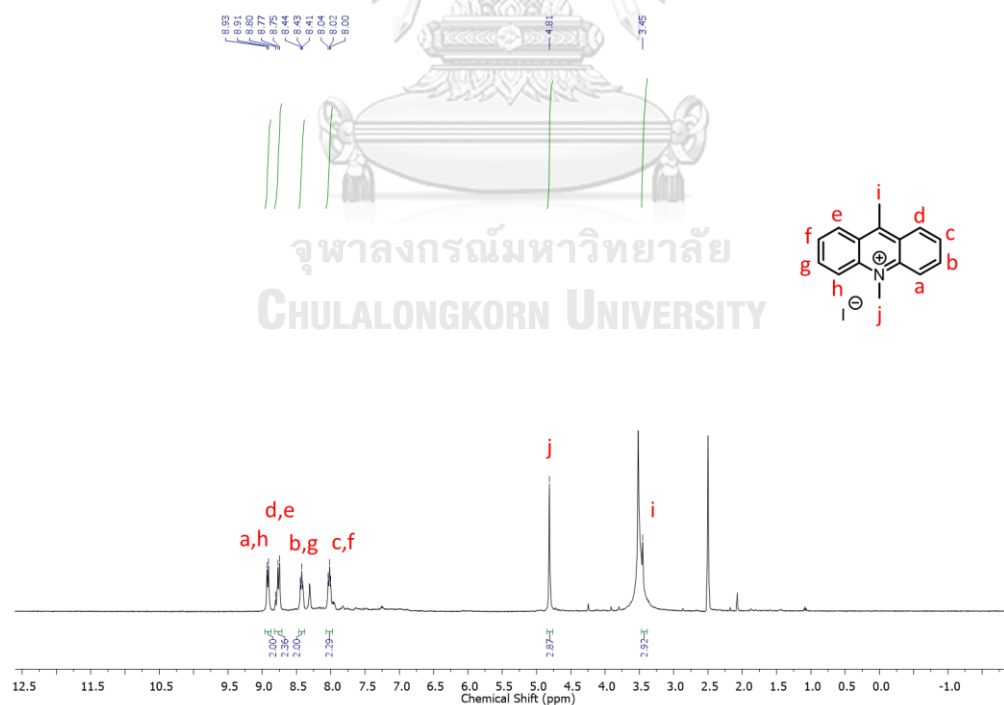


Figure A6 ^1H (500 MHz, $\text{DMSO-}d_6$) NMR spectrum of 9,10-dimethylacridin-10-ium iodide

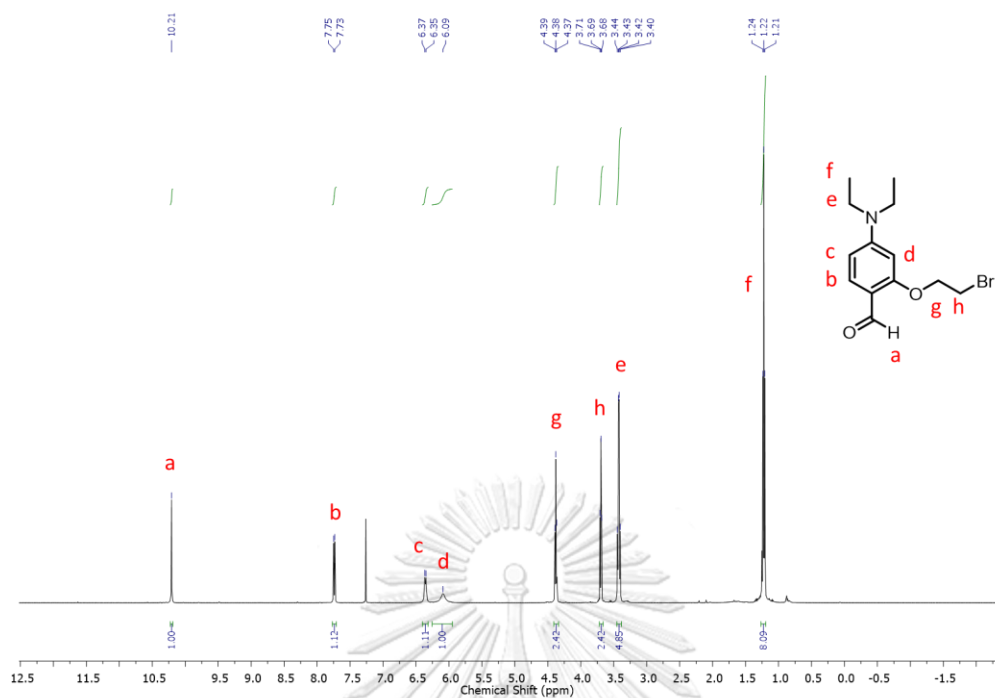


Figure A7 ^1H (500 MHz, CDCl_3) NMR spectrum of 2-(2-bromoethoxy)-4-(diethylamino)benzaldehyde

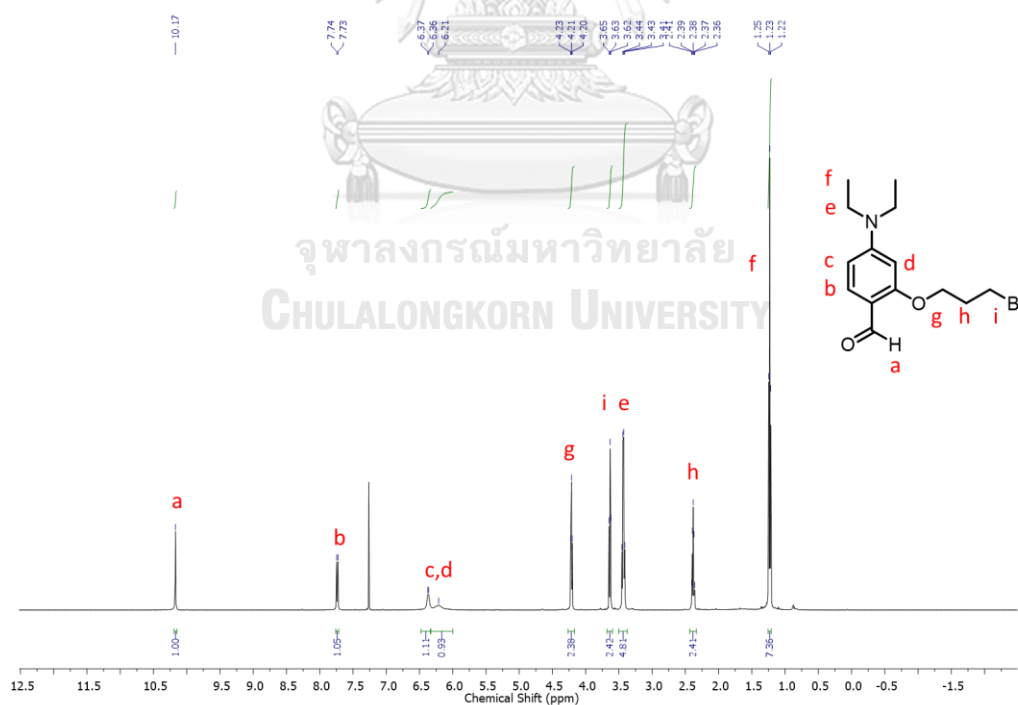


Figure A8 ^1H (500 MHz, CDCl_3) NMR spectrum of 2-(3-bromopropoxy)-4-(diethylamino)benzaldehyde

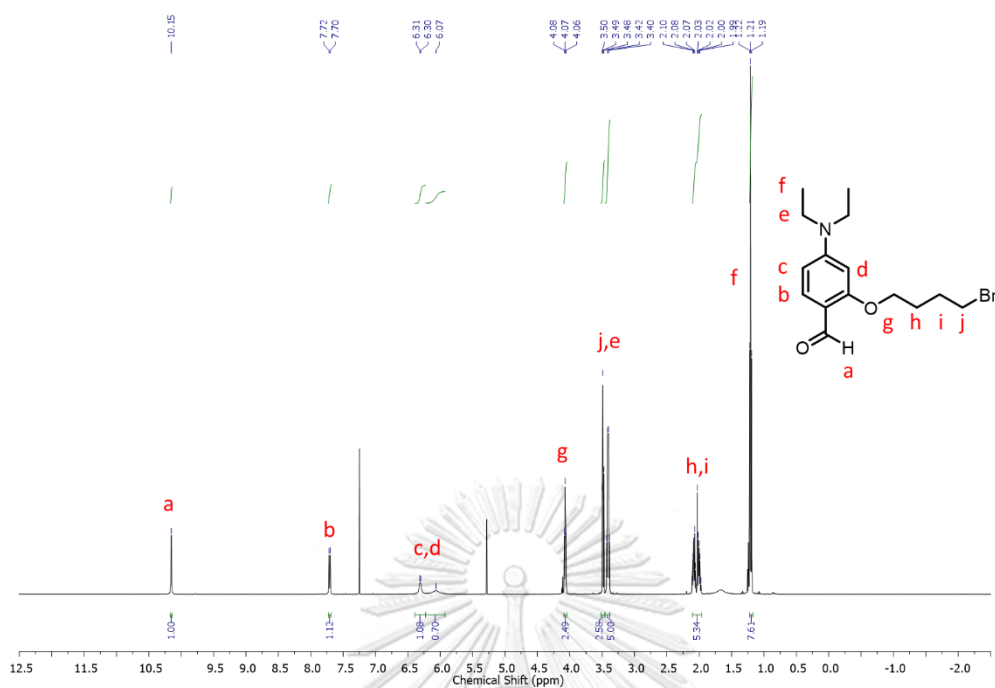


Figure A9 ^1H (500 MHz, CDCl_3) NMR spectrum of 2-(4-bromobutoxy)-4-(diethylamino)benzaldehyde

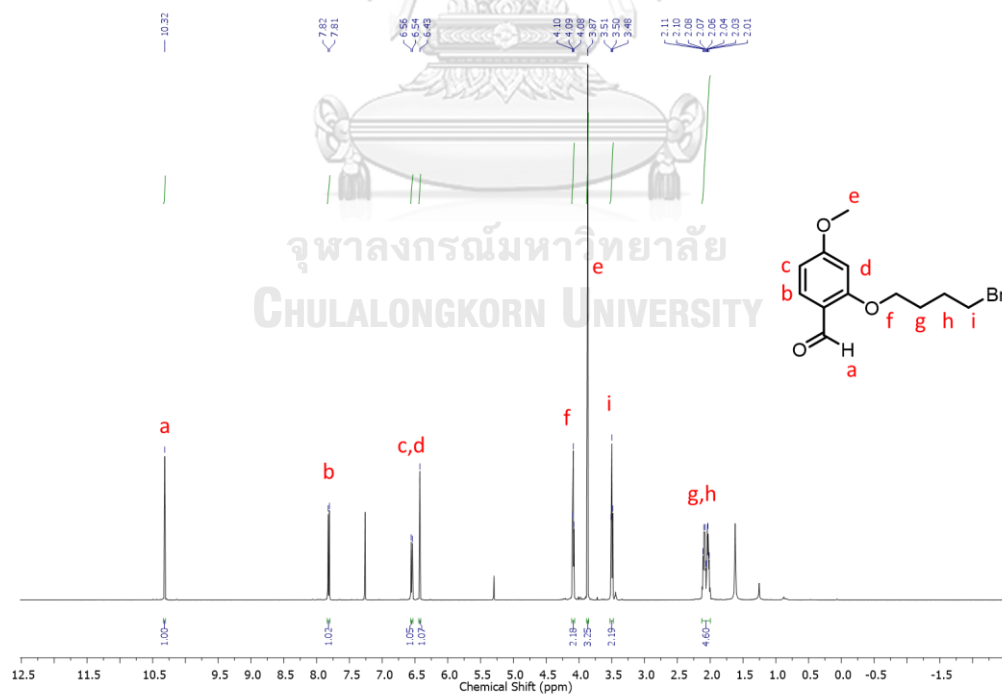


Figure A10 ^1H (500 MHz, CDCl_3) NMR spectrum of 2-(4-bromobutoxy)-4-methoxybenzaldehyde

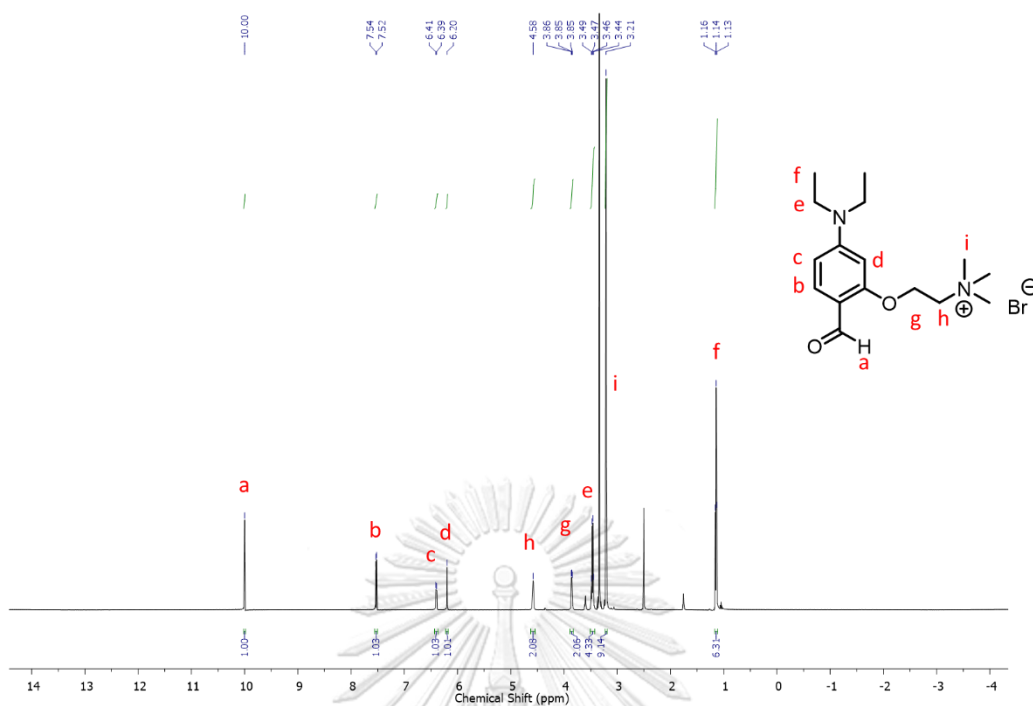


Figure A11 ^1H (500 MHz, $\text{DMSO-}d_6$) NMR spectrum of 2-(5-(diethylamino)-2-formylphenoxy)-*N,N,N*-trimethylethan-1-aminium bromide

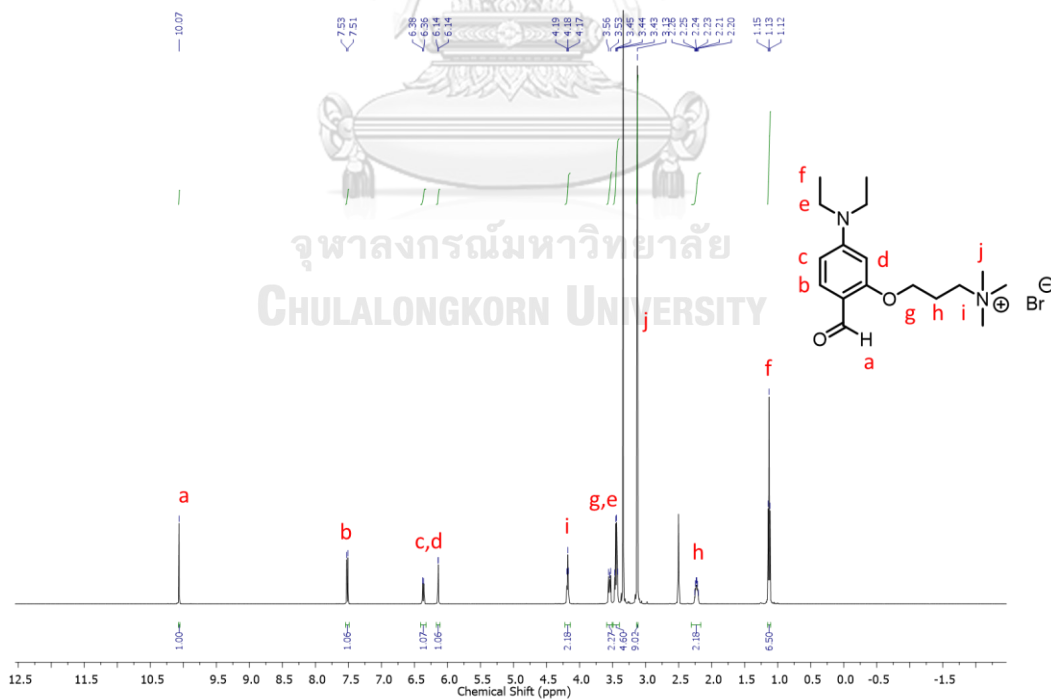


Figure A12 ^1H (500 MHz, $\text{DMSO-}d_6$) NMR spectrum of 3-(5-(diethylamino)-2-formylphenoxy)-*N,N,N*-trimethylpropan-1-aminium bromide

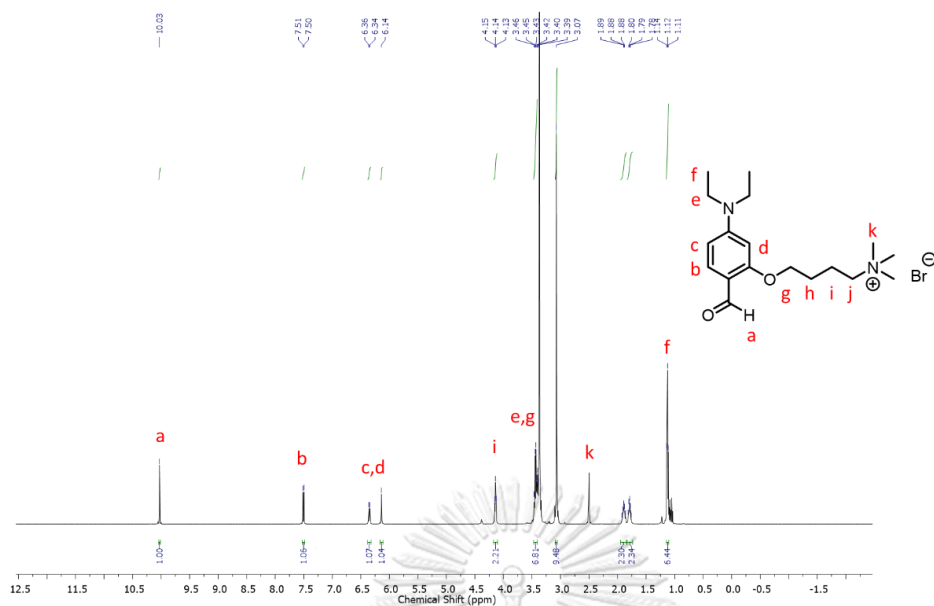


Figure A13 ¹H (500 MHz, DMSO-*d*₆) NMR spectrum of 4-(5-(diethylamino)-2-formylphenoxy)-*N,N,N*-trimethylbutan-1-aminium bromide

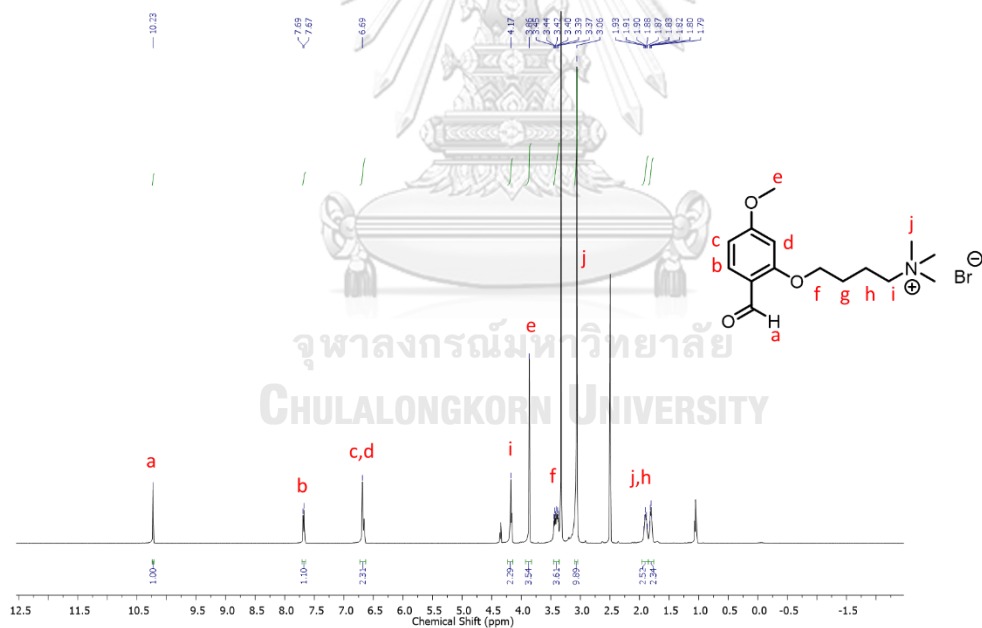
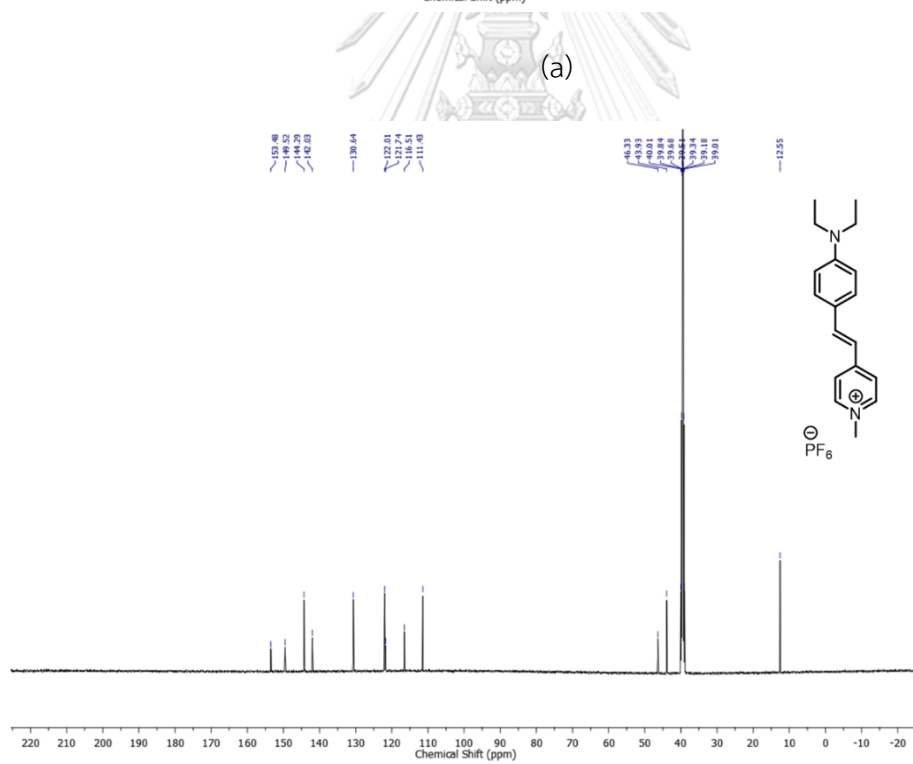
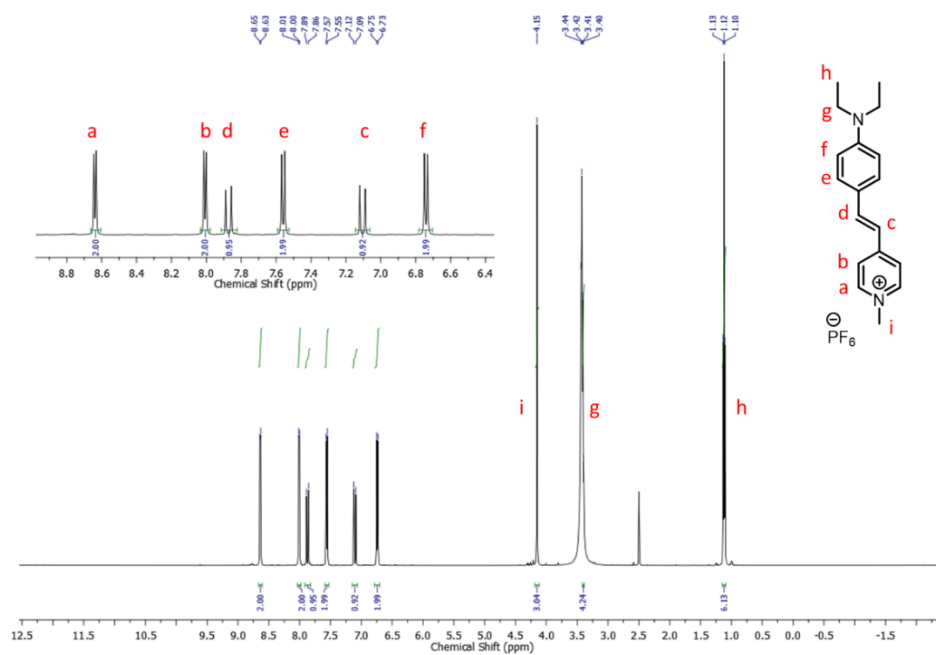
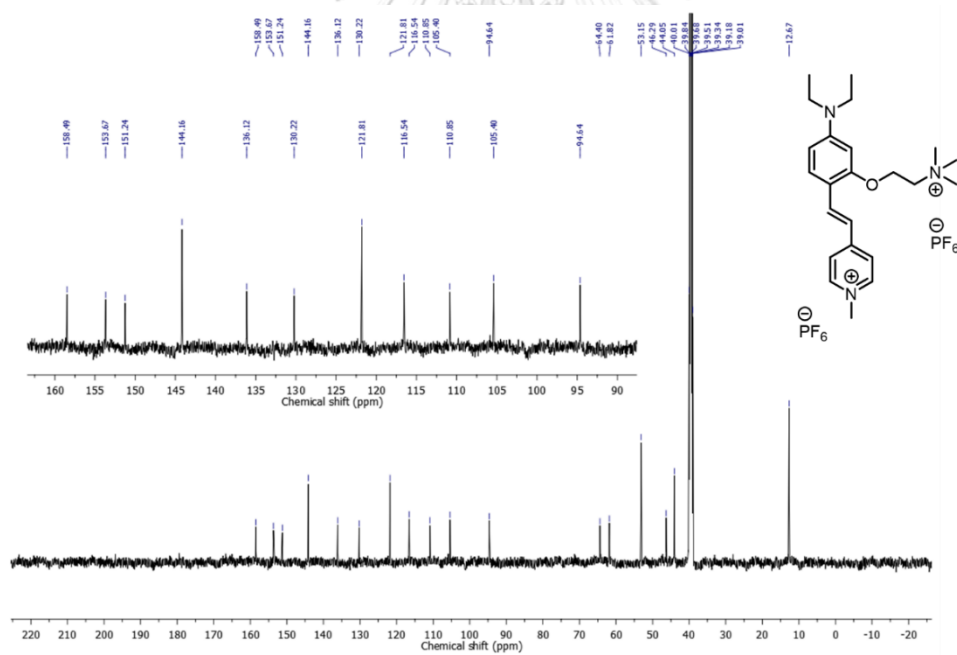
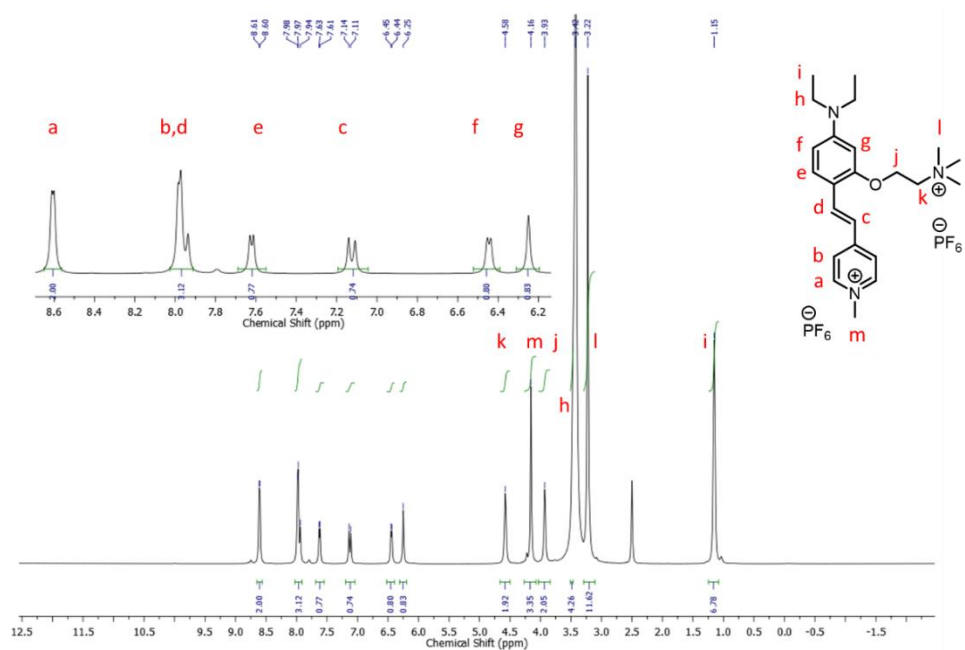


Figure A14 ¹H (500 MHz, DMSO-*d*₆) NMR spectrum of 4-(2-formyl-5-methoxyphenoxy)-*N,N,N*-trimethylbutan-1-aminium bromide



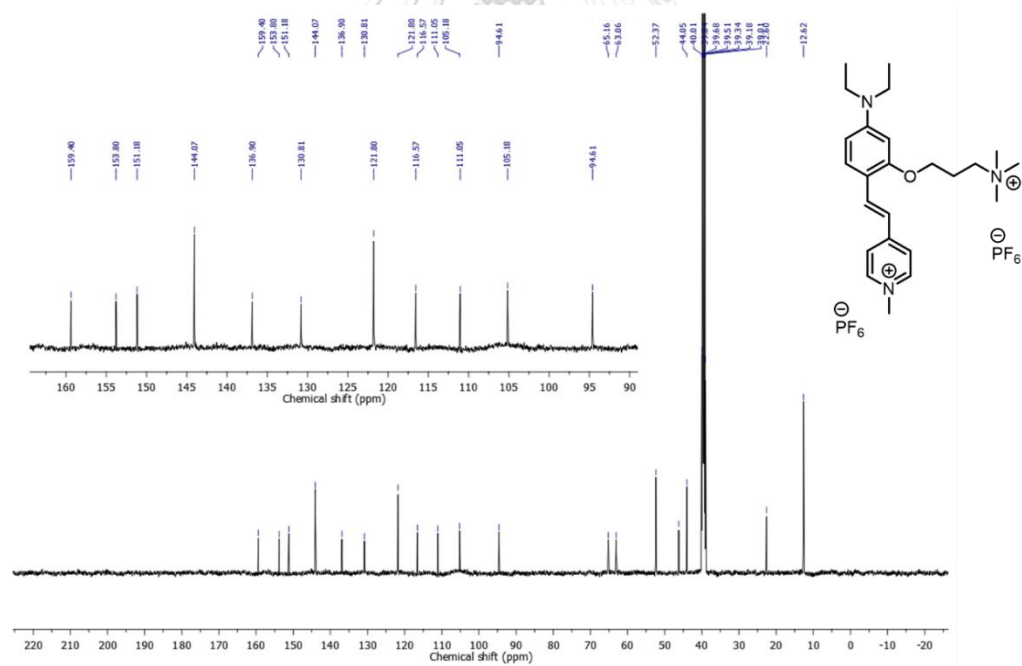
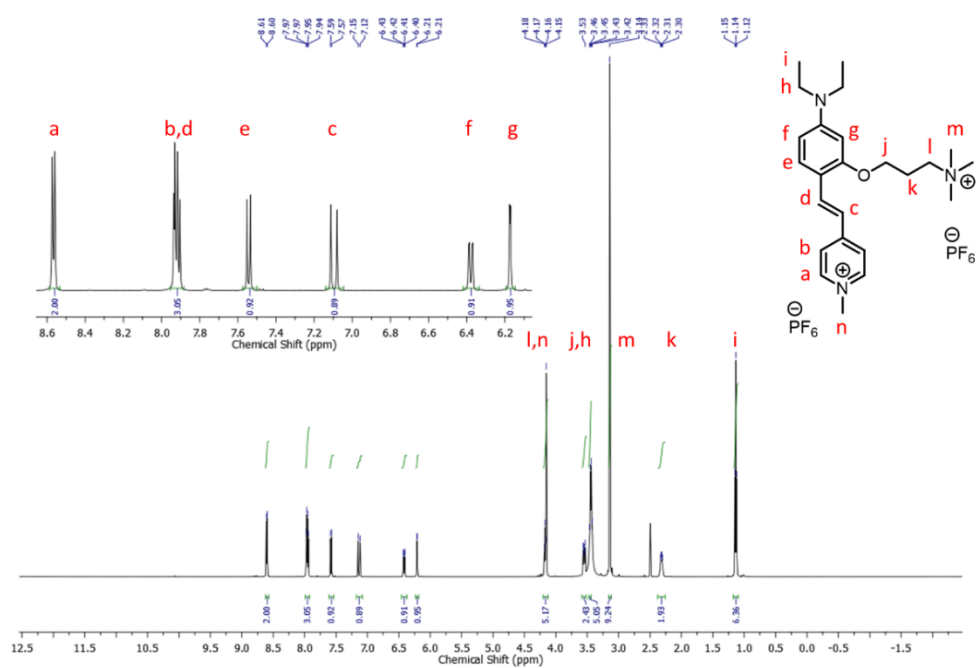
(b)

Figure A15 ^1H (500 MHz, $\text{DMSO-}d_6$) (a) and ^{13}C (126 MHz, $\text{DMSO-}d_6$) (b) NMR spectra of compound PY+



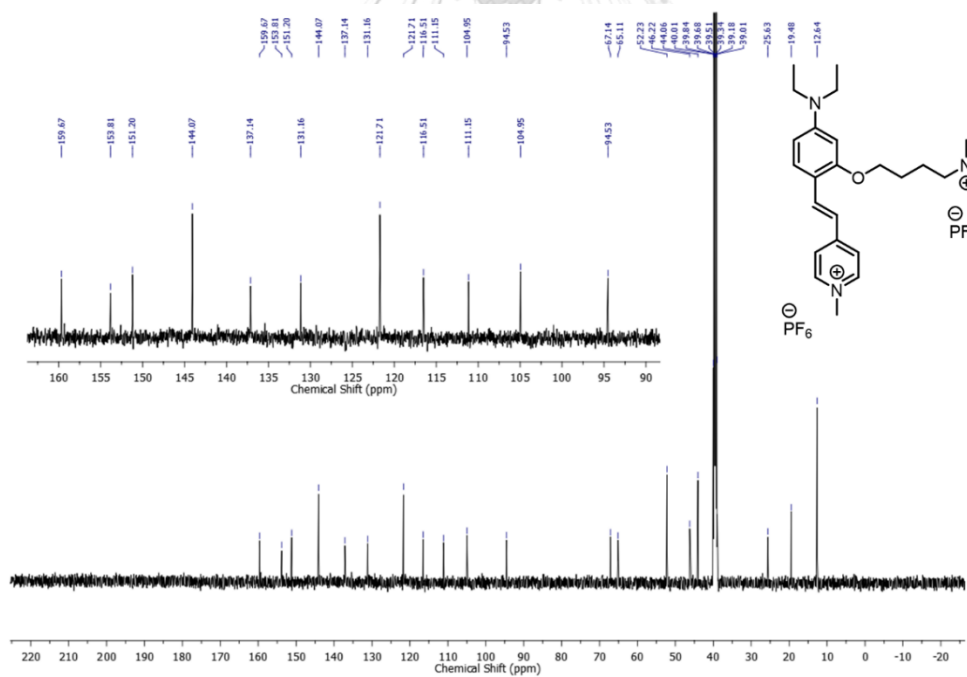
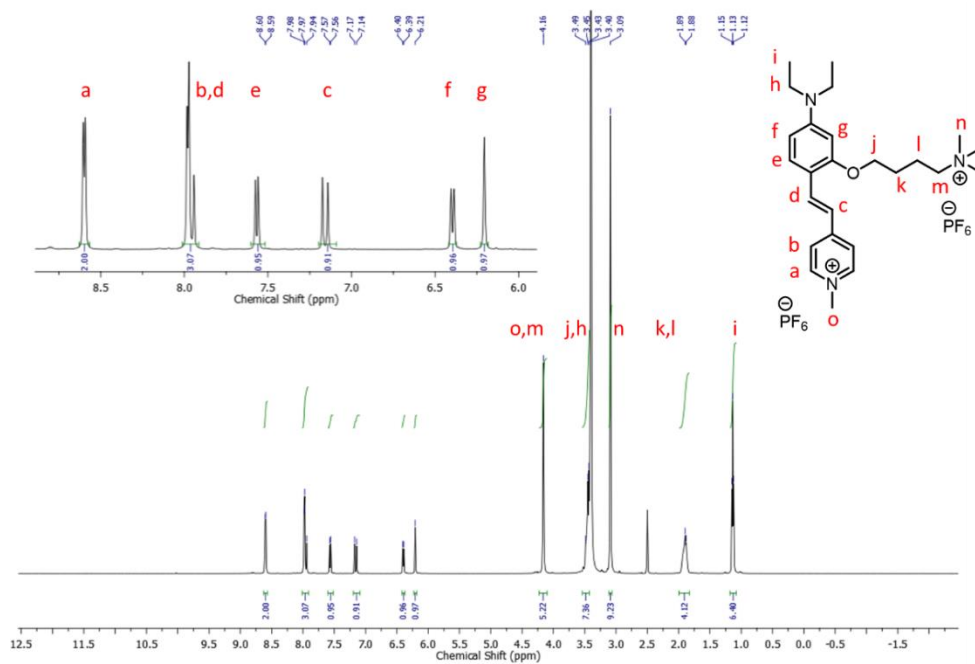
(b)

Figure A16 ¹H (500 MHz, DMSO-*d*₆) (a) and ¹³C (126 MHz, DMSO-*d*₆) (b) NMR spectra of compound PY2+(C2)



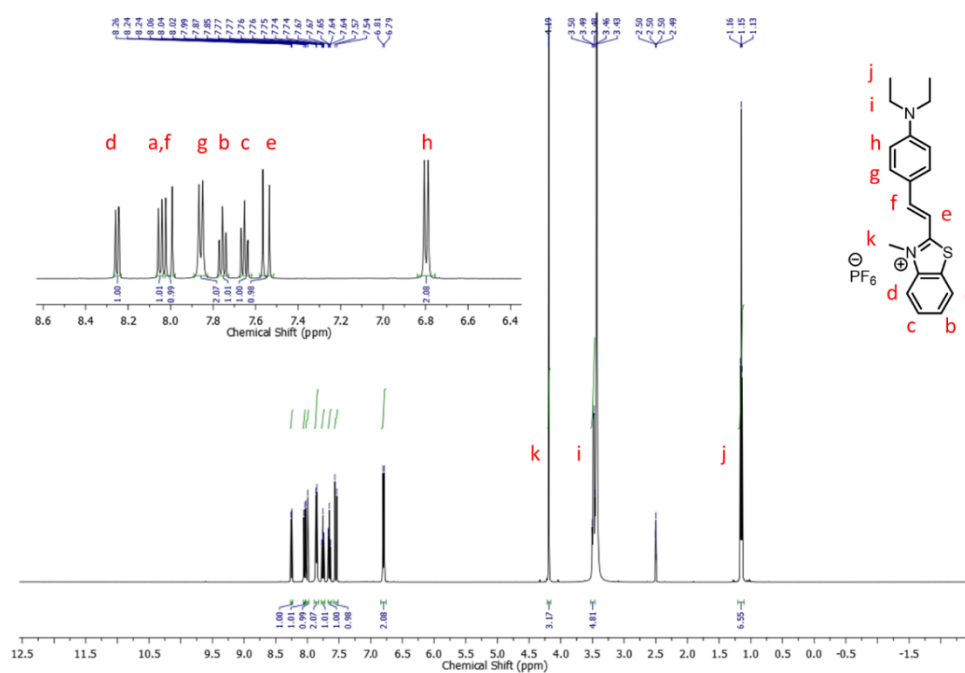
(b)

Figure A17 ¹H (500 MHz, DMSO-*d*₆) (a) and ¹³C (126 MHz, DMSO-*d*₆) (b) NMR spectra of compound PY2+(C3)

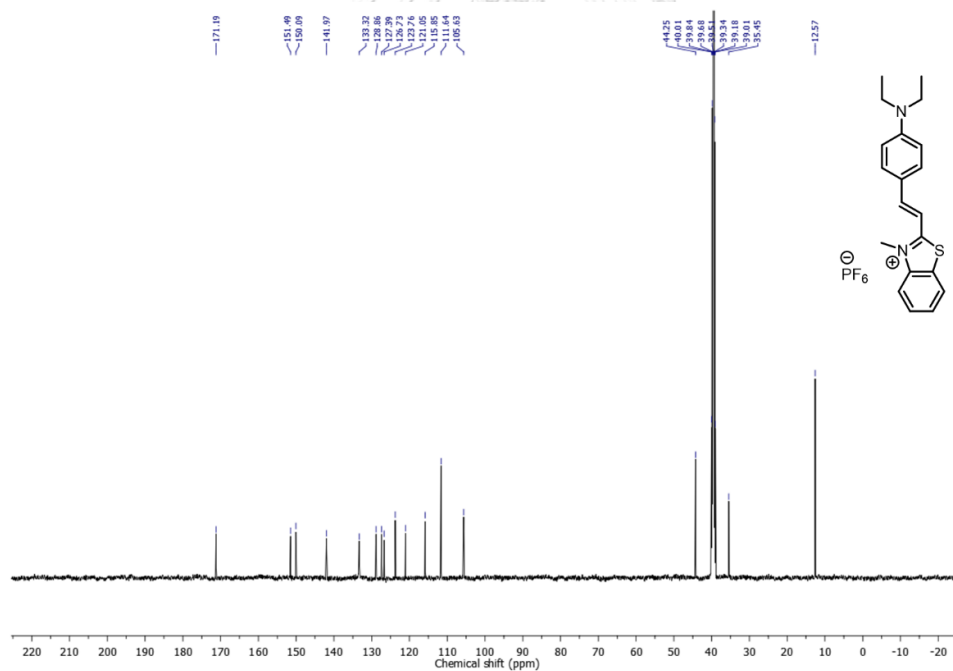


(b)

Figure A18 ¹H (500 MHz, DMSO-*d*₆) (a) and ¹³C (126 MHz, DMSO-*d*₆) (b) NMR spectra of compound PY2+(C4)



(a)



(b)

Figure A19 ¹H (500 MHz, DMSO-*d*₆) (a) and ¹³C (126 MHz, DMSO-*d*₆) (b) NMR spectra of compound **BT⁺**

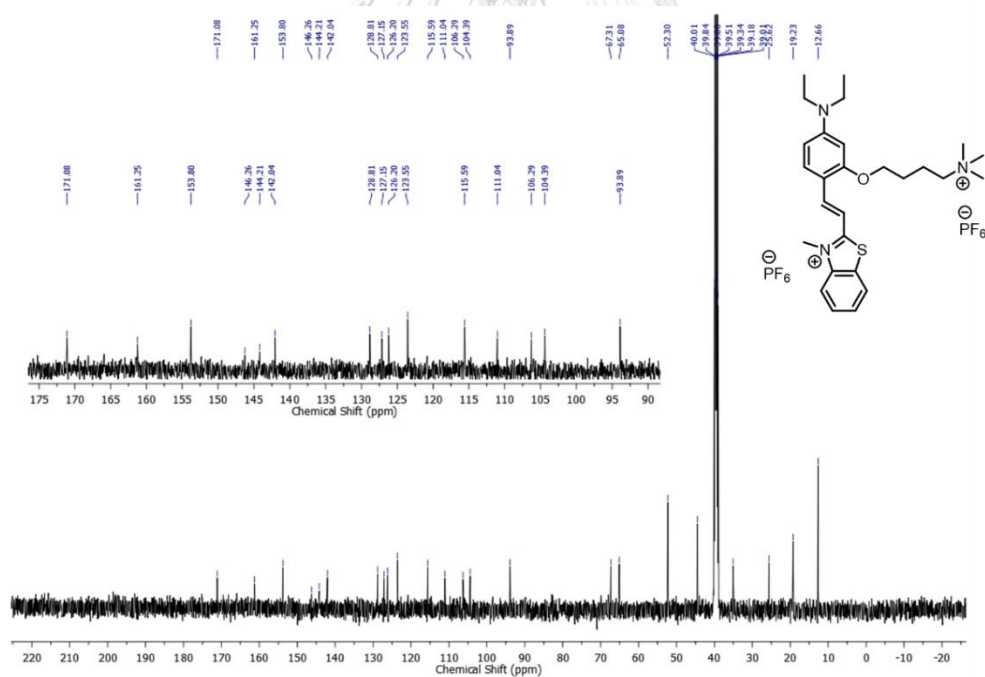
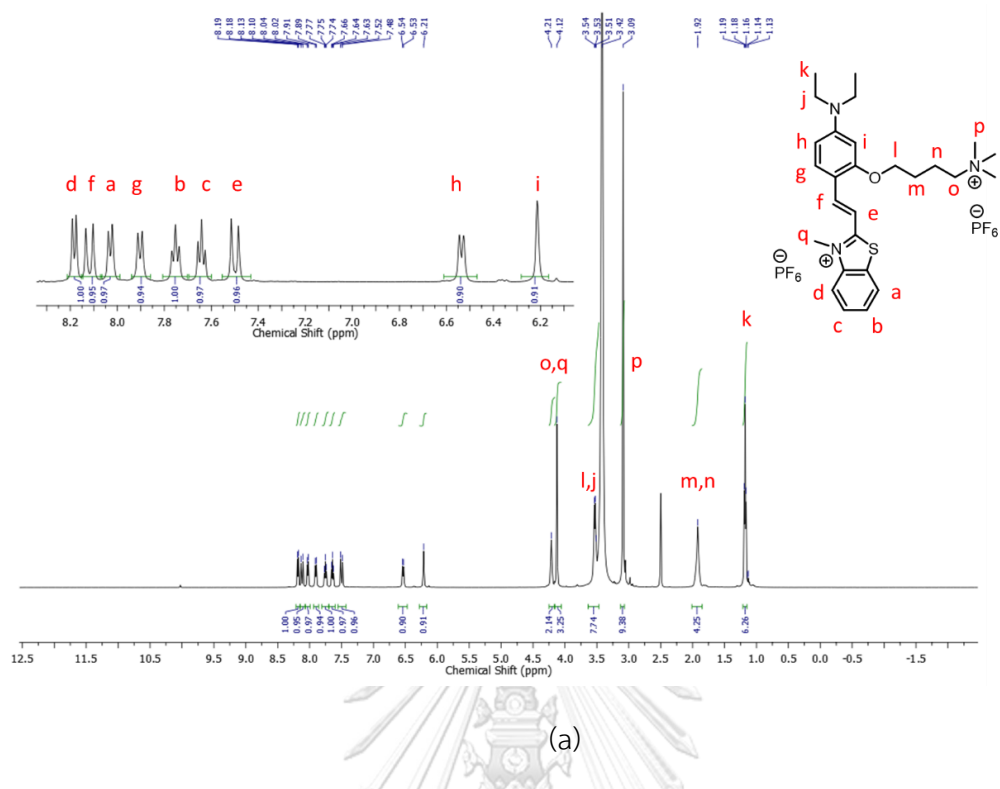
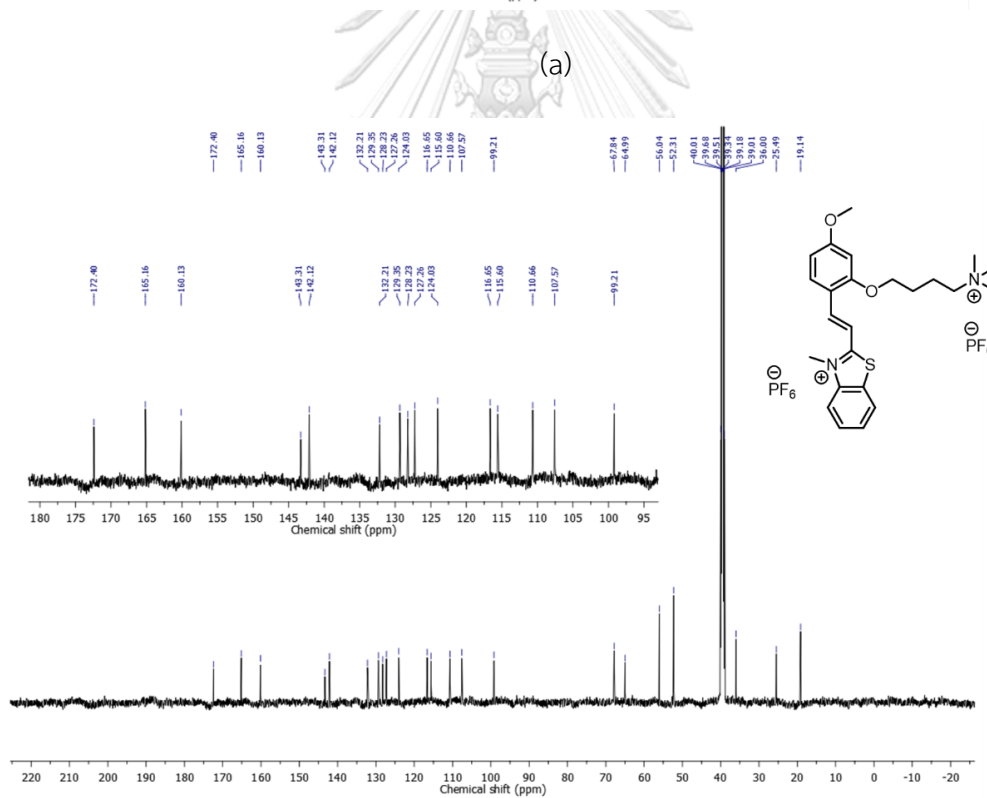
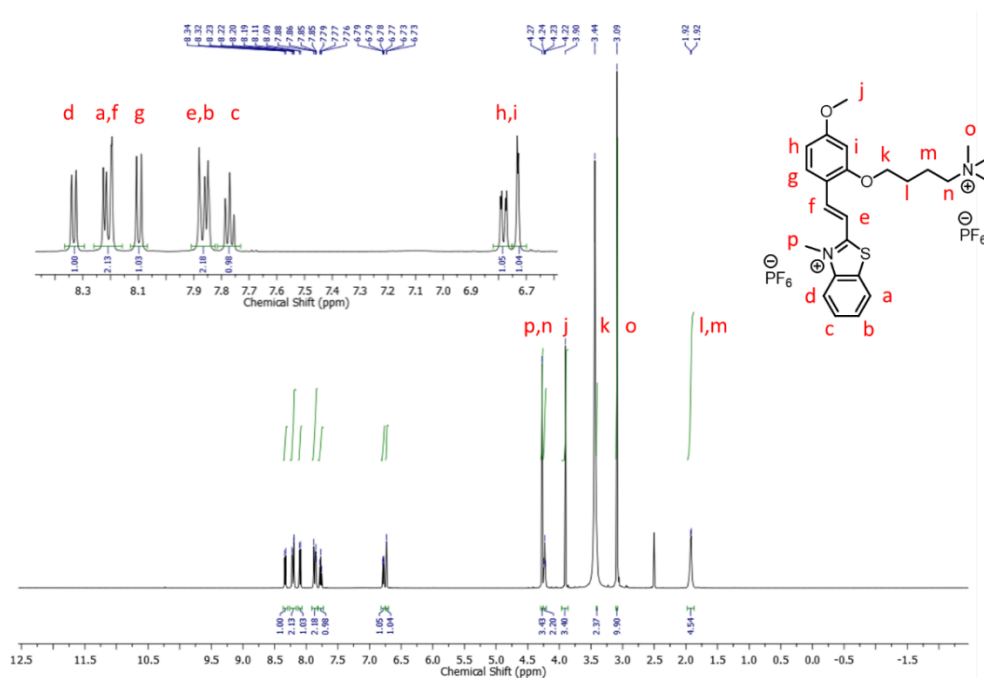
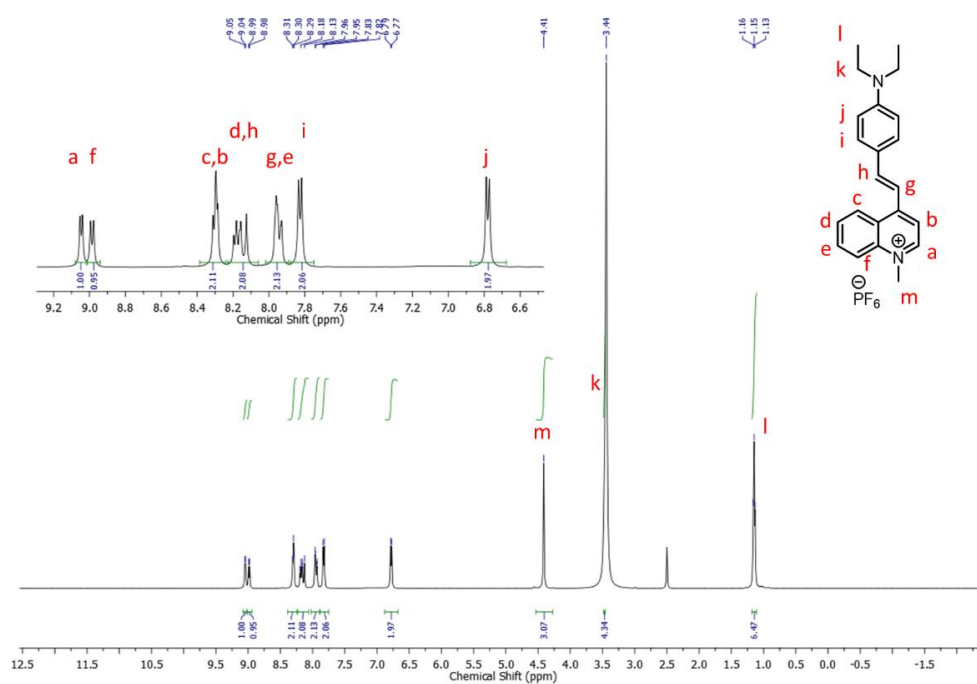


Figure A20 ^1H (500 MHz, $\text{DMSO-}d_6$) (a) and ^{13}C (126 MHz, $\text{DMSO-}d_6$) (b) NMR spectra of compound **BT2+(NEt₂)**

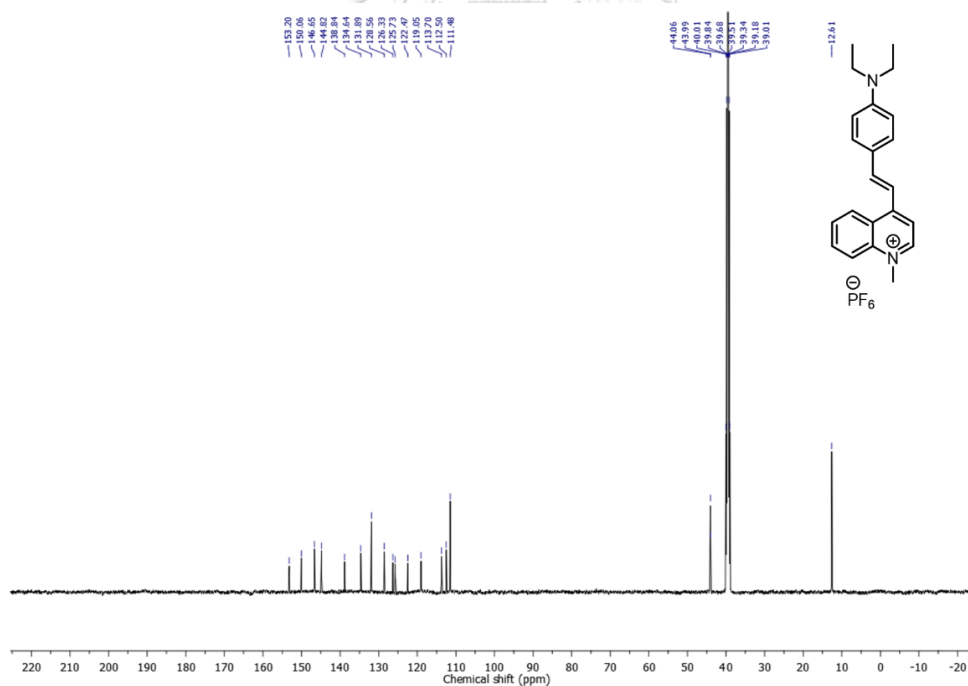


(b)

Figure A21 ¹H (500 MHz, DMSO-*d*₆) (a) and ¹³C (126 MHz, DMSO-*d*₆) (b) NMR spectra of compound BT2+(OMe)



(a)



(b)

Figure A22 ¹H (500 MHz, DMSO-*d*₆) (a) and ¹³C (126 MHz, DMSO-*d*₆) (b) NMR spectra of compound 4QL+

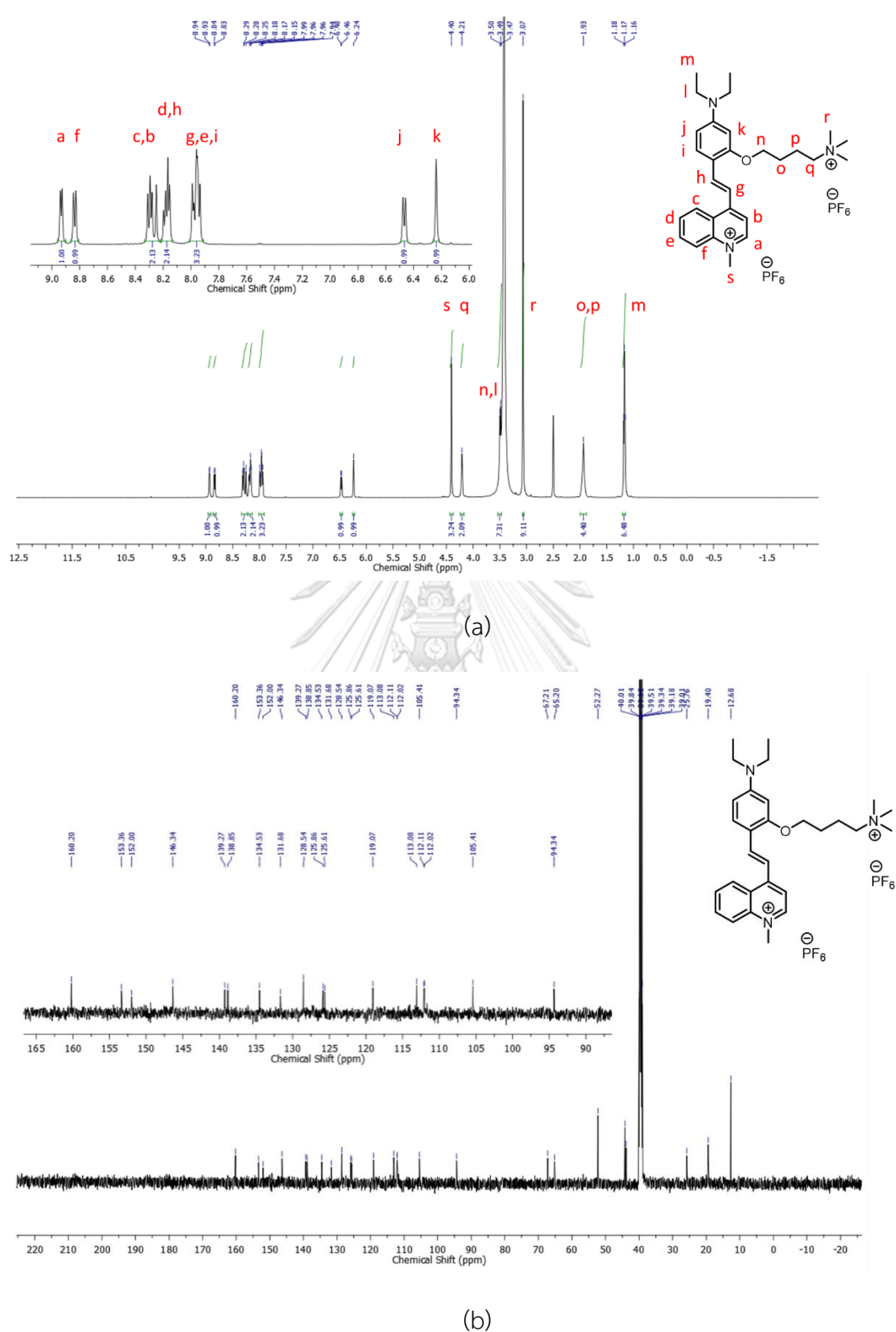


Figure A23 ^1H (500 MHz, $\text{DMSO-}d_6$) (a) and ^{13}C (126 MHz, $\text{DMSO-}d_6$) (b) NMR spectra of compound **4QL2+**

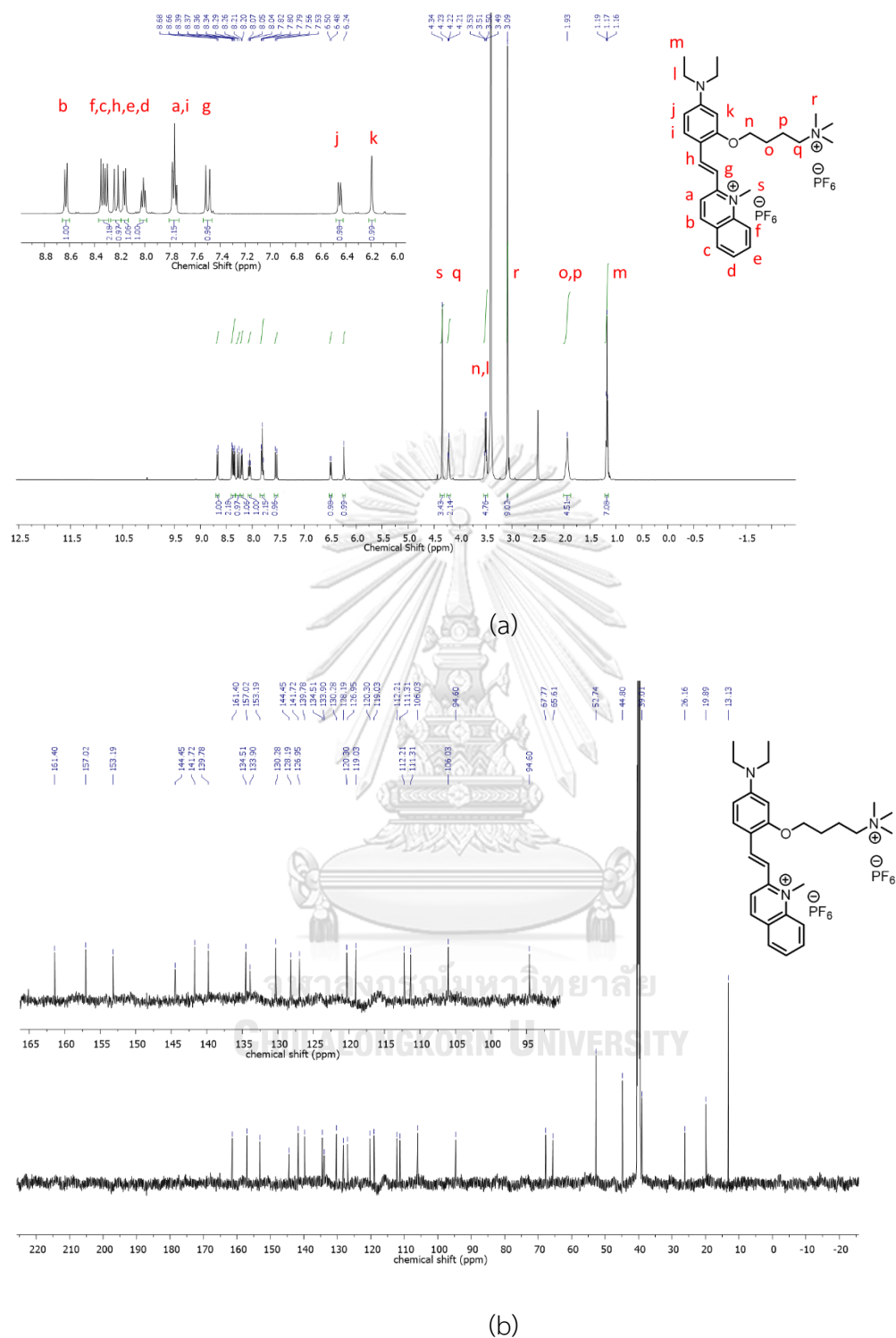
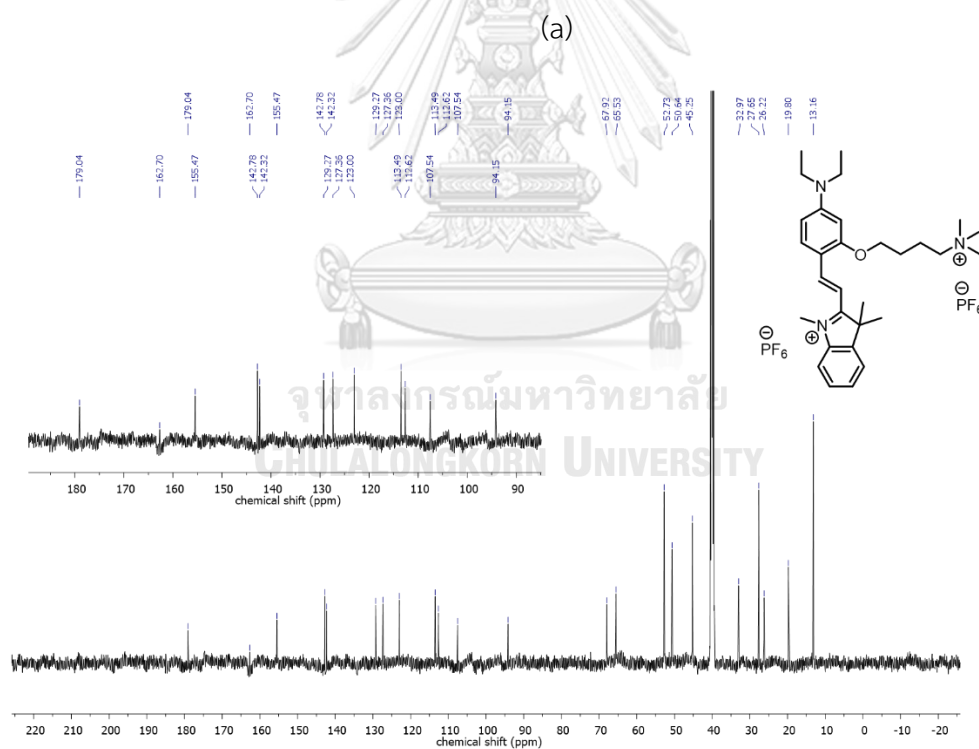
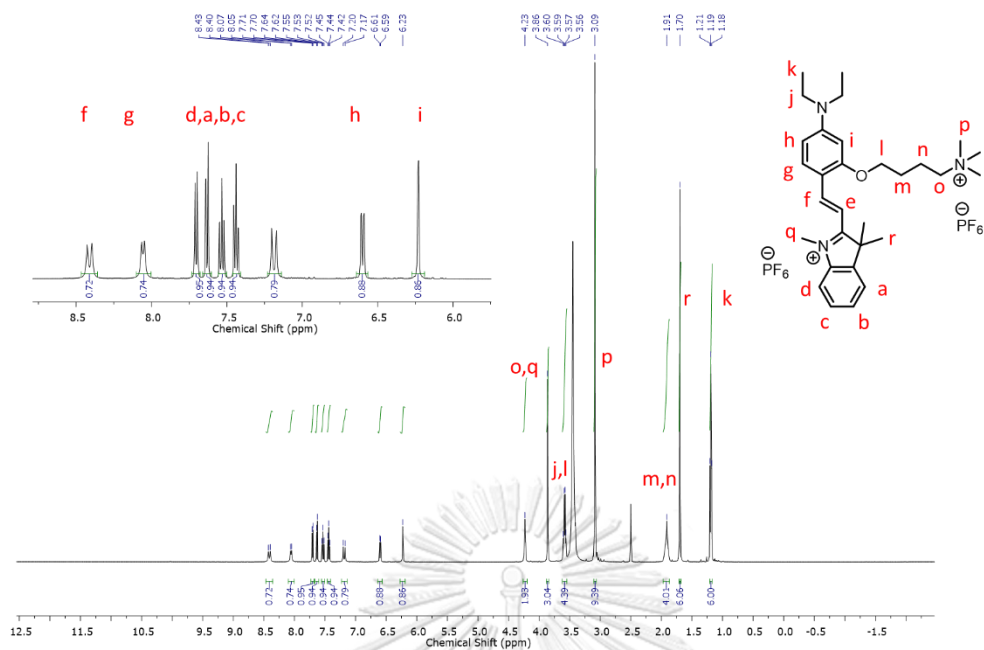


Figure A24 ^1H (500 MHz, DMSO- d_6) (a) and ^{13}C (126 MHz, DMSO- d_6) (b) NMR spectra of compound 2QL2+



(b)

Figure A25 ¹H (500 MHz, DMSO-*d*₆) (a) and ¹³C (126 MHz, DMSO-*d*₆) (b) NMR spectra of compound TMIN2+

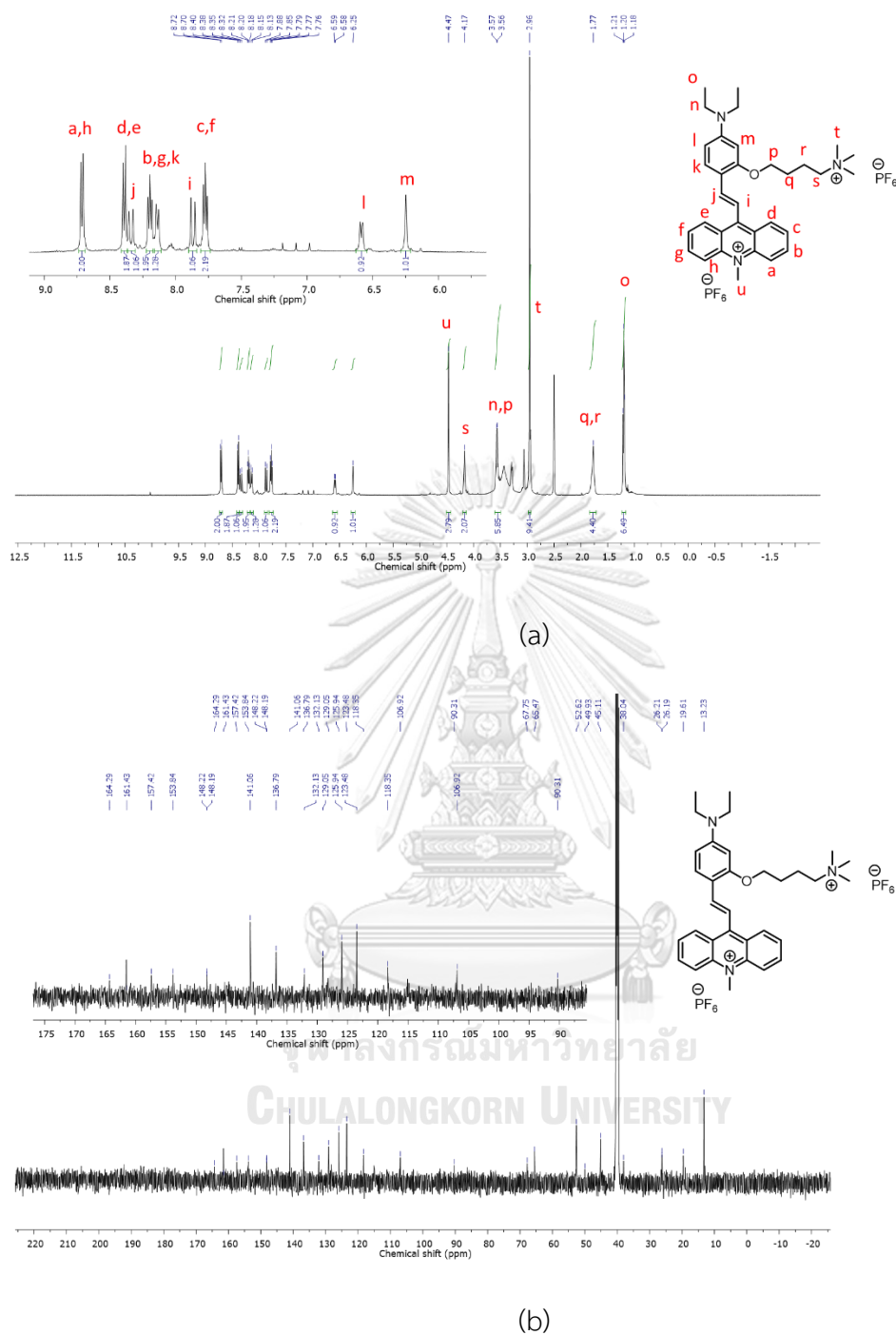


Figure A26 ^1H (500 MHz, $\text{DMSO-}d_6$) (a) and ^{13}C (126 MHz, $\text{DMSO-}d_6$) (b) NMR spectra of compound AD2+

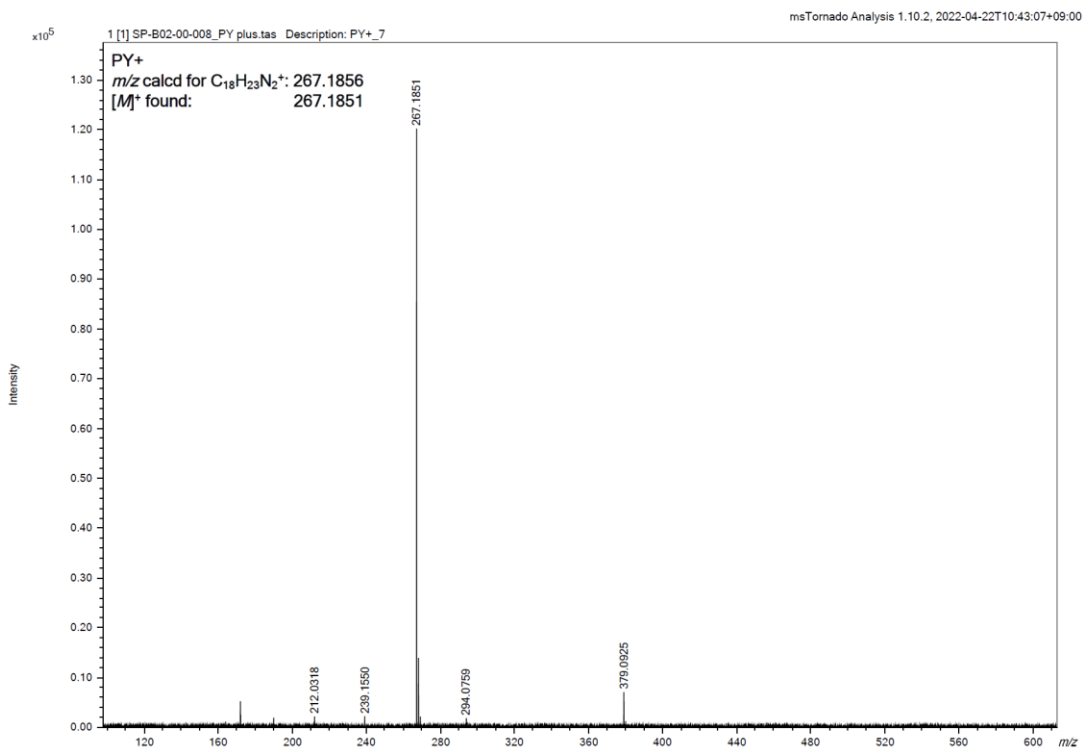


Figure A27 HRMS (MALDI-TOF) of PY+

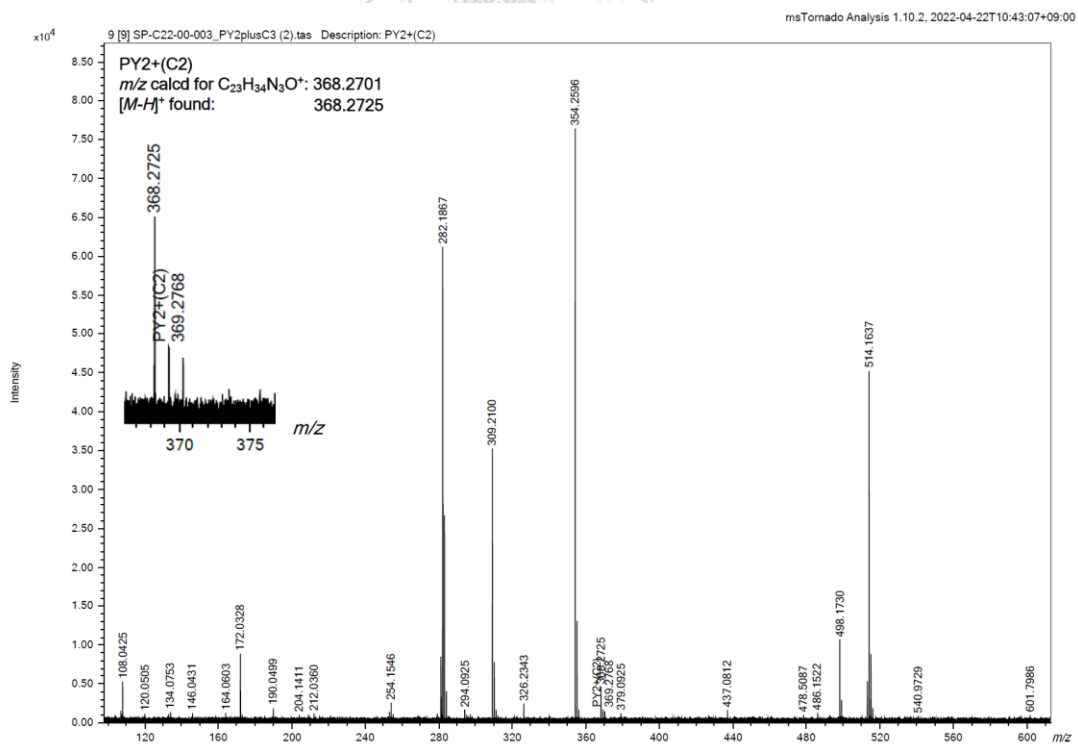


Figure A28 HRMS (MALDI-TOF) of PY2+(C2)

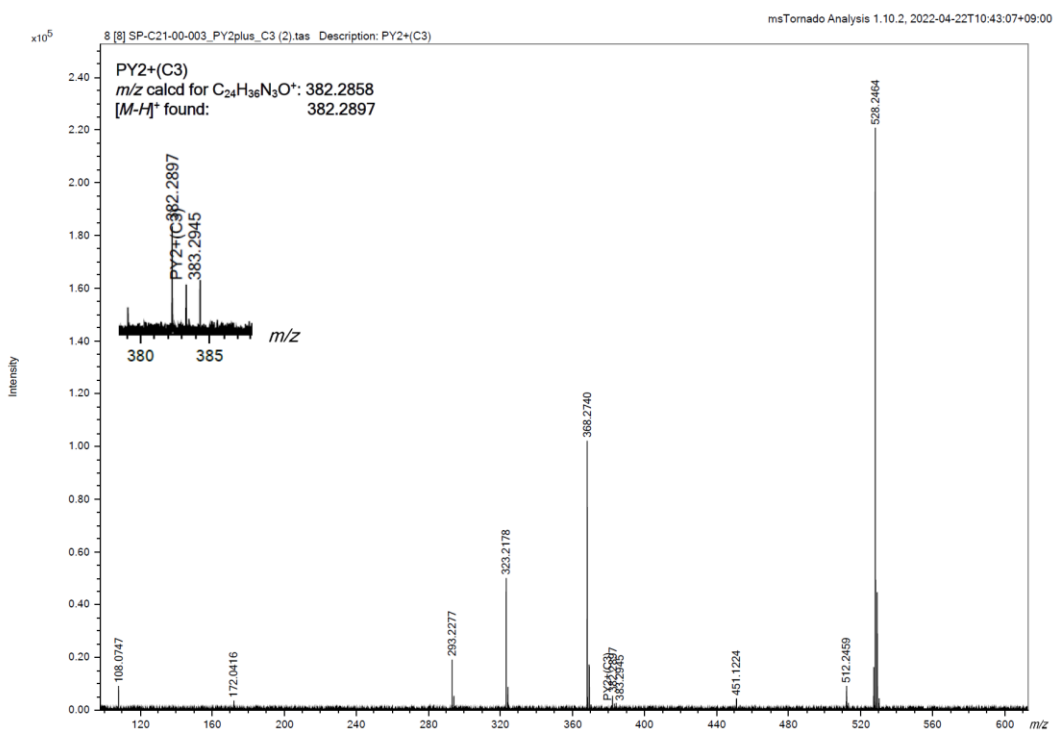


Figure A29 HRMS (MALDI-TOF) of PY2+(C3)

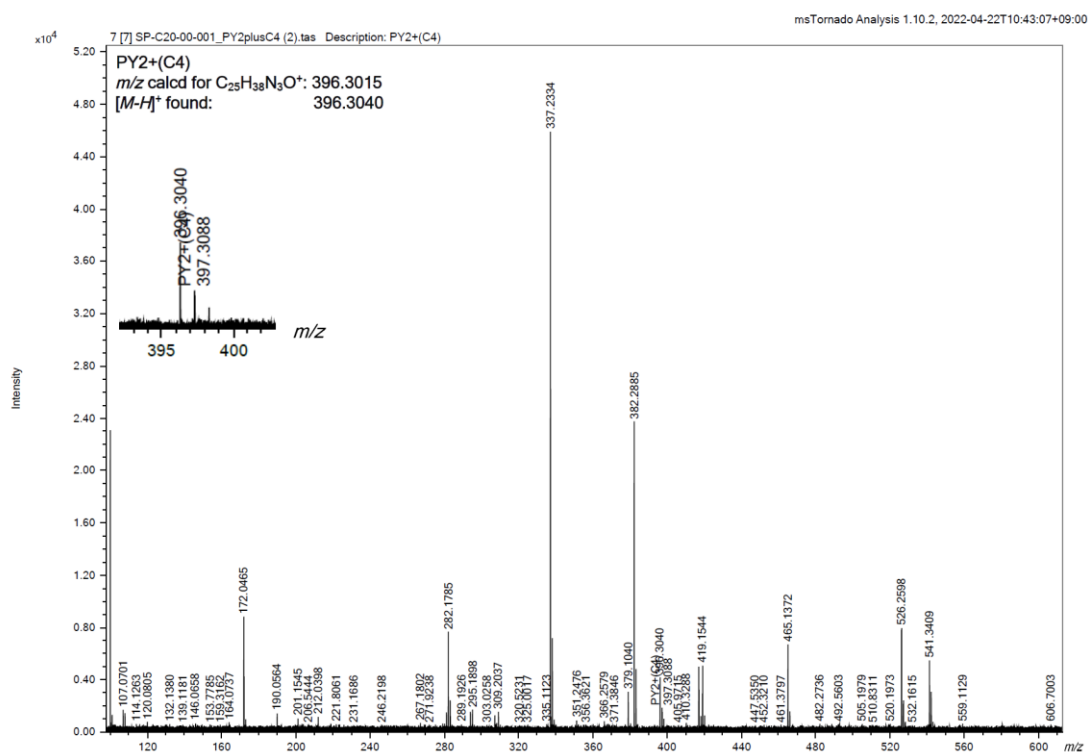


Figure A30 HRMS (MALDI-TOF) of PY2+(C4)

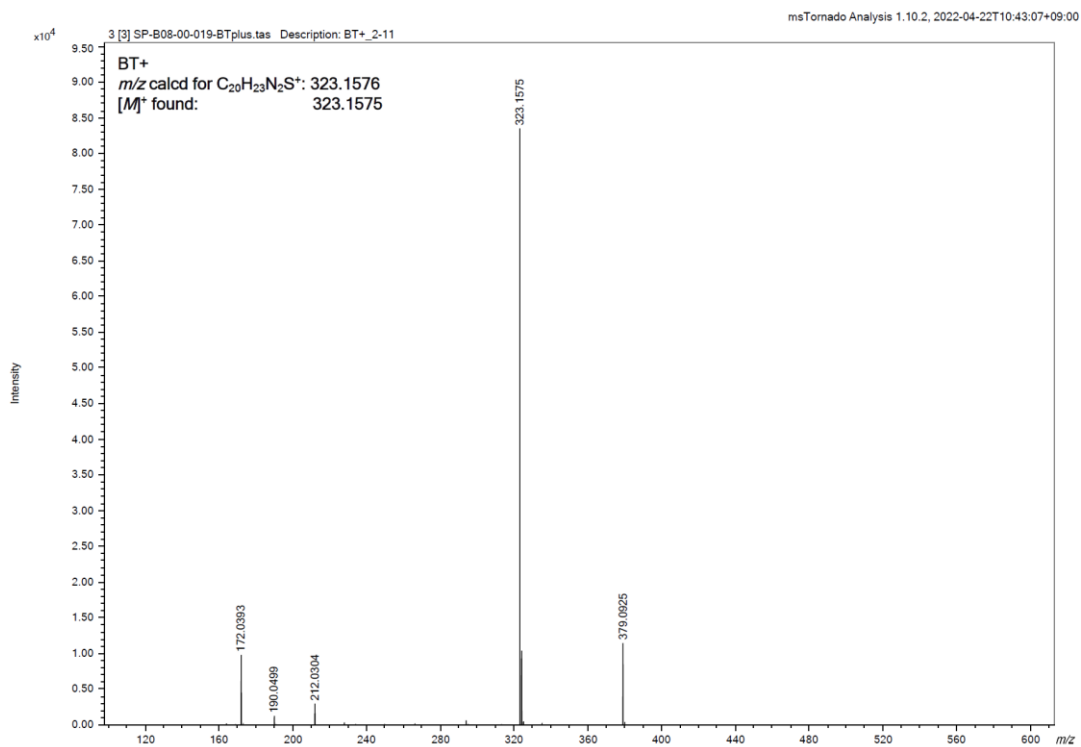
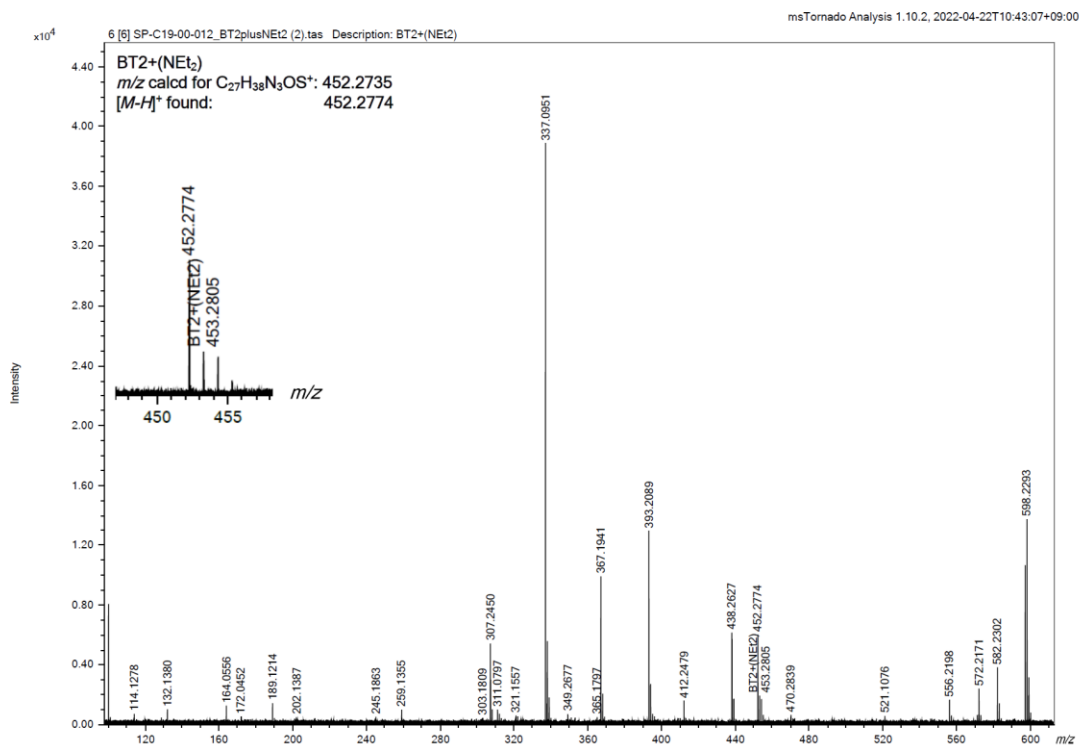


Figure A31 HRMS (MALDI-TOF) of BT+

Figure A32 HRMS (MALDI-TOF) of BT2+(NEt₂)

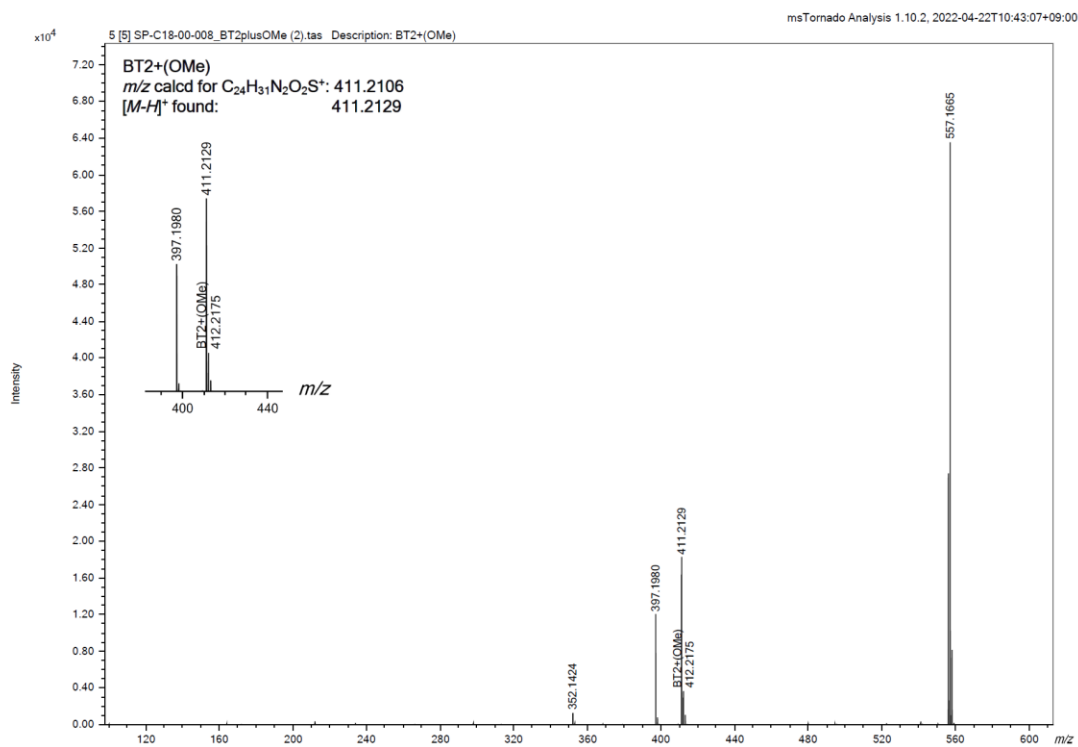


Figure A33 HRMS (MALDI-TOF) of BT2+(OMe)

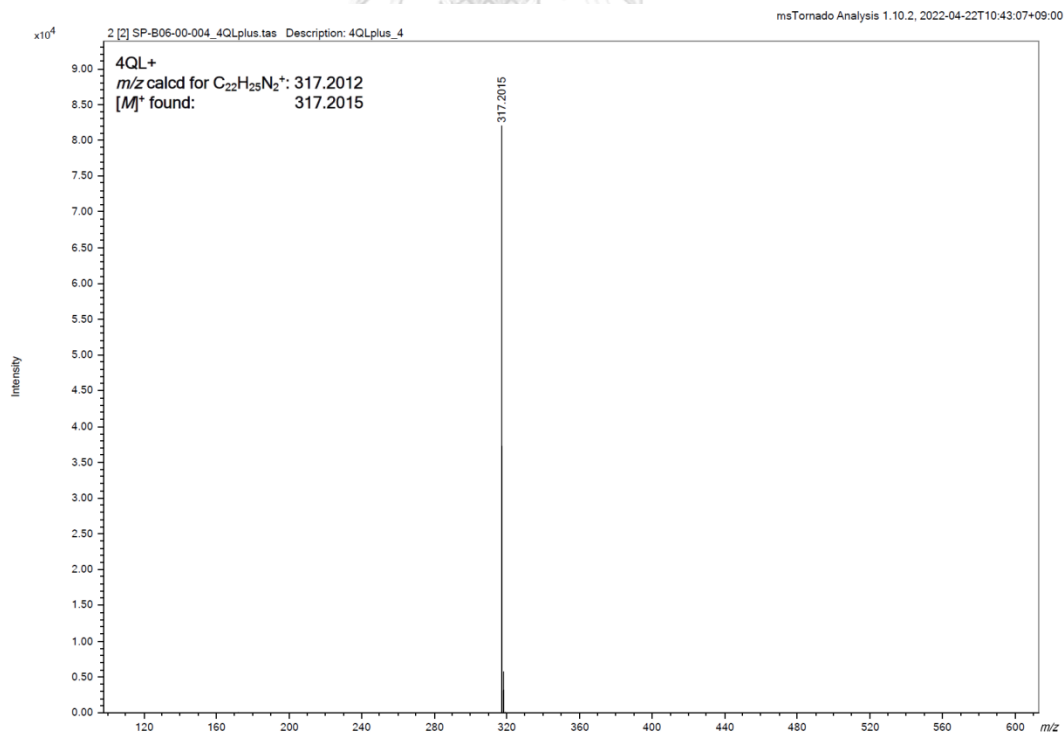


Figure A34 HRMS (MALDI-TOF) of 4QL+

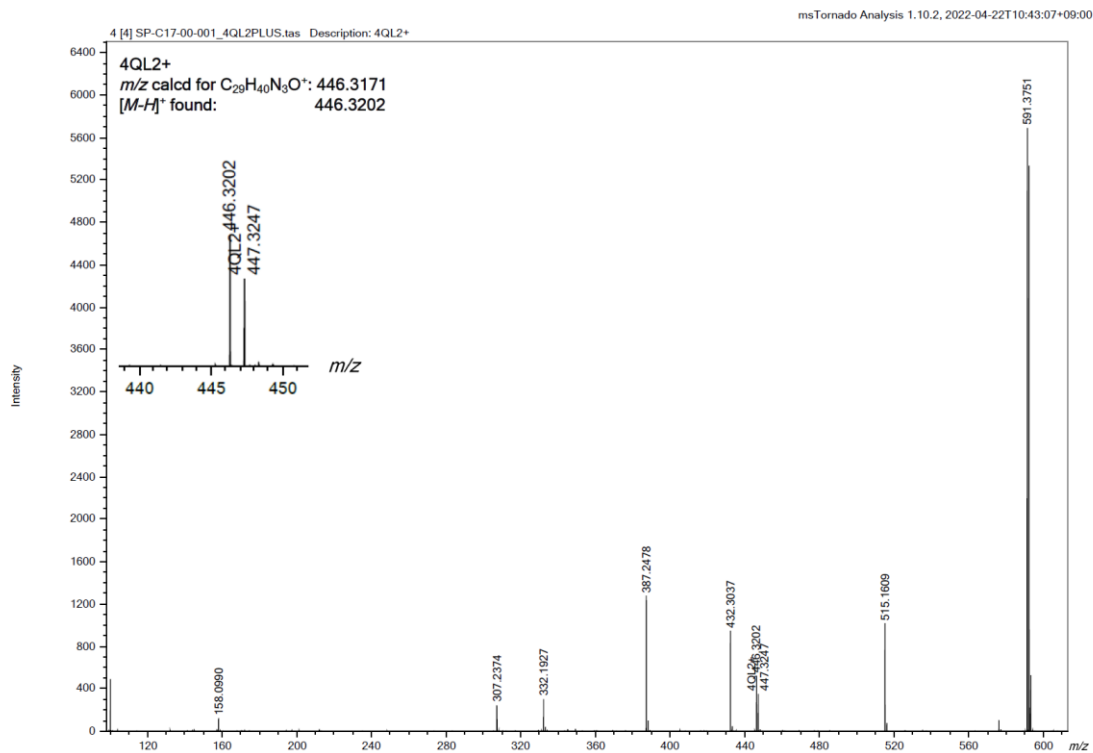


Figure A35 HRMS (MALDI-TOF) of 4QL2+



VITA

NAME Kotchakorn Supabowornsathit

DATE OF BIRTH 20 September 1992

PLACE OF BIRTH Phra Nakhon Si Ayutthaya, Thailand

INSTITUTIONS ATTENDED Bachelor's Degree of Science (Chemistry) in 2015

PUBLICATION Ditmangklo, B.; Muangkaew, P.; Supabowornsathit, K.; Vilaivan, T., Synthesis of PyrrolidinyI PNA and Its Site-Specific Labeling at Internal Positions by Click Chemistry. In Peptide Nucleic Acids: Methods and Protocols, Nielsen, P. E., Ed. Springer US: New York, 2020; pp 35-60.